Exploring Selenium Hydrogen Bonding through Gas Phase Spectroscopy Coupled with Quantum Chemical Calculations

A thesis

submitted in partial fulfillment of the requirements

of the degree of

Doctor of Philosophy

By

Kamal Kumar Mishra

ID No. 20143343

भारतीय विज्ञान शिक्षा एवं अनुसंधान संस्थान, पुणे

INDIAN INSTITUTE OF SCIENCE EDUCATION AND RESEARCH PUNE

(2019)

Dedicated to

My parents

भारतीय विज्ञान शिक्षा एवं अनुसंधान संस्थान, पुणे
INDIAN INSTITUTE OF SCIENCE EDUCATION AND RESEARCH
(An Autonomous Institution, Ministry of Human Resource Development, Govt. of India)
Dr.HomiBhabha Road, Pashan Pune – 411008

Declaration

I declare that this written submission represents my ideas in my own words and wherever other's ideas have been included; I have adequately cited and referenced the original sources. I also declare that I have adhered to all principles of academic honesty and integrity and have not misrepresented, fabricated or falsified any ideas/data/fact/sources in my submission. I understand that violation of the above will cause disciplinary action by the Institute and can also evoke penal action from the sources which have thus not been properly cited or from whom proper permission has not been taken when needed.

Kamal

Date: 06/05/2019

Mr. Kamal Kumar Mishra

20143343

भारतीय विज्ञान शिक्षा एवं अनुसंधान संस्थान, पुणे

IISER PUNE

INDIAN INSTITUTE OF SCIENCE EDUCATION AND RESEARCH
(An Autonomous Institution, Ministry of Human Resource Development, Govt. of India)
Dr.HomiBhabha Road, Pashan Pune – 411008

Certificate

Certified that the work incorporated in this thesis entitled "**Exploring Selenium Hydrogen Bonding through Gas Phase Spectroscopy Coupled with Quantum Chemical Calculations**" submitted by Mr. Kamal Kumar Mishra represents his original work which was carried out by him at IISER, Pune under my guidance and supervision during the period from 2014 to 2019. The work presented here or any part of it has not been included in any other thesis submitted previously for the award of any degree or diploma from any other University or Institution. I further certify that the above statements made by him regarding his thesis are correct to the best of my knowledge.

Aloke Das

Date: 06/05/2019

Dr. Aloke Das

(Research Supervisor)

Acknowledgment

First of all, I would like to acknowledge my research supervisor Dr.Aloke Das for his extensive help, careful guidance, motivation, inspiration and crucial suggestions during my Ph. D. Research journey. His expertise and continuous effort in work have helped me to achieve the research goals successfully. The journey of my Ph. D would not be accessible without his help and diligent participation. I want to thank him for his immense efforts to train me to become a good researcher and develop my skills in the experiments. Apart from helping me to develop my research skills he has also helped me to improve my writing and speaking skills. All of my learning from him will assist me in the future to become an independent researcher.

It is my great pleasure to thank my research advisory committee members Dr.Debashree Ghosh, Dr.SayanBagchi and Dr. H. N. Gopi for their fruitful suggestions to improve my results.

My research work would have been incomplete without help from the collaborators. I express my sincere thanks to my collaborators Dr.Debashree Ghosh, Dr. M. S. Madhusudhan a, Dr.Biplab Sarkar, Paulami Ghosh and Gulzar Singh for working with us.

I would also like to express my sincere thanks to former group members of the lab, Dr.Sumit Kumar and Dr. Santosh Kumar Singh. They have helped me a lot in performing the experiments, and it was a great pleasure to work with them. I thank Dr.Sumit Kumar for introducing me with various instruments in the lab and experimental techniques during my initial days. I thank Dr. Santosh Kumar Singh for teaching and assisting me during the experiments. Without his help, it would not have been possible for me to learn all the computational and experimental aspects of the work in a short time. I am grateful to my labmates Mr. Satish Kumar, Mr. Kshetrimayum Borish, Mr. Surajit Metya, and Mr. Prakash

Panwaria for assisting me in my work. I sincerely thank them especially Mr. Prakash Panwaria for helping me in preparing my thesis.

I am thankful to my IISER friends Ashok, Chandan, Shatrughan, Vinay, Sanjit and Ajay for their support and lively company.

I wish to express my thanks to Prof K. N. Ganesh, former Director and Prof. Jayant B. Udgaonkar, current Director of IISER Pune for providing high-quality research environment.

I thank UGC for my JRF and SRF fellowship.

I would like to acknowledge all the supporting staff members of the chemistry department for their help.

I want to express my sincere respect to my parents for their constant support during my research period. It would have been impossible for me to achieve my goal without their blessings.

Kamal Kumar Mishra

Content

List of Acronyms

REMPI	Resonantly Enhanced Multi-Photon Ionization
1C-R2PI	1 Color-Resonant Two-Photon Ionization
2C-R2PI	2 Color Resonant Two-Photon Ionization
RIDIRS	Resonant Ion-Dip Infrared Spectroscopy
HB	Hole Burn
TOF	Time Of Flight
MS	Mass Spectrometry
PV	Pulse Valve
Ar	Argon
He	Helium
He-Ne	Helium-Neon
DFT	Density Functional Theory
MP2	Moller-Plesset Second-Order Perturbation Theory
EDA	Energy Decomposition Analysis
AIM	Atoms-In-Molecules
NBO	Natural Bond Orbital
LMO	Localized Molecular Orbital
ALMO	Absolutely-Localized Molecular Orbital
ZPE	Zero Point Energy
Disp	Dispersion
Es	Electrostatics
Ex	Exchange
Pol	Polarization
Rep	Repulsion
CT	Charge Transfer
PDB	Protein Data Bank
CSD	Cambridge Structural Database
BSSE	Basis set superposition error
ΔE_e	BSSE corrected binding energy
ΔE_o	BSSE+ZPE corrected binding energy
aVNZ	aug-cc-pVNZ
SAPT	Symmetry-Adapted Perturbation Theory
OPO	Optical Parametric Oscillator
OPA	Optical Parametric Amplifier
IP	Ionization Potential

List of Figures

List of Tables

Synopsis

Non-covalent interactions play a significant role in the structure and function of biomolecules as well as materials. These weak intermolecular interactions are generally classified into different categories such as hydrogen bond, halogen bond, π-stacking, cation-π interaction, anion-π interaction, etc. Undoubtedly, the hydrogen bond is the most extensively studied non-covalent interaction among all others. The present thesis is dealt with molecular-level understanding of the nature and strength of selenium hydrogen bonding interaction through gas phase laser spectroscopy and quantum chemistry calculations.

The concept of a hydrogen bond is about a century old. It was first reported in the literature by Latimer and Rodebush in 1920. Hydrogen-bond is one of the well-studied non-covalent interactions. However, there is still an ever-growing interest in the scientific community to understand this fascinating intermolecular interaction in further detail. Hydrogen-bonding interaction is highly directional, and it plays an important role in the molecular association. This non-bonding interaction controls and directs the structures of molecular assemblies in supramolecular chemistry.

Pauling in his famous book 'Nature of Chemical Bond' mentioned that hydrogen bond is electrostatic in nature and the most electronegative atoms in the periodic table, e.g., O, N and F can only form hydrogen bond because of their high electronegativity. However, it has been found that hydrogen bond is not restricted to only conventional electronegative donor and acceptor atoms. It has also been confirmed later through Compton scattering and NMR experiments that hydrogen-bond contains the covalent character. IUPAC committee re-defined hydrogen bond in 2011. According to the recent definition of the hydrogen bond-

"The hydrogen bond is an attractive interaction between a hydrogen atom from a molecule or a molecular fragment X–H in which X is more electronegative than H, and an atom or a

group of atoms in the same or a different molecule, in which there is evidence of bond formation."

Hydrogen bond is classified into conventional and unconventional based on the electronegativity of hydrogen bond donor and acceptor atoms. Conventional hydrogen bonds include conventional donors and acceptor atoms, i.e., atoms with higher electronegativity, e.g., O, N, and F. Conventional hydrogen bonds include N-H…N, O-H…O, N-H…O, etc. The typical bond energy for conventional hydrogen bond is 20-50 kcal/mol.

On the other hand, non-conventional hydrogen bonds include hydrogen bonds having donor or acceptor atoms or both having less electronegativity. Non-conventional hydrogen bonding includes C-H…O, C-H…F, C-H…N, O-H…S, N-H…S, O-H…Se, N-H…Se, π-hydrogen bonding, etc. The typical bond energy for conventional hydrogen bond is 1-20 kcal/mol.

Selenium is considered as an essential trace element in animals and humans for growth and fertility. Selenocysteine is the 21st amino acid in ribosome-mediated protein synthesis. As oxygen and selenium atoms belong to the same group in the periodic table, they have the same physical properties. Replacement of oxygen with selenium does not change the physical properties of the nucleic acids. Rather selenium substitution facilitates the crystallization and solving the crystal structures of the nucleic acids because of higher electron density and larger size of Se. Biswal and co-workers carried out extensive protein data bank (PDB) analysis and reported that there are 24461 Mse (selenomethionine) residues present in 4472 protein structures which account for 4334 hydrogen bonds. They observed that out of these 4334 N-H...Se hydrogen bonds, 2342 are with the main chain and 1992 are with the side chain.

Se is the third element in the chalcogen family after O and S. The electronegativity of Se is 2.55 which is comparable to S (2.58) but less than O (3.44). It has been reported that S forms hydrogen bond of similar strength as compared to O although it is less electronegative than O. S-hydrogen bond is studied quite extensively and it has been reported that dispersion interaction plays a major role in stabilization of sulfur-centered hydrogen-bonded complexes. However, spectroscopic investigation of Se-hydrogen bond is sparse in the literature except the one recently reported by Biswal and co-workers.

The goal of the present thesis is the following:

1. It has already been reported in the literature that S forms hydrogen bond of similar strength as compared to O. Does selenium (Se) also forms hydrogen bond of similar strength as compared to S and O. What is the physical nature of hydrogen bond involving selenium?
2. What is the nature, strength and binding motifs of water-mediated selenium hydrogen bonding interactions which are present in proteins?
3. What will be the strength and nature of the hydrogen bond when both hydrogen bond donor and acceptor atoms are less electronegative?

Chapter 1 starts with a brief introduction of the hydrogen bond followed by the introduction of selenium hydrogen bonding. We have discussed the physical nature of the hydrogen bond, in general. Various spectroscopic techniques to probe the hydrogen bond are also discussed in detail. We have discussed the importance of selenium hydrogen bonding interaction in biomolecules and materials. This chapter ends with the aim of the thesis.

Chapter 2 gives detailed information of various spectroscopic techniques and computational details which have been used to study the complexes formed by hydrogen bond involving selenium. We have briefly discussed the principle of supersonic expansion, time of flight mass spectrometry, various spectroscopic techniques (1C-R2PI, 2C-R2PI, RIDIRS, UV-UV

hole burn, and IR-UV hole burn) used to measure the electronic and IR spectra of the clusters.

In Chapter 3, we have discussed the experimental evidence of direct selenium hydrogen bonding and the nature of selenium hydrogen bonding. We have synthesized the complexes of indole and phenol with dimethyl selenide (Me_2Se) in supersonic jet and studied these complexes by various spectroscopic techniques. We observed that Se forms hydrogen bond of similar strength as compared to S and O. We have studied both N-H...Se and O-H...Se hydrogen bonds using gas phase spectroscopy and quantum chemistry calculations. We have explored various energy decomposition analyses to determine the origin of the IR red-shift in the X-H stretch frequency of the S/Se hydrogen bond as the electrostatic interaction in these complexes is smaller compared to that in conventional hydrogen-bonded complexes. It has been found that the charge transfer component of the interaction energy plays a significant role in the IR red shift in the X-H stretching frequency.

Chapter 4 deals with the molecular level understanding of water-mediated selenium hydrogen bonding present in proteins. It has been reported from extensive PDB analysis that direct selenium hydrogen bonding between selenomethionine and other amino acid residues is abundant in proteins and this interaction plays an important role in the stability of the protein structures. However, water-mediated indirect selenium hydrogen bonding between two or more amino acid residues involving selenomethionine is not demonstrated in the literature. Generally, water molecules present in the core or interior of the proteins forming some cavities bind with two or more amino acid residues and contribute to the stability of the proteins. We have found from the PDB analysis that the number of water-mediated Se hydrogen bonding interaction is three times more than that of the direct Se hydrogen bonding interaction present in proteins. We have studied a model complex, consisting of indole (represents tryptophan), water and dimethyl selenide (represents selenomethionine), which

mimics the structural motif of single water-mediated Se hydrogen bonding interaction present in proteins.

In Chapter 5, we have discussed the nature and strength of the hydrogen bonds where both hydrogen bond donor and acceptor atoms are less electronegative, i.e., unconventional in nature. In the literature, there are reports of spectroscopic studies of unconventional hydrogen bonding involving either weak hydrogen bond donor (C-H) or weak hydrogen bond acceptor (S, Se or P), i.e., C-H..N, C-H…O or N-H…S, O-H…S, N-H…Se, N-H…P, etc. In this work, we have explored the nature and strength of the hydrogen bond interaction (S-H…S or S-H…Se) where both hydrogen bond donor and acceptor atoms are unconventional or less electronegative. Interestingly, it has been observed that S-H…S and S-H…Se interactions are of similar strength as O-H…S interaction. We have reported here that S forms a strong hydrogen bond when it is used as a hydrogen bond donor even though it is less electronegative than O.

Chapter 6, the last chapter of the thesis, summarizes the whole thesis and discusses future perspectives.

List of Publications

1. **Kamal Kumar Mishra,** Prakash Panwaria, Kshetrimayum Borish, Surajit Metya, Satish Kumar and Aloke Das*: *Observation of strong hydrogen-bond involving unconventional hydrogen bond donor as well as acceptor atoms* **(Manuscript under preparation)**
2. **Kamal Kumar Mishra,** Santosh Kumar Singh, Satish Kumar, Gulzar Singh, Biplab Sarkar*, M.S. Madhusudhan* and Aloke Das*: *Nature, strength and binding motifs of water-mediated selenium hydrogen bonding in proteins* **(Manuscript submitted)**
3. Santosh Kumar Singh, Shahaji Moore, Satish Kumar, **Kamal Kumar Mishra,** K. N. Ganesh, Aloke Das: *A conformation-specific IR spectroscopic signature for weak C=O…C=O n→π* interaction in capped 4R-hydroxyproline*. **Phys. Chem. Chem. Phys. 2019, 21, 4755-4762**.
4. Debashish Mondal, Anjana Sathyan, Sopan V. Shinde, **Kamal Kumar Mishra,** and Pinaki Talukdar*: *Tripodalcyanurates as selective transmembrane Cl^- transporters* **Org. Biomol. Chem., 2018, 16, 8690-8694**
5. **Kamal Kumar Mishra,** Santosh Kumar Singh, Paulami Ghosh, Debashree Ghosh* and Aloke Das*: *The nature of selenium hydrogen bonding: gas phase spectroscopy and quantum chemistry calculations* **Phys. Chem. Chem. Phys. 2017, 19, 24179-24187**.
6. Santosh Kumar Singh, **Kamal Kumar Mishra,** Neha Sharma, and Aloke Das*: *Direct spectroscopic evidence for an n→π* interaction.* **Angew. Chem. Int. Ed. 2016, 55, 7801-7805.**

Chapter 1

Introduction

1.1 Non-covalent Interactions

Non-covalent interactions are the backbone of life. These interactions play a vital role in the structure and function of biomolecules as well as materials.[1-5] Non-covalent interactions are classified into different categories such as hydrogen bond,[1,3,6-9] halogen-bond,[10-18] $n\rightarrow\pi^*$ interaction,[19-23] π-πstacking,[24-27] π-hydrogen bonding interaction,[28-31] cation-π interaction,[32-37] anion-π interaction[38-41], etc. Hydrogen bond is the most extensively studied intermolecular interaction among all other non-covalent interactions. As the present thesis is focused on selenium hydrogen-bonding interaction, we will restrict our discussion here to the hydrogen-bonding interaction only.

1.2 Hydrogen bond

Hydrogen bond is about a century old and one of the well-studied non-covalent interactions. However, there is still an ever-growing interest in the scientific community to understand this fascinating intermolecular interaction in further detail. Hydrogen-bonding interaction is highly directional, and it plays an important role in the molecular association. This non-bonding interaction controls and directs the structures of molecular assemblies in supramolecular chemistry.[1,3] This interaction plays a crucial role in the structural organization of biological macromolecules. It stabilizes the DNA double helical structure which is required for genetic coding in all living organisms.[7] This weak intermolecular interaction also plays a significant role in stabilizing secondary, tertiary and quaternary structures of proteins. Water, the cause of life on earth, is also stabilized by hydrogen bonding interactions.

1.2.1 Origin of the concept of hydrogen-bond and various definitions

Although there is no consensus among the scientific community about the origin of the hydrogen bond, many authors believe that this concept was known to the scientists even

before it got its proper place in the world of chemistry. Werner in 1902 used the term *Nebenvalenz* (secondary valency) to explain the binding situation in the ammonia salts (e.g., hexaminocolatperchlorate).[42] In 1913, Pfeiffer used the term *Innere Komplexsalzbildung* (internal complex salt-bridge) to describe the intramolecular hydrogen bonding in 1-hydroxyanthraquinone. In 1912, Moore and Winmill used the term *weak union* to describe the weaker basic properties of trimethyl ammonium hydroxide in comparison to tetramethylammonium hydroxide.[43] In 1920, Latimer and Rodebush while discussing the structure of the water dimer, explained that 'a free pair of electrons on one water molecule might be able to exert sufficient force on a hydrogen held by a pair of electrons on another water molecule to bind the two molecules together' and that 'the hydrogen nucleus held between two octets constitute a *weak bond*'.[44] In 1939, Linus Pauling in his famous book 'The Nature of Chemical Bond' mentioned that 'a hydrogen atom, with only one stable orbital, cannot form more than one pure covalent bond and that the attraction of two atoms observed in hydrogen-bond formation must be due largely to ionic forces.'[45] According to Pauling, the more electronegative elements like nitrogen (N), oxygen (O) and fluorine (F) which have electronegativity values 3.0, 3.44 and 4.0, respectively, can form strong hydrogen bonds. Thus, hydrogen-bonds are formed when both of the hydrogen-bond donor and acceptor atoms are highly electronegative. Pauling described the hydrogen-bond as mainly electrostatic because it involves attraction between partially charged ions.

Pimentel and McClellan proposed a relatively broader definition of the hydrogen-bond in 1960 in their famous book 'The Hydrogen Bond.'[9] According to Pimentel and McClallen:

"*A hydrogen bond exists between a functional group A-H and an atom or a group of atoms B in the same or a different molecule when*

(a) There is evidence of bond formation (association or chelation)

(b) There is evidence that this new bond linking A-H and B involves the hydrogen atom already bonded to A."

However, the definition proposed by Pimentel and McClellan did not include the chemical nature of the hydrogen-bond donor and acceptor atoms like electronegativity, polarity and net charge.[6]

IUPAC committee redefined hydrogen-bond in 2011.[46] According to the recent definition:

"*the hydrogen bond is an attractive interaction between a hydrogen atom from a molecule or a molecular fragment X–H in which X is more electronegative than H, and an atom or a group of atoms in the same or a different molecule, in which there is evidence of bond formation.*"

Conventionally, hydrogen-bond is denoted as X-H...Y where both X (hydrogen-bond donor) and Y (hydrogen-bond acceptor) are electronegative atoms. However, it has been found that hydrogen bond is not restricted to only conventional electronegative donor and acceptor atoms. Thus this interaction can be classified into conventional and non-conventional hydrogen-bonds. Conventional hydrogen bonds include conventional donors and acceptors, i.e., the atoms with higher electronegativity, i.e., O, N, and F. Conventional hydrogen bonds include N-H…N, N-H…O, O-H…N, O-H…O interactions.[9,47-49] The strength of the conventional hydrogen-bonds is 20-50 kcal/mol.[50-52] These interactions are mainly electrostatic, but other components of the interaction energy are also present there.[53]

On the other hand, non-conventional hydrogen bonds include unconventional atoms, i.e., atoms having less electronegativity. In non-conventional hydrogen bonding, either donor or acceptor or both are less electronegative atoms. Non-conventional hydrogen bonding includes C-H…O, C-H…F, C-H…N, O-H…S, N-H…S, O-H…Se, N-H…Se interactions. There is another special kind of non-conventional hydrogen bonding represented as X-H…π interaction.[54,55] In this kind of interaction, hydrogen atom from donor interacts with the π-

electron cloud of molecular systems. Here, π-electron cloud acts as a hydrogen bond acceptor. The strength of the π-hydrogen bonding interaction depends on the polarity of the X-H group. π-hydrogen bonding interaction includes C-H…π, N-H…π, O-H…π, S-H...π,etc.[56-59] In general, non-conventional hydrogen bonds (1-20 kcal/mol)[50,51] are weaker than their conventional counterparts.

1.2.2 Physical nature of the hydrogen bond

Although hydrogen bond can be classified into conventional and non-conventional ones based on the electronegativity of the donor and acceptor atoms, physical nature of various types of the hydrogen bond is not straightforward at all. The total interaction energy in the case of a hydrogen bond is not dependent only on one factor, rather several factors contribute to the different extent to the total interaction energy of the hydrogen bonding. Kitaura and Morokuma decomposed the total interaction energy of several hydrogen bonded complexes into electrostatic, polarization, exchange repulsion, charge transfer, and dispersion components.[60,61] All the terms of the interaction energy except exchange repulsion are attractive.

1.2.2.1 Electrostatic interaction

Electrostatic interaction involves attraction between partially charged atoms. Conventional hydrogen bonds involve X-H…Y kind of interaction where both X and Y are highly electronegative atoms (N, O or F) in the periodic table. Due to the high electronegativity of X, X-H bond is polar. Electron density is more shifted towards X and due to that X bears a partial negative charge, and H bears a partial positive charge. On the other hand, Y also bears partial negative charge due to its high electronegativity. This partially positive charged hydrogen is attracted towards the partially negative charged Y.

The attraction between the two oppositely charged atoms is governed by Coulomb law and hence is called electrostatic interaction. This electrostatic interaction is directional and long-range interaction. This interaction energy varies with r^{-2} and r^{-3} for monopole-dipole interaction and dipole-dipole interaction respectively where r is the distance between the two opposite charges.[6]

In general, conventional hydrogen bonding such as N-H…O, O-H…O interactions are dominated by electrostatic interaction.

1.2.2.2 Polarization or Induction interaction

Polarization/induction interaction involves deformation of the electron cloud of a non-polar molecule in the presence of a polar molecule. This interaction is also called dipole-induced dipole interaction. When a polar molecule/group approaches towards a non-polar or neutral molecule, the electron cloud of the latter gets distorted, and due to that, it becomes polar. The following relation can give it. The lowering in potential energy (P) due to polarization can be given as[62]

$$P=e^2\overline{\alpha}/2r^4 \quad \text{--------} \quad (1.1)$$

Here, $\overline{\alpha}$ is the average polarizability of the molecule.

1.2.2.3 Exchange repulsion

Exchange repulsion involves the interaction caused by the exchange of electrons between the hydrogen bond donor (X) and acceptor (Y) in X-H…Y. It is a short-range repulsion which is generated due to the overlap of electronic distribution of X with Y. The exchange repulsion varies with the distance as r^{-12}.[6]

1.2.2.4 Charge transfer

Charge transfer interaction in X-H…Y hydrogen bond involves delocalization of electron density from the lone pair/occupied molecular orbitals (MO) of the hydrogen bond acceptor

(Y) to the antibonding/vacant molecular orbital of the X-H bond. Charge transfer interaction is an extremely short range interaction, and it varies with the distance as e^{-r}.[6]

1.2.2.5 Dispersion interaction

Dispersion interaction is an attractive force which is present in non-polar molecules. This interaction arises due to the instantaneous dipole created in the molecule due to the fluctuation of the electron density. This instantaneous dipole induces dipole of opposite sign in the neighboring molecule which leads to the attraction between two molecules. Thus, this interaction is also called instantaneous dipole-induced dipole interaction or London dispersion interaction named after German physicist Fritz Wolfgang London.

The strength of the dispersion interaction depends on the polarizability of the molecules which in turn depends on the size of the molecules. More significant will be the size of the molecules; electrons will be more loosely held, and distortion of the electron cloud will be smoother. It also depends on the polarizability of another molecule because it is the polarizability only which determines how easily dipole can be induced in the second molecule. The quantitative strength of the dispersion interaction can be given by the London formula[63]

$$V = -\frac{C}{r^6}, C = \frac{3}{2}\alpha_1'\alpha_2'\frac{I_1 I_2}{I_1+I_2} \text{ -------} \qquad (1.2)$$

Here, I_1 and I_2 are the ionization energies of the molecules. α_1' and α_2' are the polarizability of the molecules. This interaction is inversely proportional to the sixth power of the distance between the interacting molecules. It is a short-range interaction, and it is the main contributing factor in the stabilization of the π–stacked molecular assembly.

Hydrogen bond is a complex interaction which involves charge-dipole, dipole-dipole, charge transfer and dispersion interactions together depending on the nature of interacting molecules. It does not depend on a single component. Although the concept of hydrogen bond is a

century old, its definition is still debated. All these individual interactions are *r* dependent. The following table summarizes about *r* dependency of various interactions.

Table 1.1 The *r* dependency of various kind of interactions in different types of molecular units. *r* is the distance between interacting atoms in the different molecules

Type of molecular unit	Type of interaction	n in r^{-n}
ions	coulombic	1
Ion-polar molecules	Ion-dipole	2
Two polar molecules	Dipole-dipole	3
Ion-non polar molecule	Ion-induced dipole	4
Polar and non-polar molecule	Dipole-induced dipole	6
Non polar molecules	Dispersion	6

The hydrogen bonded complexes formed by conventional hydrogen bond donor and acceptor atoms are stabilized mainly due to electrostatic interaction. This interaction is a long range interaction accompanied by other short range interactions in hydrogen bonded complexes. The electrostatic component varies with r^{-3}. Hence, hydrogen bond strength varies with r^{-3} for conventional hydrogen bonded complexes.

1.3 Hydrogen bonding in biomolecules

Hydrogen bonding plays a paramount role in the structure and function of all biologically essential molecules. Carbohydrates are the most abundant molecules in biological structures next to water. Carbohydrates exist in monosaccharides (e.g., glucose, fructose, mannose) disaccharides (e.g., sucrose, maltose, lactose), oligosaccharides (e.g., raffinose) and polysaccharides (e.g., amylose) forms. They occur alone or hydrogen bonded with purine and

pyrimidines. Carbohydrates contain hydroxyl group which acts as hydrogen bond donor as well as hydrogen bond acceptor.

Amino acids are the building blocks of protein structures. There are 22 naturally occurring amino acids. Amino acids, as the name suggests, it contains both an amino group and acidic group in the same molecule. These both functional groups help the individual amino acid to form the long sequence by forming a peptide bond. Primary structure of proteins contains these amino acids linked together *via* a peptide bond. Sequences containing less than 50 amino acids are called peptides while sequences containing more than 50 amino acids are referred to as proteins or polypeptides.

The secondary structure of peptides or proteins is a combination of primary structures hydrogen bonded with each other. There are three main types of secondary structures named as α-helix, β-sheet, and β-turns. α-helix and β-sheet are stabilized by N-H...O=C interaction. In a β-turn, a loop is formed when carbonyl oxygen from i^{th} amino acid residue forms the hydrogen bond with amide from $(i+3)^{th}$ residue in the sam e chain.

The various non-covalent interactions stabilize tertiary and quaternary structures of proteins involved in its overall three-dimensional folding. Hydrogen bond plays an important role in stabilizing the tertiary and quaternary structures of the protein. Water also plays an important role in stabilizing the three-dimensional structure of proteins through hydrophobic interactions.[7] Without water; proteins lose their biological functioning due to denaturation. However, water molecules present in the core or cavity of the proteins contribute to its stability through water-mediated hydrogen-bonding interactions bridging two or more amino acid residues.

The double helical structure of the deoxyribose nucleic acid (DNA), is also stabilized by a hydrogen bond between base pairs. DNA has a special place in biology because it carries genetic information from one generation to another. Watson and Crick proposed the double

helical structure of DNA in which nucleic acid-base pairs are hydrogen bonded to each other.[64]

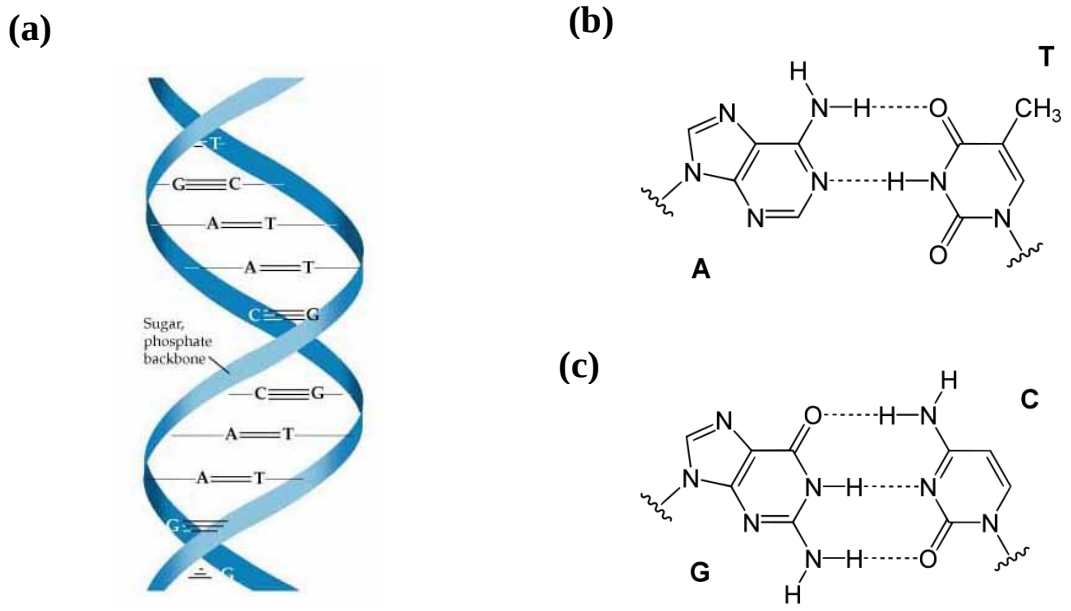

Figure 1.1: (a) Double helix structure of DNA. Hydrogen bonding between base pairs in (b) Adenine (A) and thymine (T) (c) cytosine (C) and guanine (G).

Selenium is considered as an essential trace element in animals and humans for growth and fertility. Selenocysteine is the 21st amino acid in ribosome-mediated protein synthesis [65,66]As oxygen and selenium atoms belong to the same group in the periodic table; they have the same physical properties. Replacement of oxygen with selenium does not change the physical properties of the nucleic acids. Rather selenium substitution facilitates the crystallization and solving the crystal structures of the nucleic acids because of higher electron density and larger size of Se.[67,68] Biswal and co-workers carried out extensive protein data bank (PDB) analysis and reported that there are 24461 MSe (selenomethionine) residues present in 4472 protein structures which account for 4334 hydrogen bonds. They observed that out of these 4334 N-H...Se hydrogen bonds, 2342 are with the main chain and 1992 are with the side chain.[69]

1.4 Hydrogen bonding in supramolecular chemistry

Jean-Marie Lehn coined the term supramolecular chemistry in 1969. Supramolecular chemistry may be defined as 'chemistry beyond the molecules,' bearing on the organized entities of higher complexity that result from the association of two or more chemical species held together by intermolecular forces or non-covalent interactions.[3] Among all different types of non-covalent interactions, hydrogen bond plays a crucial role in supramolecular chemistry. All the supramolecular assemblies contain carbon (C) and hydrogen (H) as the main constituting unit apart from all other heteroatoms. Hydrogen bonding interaction involving carbon as a hydrogen bond donor is well documented in the literature. First, systematic study of the C-H…O interaction in crystal structures was reported by Sutor in theophylline, caffeine, and uracil.[70] Ferguson and co-workers reported C-H...O hydrogen bonds in terminal alkynes.[71] Keegstraand co-workers observed that 1,4-benzoquinone unit in the quinonoid compound was arranged in layers through C-H…O interactions.[72] The distance (d) between the H and O atoms in the C-H…O interactions was found in the range of 2.38-2.59 Å, which was smaller than the sum of the van der waals radii of H and O (2.6 Å). Desiraju and co-workers surveyed C-H…O hydrogen bond pattern in 2306 nitro-compounds using the Cambridge Structural Database (CSD) and concluded that these patterns are of great importance in supramolecular assembly.[73]

Apart from the C-H…O interactions, hydrogen bonding interactions involving less electronegative atoms such as S and Se as hydrogen bond acceptors have been observed in the crystal structures. The crystal structures of thiourea and selenourea show similar hydrogen bonding pattern except for the fact that H...Se (N-H...Se) distance in the case of selenourea is larger than the H...S (N-H...S) distance in thiourea. This is quite obvious because selenium has a larger size than sulfur. Allen and co-workers analyzed the crystal structures containing sulfur as H-bond acceptors obtained from the Cambridge Structural

Database (CSD).[74,75] They studied >C=S and $^{-}CS_2^{-}$ systems as hydrogen bond acceptors and observed that the N-H...S interaction is more pronounced than the O-H...S interaction for both the systems. The hydrogen bond angle (∠N-H...S or ∠O-H...S) has been found to vary from 140^0 to 165^0 depending on the molecules containing sulfur as H-bond acceptor.

Intermolecular, as well as intramolecular hydrogen bonds involving selenium as a hydrogen bond acceptor, has been observed in crystal structures. Peng and co-workers reported that chiral selone exists as a dimer linked via intermolecular selenium hydrogen bonding.[76] Bhattacharya and co-workers reported that neutral $NH(SePPh_2)_2$ exists as a dimer after crystallization.[77] The H...Se distance observed in $NH(SePPh_2)_2$ dimer is 2.52 Å which is

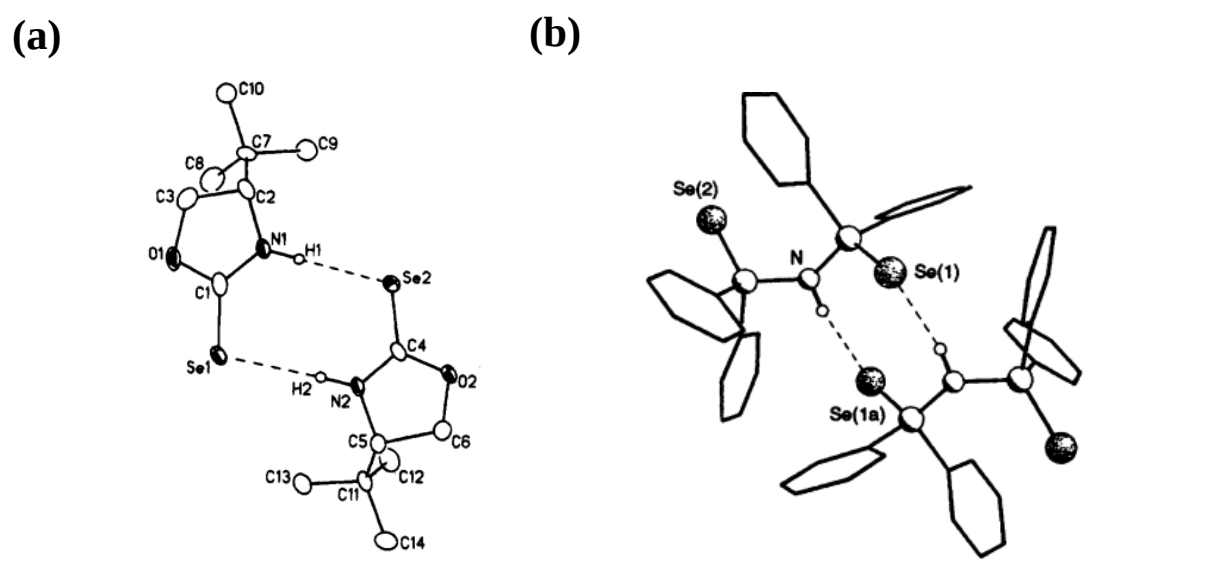

Figure 1.2: Intermolecular N-H...Se interaction in (a) selone (b) $NH(SePPh_2)_2$dimer. Figure (a) adapted in part with permission from reference 76. Copyright (1994) Americal Chemical Society. Figure (b) adapted in part with permission from reference 77. Copyright (1995) Royal Society of Chemistry.

less than the sum of the van der waals radii of H (1.20 Å) and Se (1.90 Å). Interestingly, the observed ∠N-H...Se of 166^0 is in the acceptable range of the hydrogen-bond angle for conventional hydrogen bonding. It has been observed that there is a difference in the bond length between P=Se(1) and P=Se(2) [Figure 1.2]. The bond length of P=Se(1) is longer than

that of P=Se(2) due to the presence of hydrogen bonding interaction in the former one. Iwaoka and Tomoda reported the observation of intramolecular C-H...Se hydrogen bonding in diselenocin from X-ray crystallography and FT-IR spectroscopy.[78] They observed the chair form of diselenocin having H...Se distance of 2.92 Å (Se1...H_a as well as Se1'...H_a) by single crystal X-ray diffraction analysis.

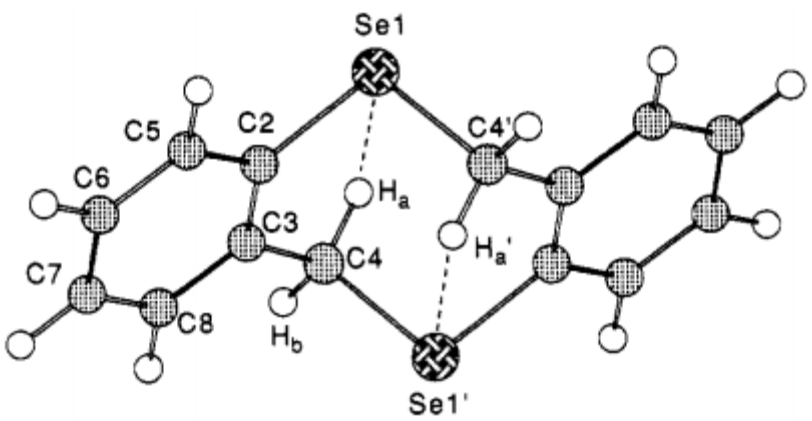

Figure 1.3: Chair form of diselenocin determined by X-ray analysis. Location of H atoms was determined by *ab initio* MO calculations. Adapted in part with permission from ref. 78 Copyright (1994) Americal Chemical Society.

The IR spectrum of the diselenocin exhibited the C-H…Se bound benzylic C-H stretching frequency at 2800 cm^{-1}, which is 53 cm^{-1} red-shifted compared to the free C-H stretching frequency (2853 cm^{-1}) of the normal methylene groups present in the compound. This observation of the significant red-shift complemented with the shorter H...Se distance gave evidence for the presence of C-H...Se hydrogen bond in diselenocin.

1.5 Spectroscopic study of hydrogen bond

Spectroscopy has played a significant role in the detection of the hydrogen bond. IR spectroscopy is one of the most potent tools to characterize the hydrogen bond. Badger and Bauer have shown that the X-H stretching frequency in the IR spectrum gets red-shifted, i.e., gets shifted towards lower wavenumber after the hydrogen bond formation.[79,80] The IR red shift in the X-H stretching frequency of the X-H…Y system is a characteristic feature for the

hydrogen bond. More significant will be the red-shift, stronger will be the hydrogen bond. This red shift in the X-H stretching frequency occurs with an increase in the intensity as well as FWHM of the IR band.

It has also been observed that the X-H stretching frequency is not always red-shifted due to hydrogen bond formation. There could be hydrogen bonded systems where X-H stretching frequency is blue-shifted with respect to that in the corresponding monomer. The blue-shift in the X-H stretching frequency was observed for the first time in the IR spectrum of triformylmethane in chloroform.[81] Buděšínský and co-workers observed the C-H stretching frequency of chloroform in triformylmethane at 3028 cm^{-1}, which was 7 cm^{-1} blue shifted than the typical C-H stretching frequency of chloroform (3021 cm^{-1}). Blue-shift in the X-H stretching frequency was observed in the gas phase by Hobza and co-workers in the complex of chloroform with fluorobenzene.[29,82] They observed 12 cm^{-1} blue shift in the C-H stretching frequency of chloroform.

Nuclear magnetic resonance (NMR) has also been proved to be an excellent spectroscopic tool for the study of the hydrogen bond. In the ^{1}H NMR of a hydrogen-bonded complex, the proton magnetic resonance of X-H shows downfield shift due to the hydrogen bond formation compared to that of the free X-H. This happens due to strong deshielding of the hydrogen-bonded proton which is a consequence of the electronic redistribution around the hydrogen-bonded proton.

Apart from the IR and NMR spectroscopy, microwave spectroscopy is also a powerful tool in extracting structural information of isolated hydrogen-bonded complexes. The strength of hydrogen-bonded complexes has been studied in isolated condition using various techniques like Stark-modulation microwave spectroscopy, molecular beam electric resonance spectroscopy and pulsed nozzle Furrier-transform microwave spectroscopy by applying microwave radiations.[83]

Mass-selected IR-UV double resonance spectroscopy has been used extensively in the determination of the strength of the hydrogen bond of molecules and complexes in the isolated gas phase. Suhm and co-workers have used jet-FTIR and jet-Raman Spectroscopy to characterize the hydrogen bonds in several molecular complexes.[84] Apart from all these spectroscopic techniques, terahertz spectroscopy and vibrational circular dichroism spectroscopy also provide a piece of useful information regarding the strength of the hydrogen bond in molecular complexes.

1.6 Hydrogen bond involving unconventional donor and acceptor atoms

It is well known that highly electronegative atoms like N, O, and F as hydrogen bond donors and acceptors readily form strong hydrogen bonds. Hydrogen bonds formed by these atoms are mainly electrostatic and have energy ranging from 20-40 kJ/mol. However, scientists were aware of the fact that hydrogen bond can involve other atoms apart from N, O and F. Pimentel and McClellen in their famous book 'The Hydrogen Bond' mention that halogen activated C-H, acetylenic C-H and S-H form hydrogen bonds.[9] Kumler was the first to report C-H...N hydrogen bond in HCN molecule. He suggested that HCN molecules are associated with each other via hydrogen bonds as H-CN...H-CN...H-CN arrangement.[85] Pauling reported that acetyl chloride has a higher boiling point than trifluoroacetyl chloride due to hydrogen bonding in the former one.[45] Shallcross and Carpenter reported C-H...N hydrogen bonding in the crystal structure of cyanoacetylene.[86] Dougill and Jeffrey anticipated C-H...O hydrogen bonding in the crystal structure of dimethyl oxalate.[87] Sutor reported C-H...O hydrogen bond in crystalline theophylline, caffeine, uracil and some other compounds containing C (sp^2)-H groups.[70] Later, Taylor and Kennard concluded that C-H...O interactions exist in crystals and these interactions are electrostatic. Desiraju and co-workers have reported C-H...O and C-H...F hydrogen bonds in several crystal structures.[88-92]

Hydrogen bond donor can interact with electrons of the π-bonding orbital assuming that it is

sterically favorable and this type of interaction is called π-hydrogen bond. The examples of π-acceptors are benzene, phenyl ring and multiple bonds like ethylene bond and acetylene bond. Wulf and co-workers first reported first intramolecular O-H...π hydrogen bonding ortho-substituted phenols in CCl_4 solution.[93] They observed a red-shift of 45 cm^{-1} in the O-H stretching frequency of o-phenylphenol. Yoshida and Osawa reported intermolecular O-H...π hydrogen bonding in the solution of phenol and benzene dissolved in CCl_4.[94] They observed a red-shift of 49 cm^{-1} in the O-H stretching frequency of phenol. McPhail and Sim reported O-H…π hydrogen bond in the cyclic peptide.[95] Davies and Staveley reported N-H…π hydrogen bond in ammonium tetraphenylborate.[96]

Benzene is the most common among all π-acceptors. There are many reports where benzene or substituted benzene forms complex with H_2O, HF, HCl, and other hydrogen bond donors.[30,97-101] Kollman and Allen reported in 1972 that hydrogen bond donor could be any atom which has electronegativity larger than hydrogen, i.e., C, N, O, F, P, S, Cl, Se, Br and I and hydrogen bond acceptor could be any of these elements and molecules which have π electrons.[102] Biswal and co-workers have studied S and Se centered hydrogen bonds in the gas phase.[103,104] Phosphorous (P)-centered hydrogen bond has been reported recently by Kjaergaard and co-workers using FTIR spectroscopy.[105] However, the list of hydrogen bond acceptors has gone beyond the atoms mentioned by Kollman and Allen. Brammer and co-workers reported that transition metal Cobalt (Co) can also act as hydrogen bond acceptor.[106] They synthesized and characterized salts having $[Co(CO)_4]^-$ with substituted ammonium cations. The neutron diffraction study of $[HNEt_3]^+[Co(CO)_4]^-$ salt showed N-H bond length slightly elongated, and a linear Co...H-N arrangement was observed. The energy decomposition for $[Co(CO)_4]^-$ and $[NMPH]^+$ where NMP is N-methylpiperazine shows that electrostatic interaction contributes more in the stabilization of the complex followed by orbital interaction. Brammer *et al.* reported N-H...Pt interaction in $[NPr^n_4]_2[PtCl_4]$·*cis*-

$[PtCl_2(NH_2Me)_2]$ salt.[107] Braga and co-workers reported that X-H…M (M= transition metal) hydrogen bonding interaction is common when the donors (X) such as C, N, and O can approach to the nucleophilic metal center.[108]

There are reports in the literature where transition metals (M) act as hydrogen bond donors. Pearson reported that M-H bond is highly polarizable. Braga et al. reported M-H…O interactions in organometallic crystals obtained from Cambridge Structure Database (CSD).[109] Very recently, Biswal and co-workers reported from the theoretical calculations that M-H…S and M-H…Se hydrogen-bonded complexes (M= Fe, Co, and Ni) show significant red-shift in the M-H stretching frequency.[110]

1.7 Aim of the thesis

As it has been mentioned in previous sections that conventional hydrogen bond is denoted by X-H...Y where both X and Y are electronegative atoms. However, the recent definition of the hydrogen bonding by the IUPAC committee goes beyond the conventional wisdom on this non-covalent interaction.[111] Consequently, there has been a growing search for finding the presence of this ever interesting non-bonded interaction considering different atoms in the periodic table as hydrogen bond donor (X-H) and acceptor (Y). Undoubtedly, it is required to have a quantitative understanding of these unconventional hydrogen bonding interactions in terms of their strength and physical nature.

Biswal and co-workers have done extensive study on sulfur (S) centered hydrogen-bond interaction using sulfur as a hydrogen-bond acceptor. They have studied several binary complexes bound through sulfur-centered hydrogen bond in the isolated gas phase using fluorescence-dip infrared (FDIR) or resonant ion-dip infrared (RIDIR) spectroscopy techniques combined with quantum chemistry calculations. Interestingly, it has been found from their work that sulfur forms hydrogen bond of similar strength as compared to the conventional electronegative atoms oxygen (O) and nitrogen (N).[112-114] The result is quite

surprising as the electronegativity of sulfur is 2.58 while the same for oxygen and nitrogen is 3.44 and 3.04, respectively, according to the Pauling electronegativity scale. It is quite obvious that the contribution of the electrostatic interaction to the stability of the sulfur centered hydrogen-bonded complexes is relatively less than that of the conventional hydrogen-bonded complexes. Biswal and co-workers found that the dispersion interaction dominates over all other interactions in the stabilization of the sulfur-centered complexes and they called this non-covalent interaction as a dispersion-stabilized hydrogen bond.[103,113,115] Kjaergaard and co-workers have also reported from the IR red-shift values in the FTIR spectroscopy studies of oxygen and sulfur-centered hydrogen bonded complexes that N-H…O and N-H…S interactions are of similar strength.[116] They have further observed from their IR spectroscopy experiment that positively charged phosphorus (P) can also act as a strong hydrogen bond acceptor although electronegativity values of P (2.20) and H (2.19) are similar.[105]

Recently, Biswal and co-workers have investigated N-H...Se interaction in the isolated gas phase by studying the complexes 2-pyridone and N-phenylacetamide with dimethyl selenide.[104] They have reported that both S and Se forms hydrogen bond of similar strength as compared to O.Significant IR red-shift was observed in the X-H stretching frequency of both S and Se centered hydrogen bonds. It has been attributed to the higher polarizability, lesser electronegativity and lesser charges of S and Se compared to those of O. Patwari and co-workers[117] reported that electrostatic, induction, and charge transfer components of the interaction energy contribute to the IR red-shift in the stretching frequency of the hydrogen bond donor for several C-H...X (X=N, O) hydrogen-bonded complexes. Moreover, the dispersion interaction governs the overall binding energy of these complexes. Iwaoka *et al.*and Madzhidov *et al.* reported that orbital interaction could have a significant contribution to the appreciable strength of the Se hydrogen bond.[78,118] Thus the origin of the strength of

the sulfur and selenium hydrogen bonds in terms of notable IR red-shift in the X-H stretching frequency needs to be explored further in detail through isolated gas phase experiment as well as quantum chemistry calculations. In the present thesis, we have addressed the following points for better understanding of nature, binding motif and the strength of these unconventional hydrogen bonds of strength similar to conventional hydrogen bonds.

1. It has been found from the literature that the gas phase spectroscopic study of the Se-centered hydrogen bond is very limited compared to that of the S-centered hydrogen bond. We have studied both N-H...Se and O-H...Se hydrogen bonds using gas phase spectroscopy and quantum chemistry calculations. We have explored various energy decomposition analyses to determine the origin of the marked IR red-shift in the X-H stretch frequency of the S/Se hydrogen bond as the electrostatic interaction in these complexes is smaller compared to that in conventional hydrogen-bonded complexes.

2. It has been reported from extensive PDB analysis that selenium hydrogen bonding between selenomethionine and other amino acid residues is abundant in proteins and this interaction plays an important role in the stability of the protein structures.[104] However, water-mediated indirect selenium hydrogen bonding between two or more amino acid residues involving selenomethionine is not demonstrated in the literature. Generally, water molecules present in the core or interior of the proteins bind with two or more amino acid residues and contribute to the stability of the proteins.[119] We have found from the PDB analysis that the number of water-mediated Se hydrogen bonding interaction is three times more than that of the direct Se hydrogen bonding interaction present in proteins. We have studied a model complex, consisting of indole (represents tryptophan), water and dimethyl selenide (represents of selenomethionine), which mimics the structural motif of single water-mediated Se hydrogen bonding interaction present in proteins.

3. In the literature, there are reports of spectroscopic studies of unconventional hydrogen bonding involving either weak hydrogen bond donor (C-H) or weak hydrogen bond acceptor (S, Se or P). In this work, we have explored the nature and strength of hydrogen bond interaction (S-H…S or S-H…Se) when both hydrogen bond donor and acceptor atoms are unconventional or less electronegative.

Chapter 2

Experimental and Computational Methods

In this chapter, we will discuss experimental setup, experimental methods and various spectroscopic techniques along with computational details.

2.1 Experimental Methods

2.1.1 Supersonic jet expansion

We have used supersonic jet expansion technique[120-122] to study high resolution electronic and vibrational spectra of isolated molecules as well as weakly bound molecular complexes. This technique is the most essential part of the experiments reported in this thesis. Supersonic jet expansion technique involves expansion of gas molecules from a high-pressure region to a sufficiently low-pressure region through a small orifice. The diameter of the orifice plays a vital role in the formation of a supersonic beam. If the diameter (D) of the orifice is smaller than the mean free path (λ_0) of the gaseous atoms or molecules in the reservoir,i.e., $D << \lambda_0$, there will be insufficient collisions between atoms or molecules near the orifice during the expansion. This kind of flow is called effusive flow, which leads to the formation of an effusive beam. In an effusive beam, the velocity distribution of the expanding gas molecules follows Maxwell-Boltzmann velocity distribution.

The supersonic beam is formed when the expansion of gas takes place from a high-pressure region (~ 10^3torr) to a low-pressure region (~10^{-6}torr) through a small orifice (Figure 2.1). In this case, the diameter (D) of the orifice is much larger than the mean free path (λ_0) of gaseous molecules ($D >> \lambda_0$). As a result of it, gaseous molecules suffer enormous collisions at the orifice and downstream of the orifice during the expansion. The collision is maximum near the orifice, and it decreases with the increase in the distance (d) from the orifice. Due to these enormous collisions, the thermal energy associated with the molecules is converted into directed mass flow along the beam axis. Since most of the thermal energy associated with the molecules are converted into directed kinetic energy, there is rapid cooling of the gas

molecules to very low temperature. It is this reduction in translational temperature which leads to a significant narrowing of the velocity distribution accompanied by an overall increase in the velocity (u) of the molecules. The translational temperature is related to the speed of the sound (a) by the relation $(\gamma kT/m)^{1/2}$, where γ is the ratio of the heat capacity C_p/C_v, k is the Boltzmann constant and m is the mass of the molecule. Since the velocity of molecules increases and speed of sound decreases, Mach number (M) which is given as M=u/a increases. When M>1, the flow is termed as supersonic. To obtain a well-defined coherent supersonic beam, a small hyperbolic cone-shaped device with an aperture on its tip, which is called skimmer (Figure 2.1) is placed in front of the expanding supersonic beam.

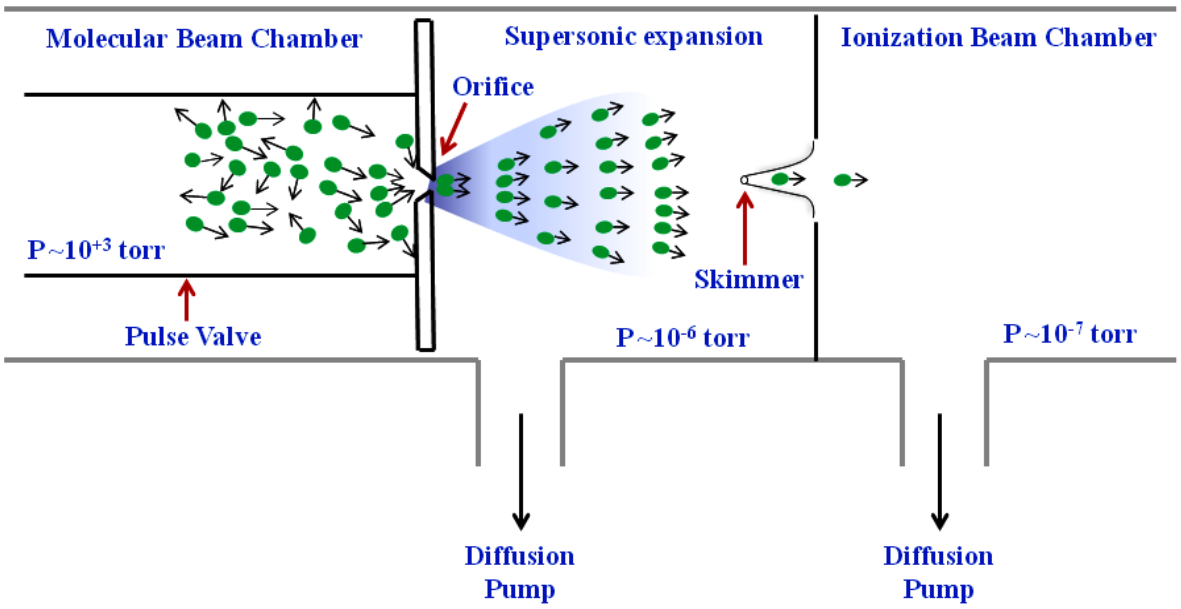

Figure 2.1: A schematic representation of supersonic expansion.

Figure 2.2 depicts the velocity distribution of gas molecules before and after the supersonic expansion. Figure 2.2a shows the velocity weighted Maxwell-Boltzmann distribution of gas molecules in the reservoir before the expansion. After supersonic expansion, velocity distribution narrows down as shown in Figure 2.2b, and peak maximum shifts towards higher velocity side. It is evident from the narrow velocity distribution curve that the translational

temperature of molecules decreases in the post-expansion region (Figure 2.2b). The translational temperature of the supersonic molecular beam reaches up to ~0.1 K. This low translational temperature acts as a bath for further cooling of rotational and vibrational degrees of freedom. The equilibrium between translational and rotational degrees of freedom is very fast, and hence the rotational cooling of molecules is quite efficient. The rotational temperature of molecules can go down to a few Kelvin. However, the rate of translational-vibrational equilibrium is generally slow, and hence vibrational cooling is not as effective as rotational cooling. The vibrational temperature of molecules can reach up to 20-50 K. The molecular density decreases downstream of the expansion, and hence rotational and vibrational cooling stops when the density becomes too low because of the absence of collisions.

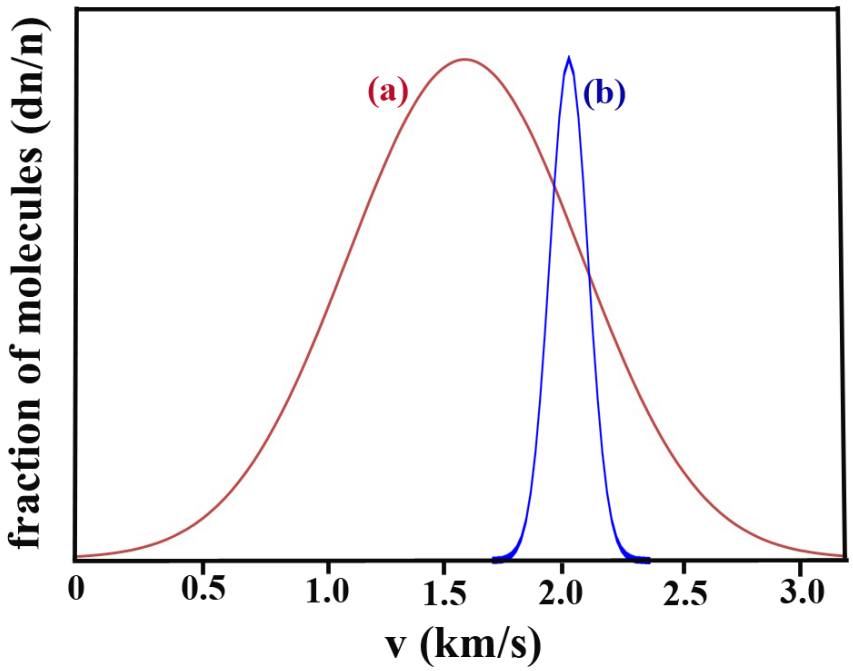

Figure 2.2: A schematic representation of velocity distributions in the (a) reservoir and (b) supersonic beam. Both curved are normalized to unity at the most probable velocity.

The process of supersonic expansion is isentropic under adiabatic reversible flow conditions. Considering the expanding gas as an ideal gas, the relationship between the temperature pressure, density and Mach number of the expanding gas is following[120,121]

$$\frac{T}{T_0} = \left(\frac{P}{P_0}\right)^{(\gamma-1)/\gamma} = \left(\frac{\rho}{\rho_0}\right)^{\gamma-1} = \frac{1}{1+\frac{1}{2}(\gamma-1)M^2} \quad \ldots\ldots\ldots\ldots (2.1)$$

Where, T_0, P_0, and ρ_0 are temperature, pressure, and density of the gas in the reservoir, respectively. T, P, and ρ are the same quantities of the gas molecules after supersonic expansion. γ ιs the ratio of heat capacity (C_p/C_v) and M is the Mach number (u/a). For a continuous gas, the Mach number can be given by the following relation[120]

$$M=A(X/D)^{\gamma-1} \quad \ldots\ldots\ldots\ldots(2.2)$$

Where X is the distance from the orifice and D is the orifice diameter. A is a constant that depends on γ, and its value is 3.26 for a monoatomic gas. From equations 2.1 and 2.2, it appears that the Mach number (M) increases while the temperature, pressure, and density of the molecular beam decrease as we go downstream of the orifice.

Anderson and Fenn showed that Mach number could not keep on increasing continuously. Equation 2.2 is derived for continuous gas flow, but in the actual case, the gas molecules are discrete particles. The density of the molecules decreases downstream of the orifice; hence the number of collisions between them are finite, and as a consequence, the Mach number (M) has a terminal value. The following equation gives the terminal Mach number (M_T),

$$M_T = 2.05\in^{-(1-\gamma)/\gamma} (\lambda_0/D)^{(1-\gamma)/\gamma} \quad \ldots\ldots.(2.3)$$

$$=133(P_0D)^{0.4} \text{ (for Argon)} \quad \ldots\ldots.(2.4)$$

where, $\in$ is the collisional effectiveness constant, D is the orifice diameter, λ_0 is the mean free path of the gas molecules in the reservoir, and γ is the ratio of heat capacity (C_p/C_v).

From equation 2.4, it is evident that terminal Mach number is directly proportional to gas pressure in the reservoir and orifice diameter. Since the probability per unit time for a molecule to make a binary collision is proportional to the pressure (P_0), the quantity P_0D is proportional to the total number of binary collisions. Hence, the terminal Mach number (M_T)

is directly proportional to the total number of binary collisions that an average molecule make.

2.1.2. Resonantly enhanced multiphoton ionization (REMPI) coupled with Time of Flight (TOF) mass spectrometry

2.1.2.1. REMPI

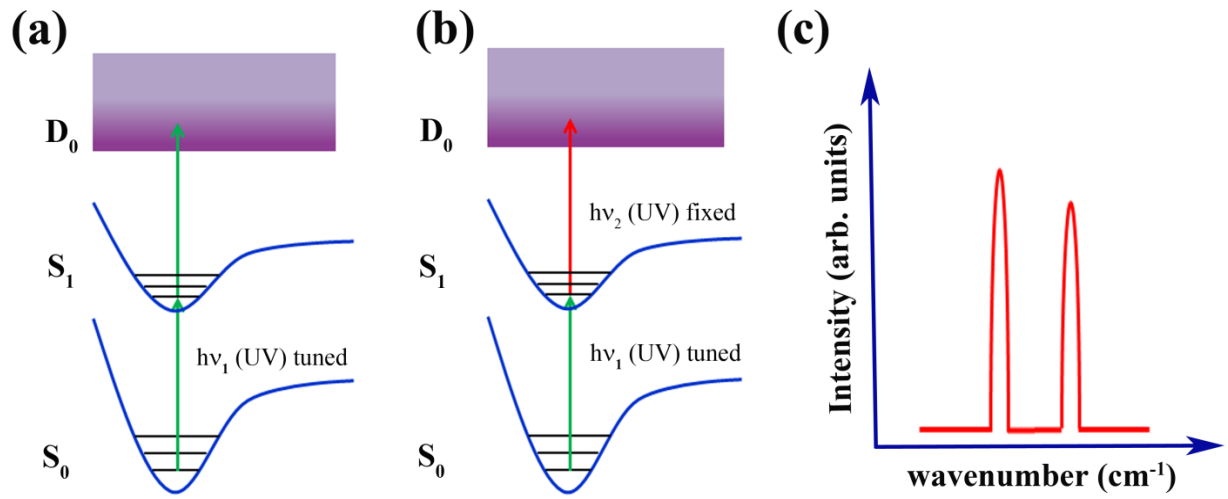

Figure 2.3: A schematic diagram of (a) 1C-R2PI and (b) 2C-R2PI techniques, (c) R2PI spectrum.

Resonantly Enhanced Multi-Photon Ionization (REMPI) method is an efficient technique to ionize the molecules and study their electronic spectra. Figure 2.3 shows a schematic representation of the REMPI method. In the schematic representation, S_0, S_1, and D_0 stand for the ground electronic state, first excited electronic state and ground ionic state, respectively. When one photon of a specific wavelength is used for electronic excitation of the molecules and consecutively another photon of the same wavelength from the same laser is used for ionization of the molecules, the technique is called 1C-R2PI (1-color resonant 2-photon ionization)or (1+1) REMPI (shown in Figure 2.3a). In 1C-R2PI, the total energy of the two photons is higher than the ionization potential of the molecules.

Sometimes, 1C-R2PI method is not suitable to ionize the molecules. If the ionization energy

of the molecules is more than the sum of the two photons of a laser used for $S_1 \leftarrow S_0$ electronic excitation, the second photon of a different wavelength from another laser is employed to ionize the molecules. This technique is called 2C-R2PI (2-color resonant 2-photon ionization) or (1+1') REMPI technique. In this technique, one photon from the first laser excites the molecules, and another photon of shorter wavelength from another laser is used to ionize the molecules.

2C-R2PI or (1+1') REMPI technique is also used to prevent fragmentation of the molecules or weakly bound clusters in the D_0 state. If the ionized molecules produced by the 1C-R2PI technique has large excess of energy, the fragmentation of the ions can take place. To prevent the fragmentation, the second photon of longer wavelength is used to ionize the molecules. Figure 2.3c shows a typical high-resolution electronic spectrum of a molecule or weakly bound complex measured by the R2PI technique.

2.1.2.2. Time of Flight mass spectrometry

The ions produced in the 1C-R2PI or 2C-R2PI techniques can be detected via Time-Of-Flight mass spectrometry (TOF-MS). In the mass spectrometry, ions are separated according to their masses and hence their time of flight. In the TOF-MS, the ions are accelerated by a uniform electric field to the same kinetic energy. Therefore the ions of different mass to charge ratio have different velocity, and thus they reach the detector at different time. If only singly charged ions are present, the lighter ion reaches the detector faster than the heavier ions and hence, the time of flight of the lighter ion is less than that of, the heavier ions.

The TOF-MS has been built according to Wiley-McLaren configuration[123] in which the ions are accelerated into two regions of different electric field strength. The TOF-MS employs three electrode design for improved mass resolution of molecules and clusters. Figure 2.4 shows a schematic diagram of a TOF-MS. It is comprised of three electrode plates, a field-free TOF tube, a ground plate, and the MCP detector. The three plates are called repeller

plate, extraction grid, and ground plate. The repeller plate has a higher positive voltage than the extraction grid.

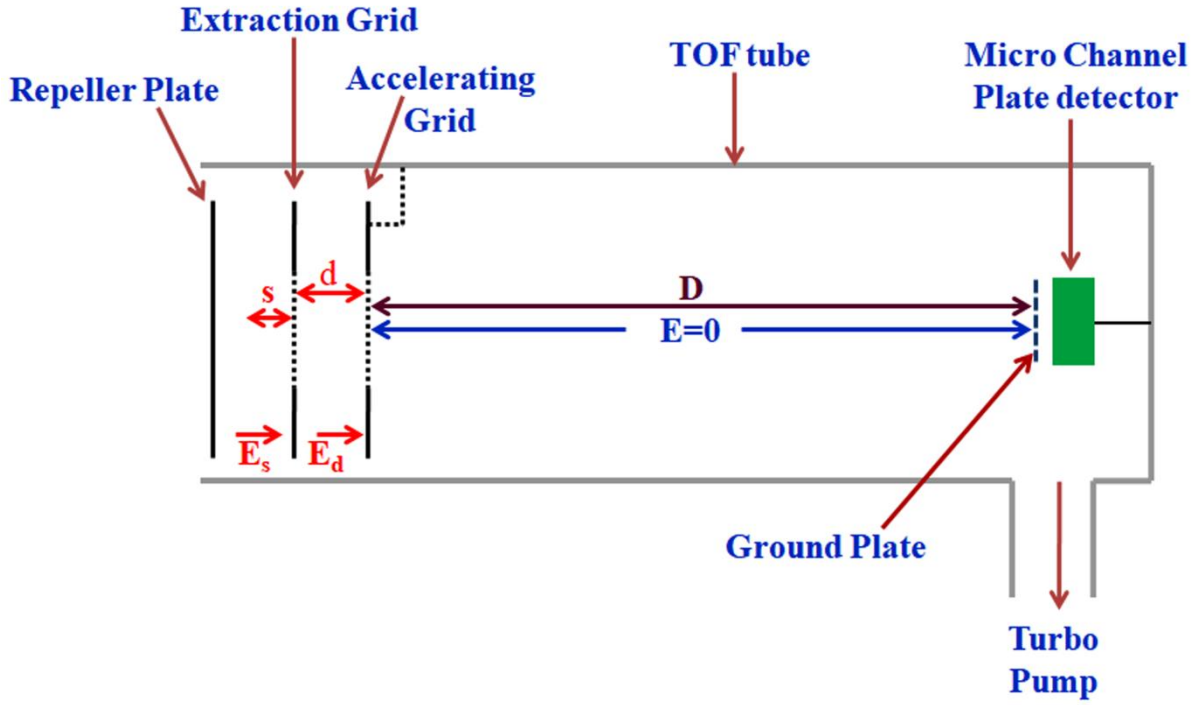

Figure 2.4: A schematic diagram of a Time of Flight-Mass Spectrometer (TOF-MS).

The ions are mostly formed at the halfway between the repeller plate and extraction grid by using a laser beam of diameter about 2-3 mm. The distance from the ionization position to the extraction grid is denoted by s. The ions generated through 1C-R2PI or 2C-R2PI technique experience an electric field E_s between the repeller plate and extraction grid and afterward move towards the extraction grid. The region between the repeller plate and extraction grid is called the ionization region. After passing through the extraction grid, the ions experience an electric field E_d between the extraction grid and ground plate which are separated by distance d. As $E_d > E_s$, the ions get highly accelerated. The region between the extraction grid and the ground plate is called the acceleration region. It is this acceleration which helps them to move in TOF tube of length D where no electric field (E=0) is present.

If the ion has initial energy U_0 at the time of its formation and it increases to U after

experiencing the electric fields $E_s$and E_d then

$U = U_0 + qsE_s + qdE_d$, ……(2.5)

The total time of flight T taken by an ion of mass m and charge q is given by

$T= T_s + T_d + T_D$, ……(2.6)

Where, T_s is the time taken by ion source to travel the ionization region, T_d is the time taken by ion source to travel the acceleration region and T_D is the time taken by ion source to travel field free drift tube.

$T_s = 1.02\frac{(2m)^{1/2}}{qE_d}[(U_0+qsE_s)^{1/2} \pm (U_0)^{1/2}]$ ……(2.7)

Here, + and – signs correspond to initial velocities directed away from and towards the detector respectively.

$T_d = 1.02\frac{(2m)^{1/2}}{qE_d}[U^{1/2}-(U_0+qsE_s)^{1/2}]$ ……..(2.8)

$T_D = 1.02(2m)^{\frac{1}{2}}(\frac{D}{2U})^{\frac{1}{2}}$ ... ... (2.9)

In our experimental setup, the TOF mass spectrometer, pulsed molecular beam axis, and pulsed laser beam axis are mutually perpendicular to each other. The skimmed molecular beam is ionized by a laser pulse inserted between the repeller plate and extraction grid which are 1 cm apart from each other. The ions move towards the extraction grid due to the potential difference between the repeller plate (e.g., V=3060 volts) and extraction grid (e.g., V=2800 volts). The ions are further accelerated between the extraction grid and the ground plate (V= 0 volts). After passing through the ground grid, ions travel into a field free (E=0) TOF tube of 1 m length. These ions are detected by an 18 mm microchannel plate detector (V= -3000V) placed at the end of the TOF tube.

2.1.3 Tunable laser systems used for experiments

2.1.3.1 Dye laser

An active medium in a dye laser is generally organic dyes i.e., rhodamine, fluorescein, coumarin, LDS, etc. dissolved in a suitable solvent (e.g., methanol). The dye molecules should have strong absorption/fluorescence at the excitation wavelength, excellent photochemical stability and minimum intersystem crossing for the productive performance of the laser.[124-126]

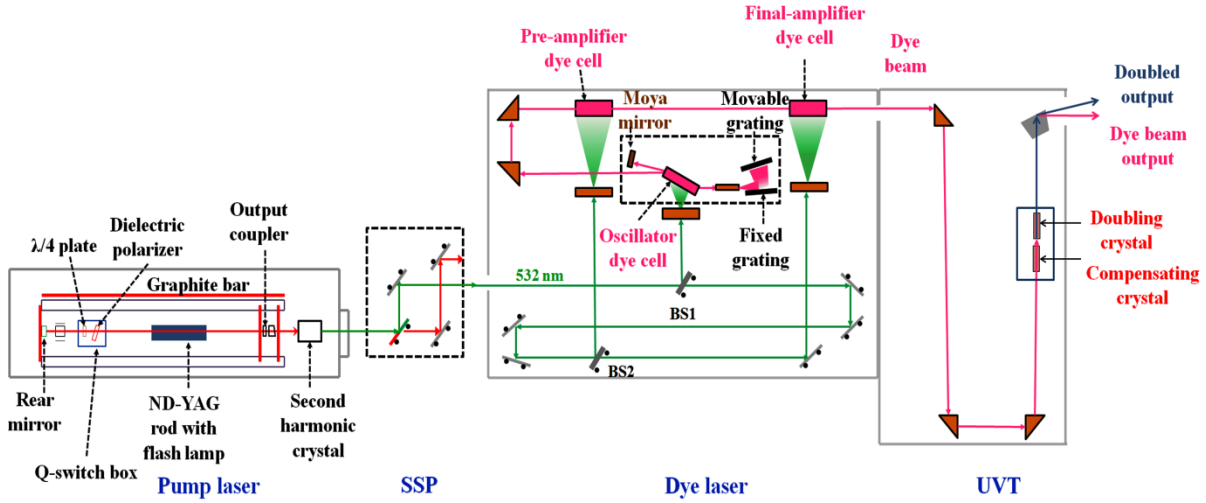

Figure 2.5: A schematic diagram of a dye laser.

The dye laser used for our experiments is pumped by second harmonic output (532 nm) of an ND: YAG laser (Continuum, Surelite II-10, 10 Hz, 10 ns) having pulse energy of ~ 250 mJ. The dye laser consists of one oscillator cell and two amplifiers cells called pre-amplifier and final amplifier cell. The vertically polarized 532 nm pump beam, after reaching to a beam splitter (BS1) gets split into two parts. 5% of the input 532 nm pump beam is reflected into the oscillator cavity whereas the remaining portion of the 532 nm pump beam gets transmitted through beam splitter BS1. The transmitted portion of the 532 nm pump beam, after reflection from various mirrors, reaches to another beam splitter BS2. The BS2 diverts 10% of the input pump energy into the first amplifier. The remaining energy is transmitted to

the final amplifier. The oscillator cavity consists of a grating, beam expander, cavity mirror, focusing lens, and dye cell. The light reflected from BS1 falls on dye cell after passing through the focusing lens. Dye cell contains dye molecules dissolved in a suitable solvent. The pump light excites the dye molecules. When these dye molecules return to their ground state; they emit light via fluorescence. This fluorescent light from the oscillator dye cell passes through the beam expander before falling on the grating (2400 lines/mm). The grating helps in proper wavelength selection from the whole output range of dye. The output from the oscillator cavity is amplified using the preamplifier and final amplifier. The final amplified beam then enters into UV Tracker (UVT) where it gets frequency doubled and generates UV beam after passing through KD*P crystal.

2.1.3.2 IR Optical Parametric Oscillator (OPO)/ Optical Parametric Amplifier (OPA) System

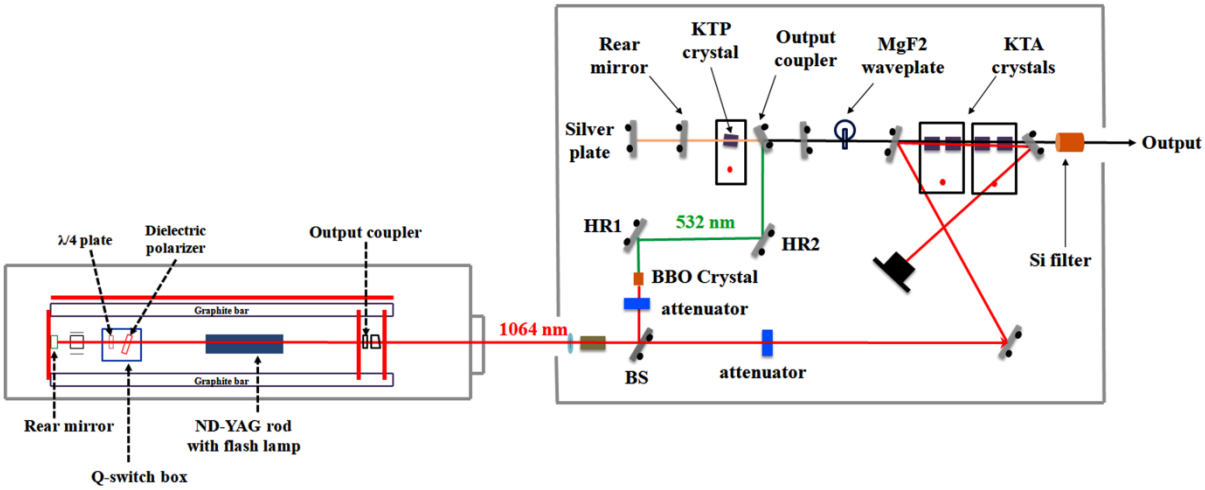

Figure 2.6: A schematic diagram of an IR laser.

The infrared laser (LaserVision) produces IR radiation in the mid-IR region (1.35μ–5μ). The IR laser is pumped by 1064 nm output of NdYAG laser (Surelite II-10, 10 ns, 10 Hz) having pulse energy ~530 mJ. Generation of IR radiation employs nonlinear KTP crystal at the OPO

stage and four nonlinear KTA crystals at the OPA stage. A schematic diagram of the IR stage is shown in Figure 2.7.

The horizontally polarized 1064 nm pump beam, after focussing from the telescope falls on the beamsplitter (BS) which divides the pump beam into two parts. One part is directed towards the OPO where after passing through the BBO crystal, it gets frequency doubled. At the OPO stage, this 532 nm beam passes through KTP crystal after reflection from mirrors HR1 and HR2. KTP crystal generates two new photons, idler (ω_i) and signal (ω_s) via optical parametric oscillation process. The sum of idler and signal frequencies is equal to the frequency of the pump beam. Both idler and signal pass through dove prism which improves the collimation of beams. A MgF_2 waveplate is placed before the OPA stage which changes the polarization of idler from vertical to horizontal and rejects signal. Thus the only idler reaches to OPA stage.

At OPA stage, there are four KTA crystals. The idler (ω_i) after passing through MgF_2waveplate, mixes with 1064 nm pump beam which was transmitted through a beam splitter (BS). The combined idler (ω_i) and 1064 nm beams then pass through four KTA crystals. The positions of the KTA crystals were optimized to maximize the output energy. After passing through KTA crystals, difference frequency mixing takes place, and a new idler (ω_I) is generated according to the relation $1/\lambda_i - 1/1064=1/\lambda_I$ where λ_I is the wavelength of idler photon after OPA stage. A new signal photon (ω_S) is also generated at this stage according to the relation $1/\lambda_S=1/1064-1/\lambda_I$ where λ_S is the wavelength of the signal photon after OPA stage. Both idler (ω_I) and signal (ω_S) are vertically and horizontally polarized respectively. Both idler (ω_I) and signal (ω_S) then pass through silicon polarizer which is used to separate both the beams. Idler beam is selected by the polarizer which is in the mid-IR region and is used for further experimental purposes.

2.1.4 Experimental set-up

The experimental setup shown in Figure 2.7 consists of a home-built jet-cooled REMPI-TOF mass spectrometer. The installation consists of two differentially pumped vacuum chamber (ionization chamber and molecular beam chamber) connected through a skimmer of 2 mm diameter. A commercial series 9 pulse valve having a 10 Hz repetition rate and 0.5 mm diameter operated by pulse driver (IOTA ONE, Parker Instrumentation) is incorporated into the molecular beam chamber. Molecular beam chamber is pumped by a 10-inch diffstack diffusion pump (OD 250, Hind Hivac) having pumping speed 3000 L/s. This diffusion pump is backed by a roughing pump (FD60, HindHivac) with a pumping speed of 17 L/s. The ionization chamber is pumped by a 4.5-inch diffstack diffusion pump (OD 114, Hind Hivac) having a pumping speed of 280 L/s. This small diffusion pump is backed by a roughing pump

Figure 2.7: Laboratory photograph showing home built jet cooled TOF-MS.

(ED-21, Hind Hivac) having a pumping speed of 6 L/s. The walls of both diffusion pumps are cooled by circulating water maintained at 18^0 C from a chiller (Refricon Hvac System). Both the vacuum chambers are separated from the diffusion pumps by the gate valves. Liquid

nitrogen traps are used between vacuum chambers and diffusion pumps which prevent the contamination of diffusion pump oil. Cold cathode ion gauges measure the pressure inside the vacuum chambers. The base pressure in the molecular chamber and ionization chamber is $8*10^{-8}$ torr and $1*10^{-7}$ torr, respectively.

The time of flight (TOF) tube is placed on the top of the ionization chamber in a direction perpendicular to the molecular beam axis. An 18 mm dual Micro Channel Plate (MCP) detector (Jordon TOF Products) is accommodated in a small vacuum chamber which is placed at the end of the TOF tube. The detector chamber is pumped by turbopump having pumping speed 70 L/s. The turbopump is backed by a dry scroll pump (SH-110, Varian) having pumping speed 1.5 L/s. A TOF power supply (Jordon TOF products) is used to provide negative voltage to the detector and positive voltage to repeller plate and extraction grid. The ion signal generated from the detector is amplified by a preamplifier (SRS, Model SR445A) and sent to a digital oscilloscope (Tektronix, 350 MHz, DPO 4034) interfaced to a PC via a USB port. The temporal synchronization between lasers was provided by the digital delay generator (BNC, Model 575).

2.1.5 Experimental Scheme

A schematic diagram of the experimental scheme is shown in Figure 2.8. Usually, the sample having low vapor pressure is kept inside a sample holder placed behind the pulse valve and this sample holder is heated between 50^0 C-100^0 C inside the vacuum to generate sufficient vapors. On the other hand, samples which have high vapor pressure are kept inside a steel container, and this container is cooled at a sufficiently low temperature outside the vacuum chamber to generate sufficient vapors for our experiment. The sample vapors seeded in the He/Ne or Argon carrier gas at 40-50 psig are expanded inside the vacuum through a pulsed nozzle. The pulse valve is operated at 10 Hz. The pulsed molecular beam, collimated with the skimmer interacts with the UV laser in the ionization chamber.

The ions are produced in the ionization chamber by REMPI technique. The ions are extracted and accelerated by applying typical voltages of +3060 V to repeller plate (VA1) and +2800 V to extraction grid (VA2). The ground plate is kept at ground potential. The ions of different masses get separated according to their different time of flight inside field free time of flight tube and are detected by MCP detector. The ion signal from the detector is further amplified by 125 times using a preamplifier and then sent to an oscilloscope which is interfaced to PC via USB port.

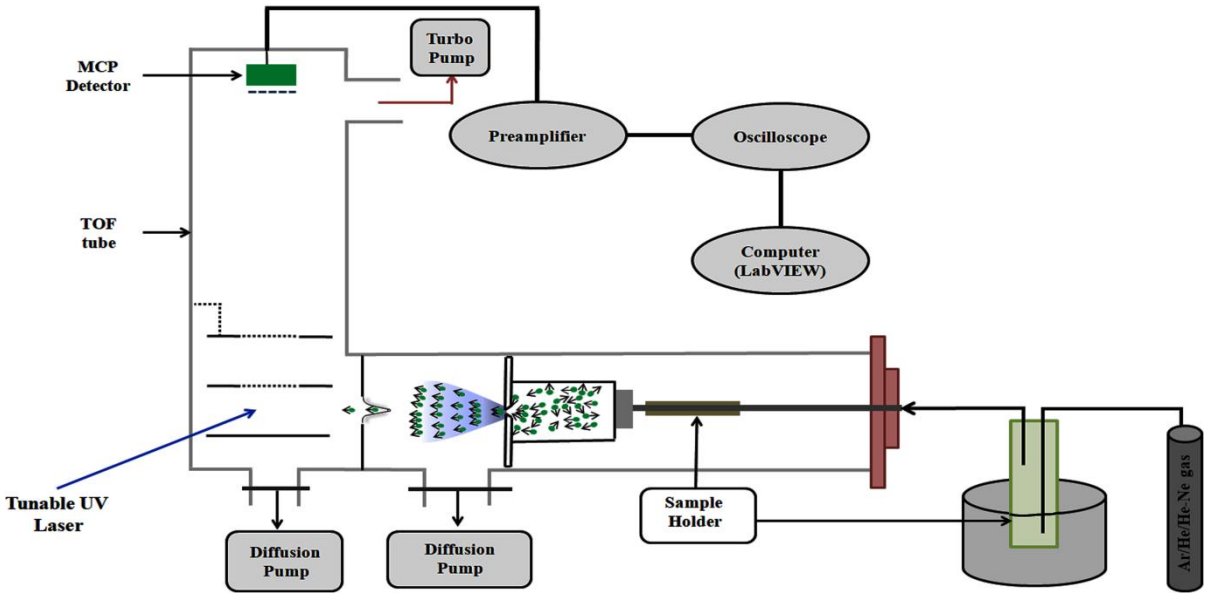

Figure 2.8: A schematic diagram of the experimental procedure.

A LabVIEW based program developed in the laboratory has been used to capture the data from the oscilloscope and to scan the laser wavelength. The time of flight of different ions is given by the relation $t_2=t_1*(m1/m2)^{1/2}$ where t_1 and m_1 are the time of flight and mass of a reference molecule, respectively while t_2 and m_2 are the time of flight and mass of an unknown molecule, respectively. This equation is based on the fact that ions of different masses have the same kinetic energy. The oscilloscope displays ions of different masses as a function of their time of flight. The time window of a particular mass is selected using a LabVIEW program, and the electronic spectrum was recorded using the same program.

2.1.6 Spectroscopic Techniques

We have used various spectroscopic techniques combined with quantum chemical calculations to determine the structures of molecular complexes formed in the supersonic jet.1C-R2PI[127] and 2C-R2PI spectroscopy have been used to record the mass selected electronic spectra of the complexes. IR-UV hole burn and UV-UV hole burn techniques were used to determine various isomers present in the electronic spectrum of the complex. IR spectra of the molecules and clusters were measured by Resonant ion dip infrared spectroscopy (RIDIRS) technique.

2.1.6.1 1C-R2PI spectroscopy

This technique has already been discussed in section 2.1.2.1

2.1.6.2 Resonant ion-dip infrared spectroscopy (RIDIRS)

The schematic diagram of RIDIRS is shown in Figure 2.9. This technique involves the use of UV and IR laser. Both UV and IR beams are spatially overlapped and are at the right angle to the molecular beam axis. IR laser beam has pulse energy 2-3 mJ whereas UV laser has pulse energy 0.2-0.3 mJ. IR laser is focussed by 100cm CaF_2 lens before entering inside the vacuum chamber.

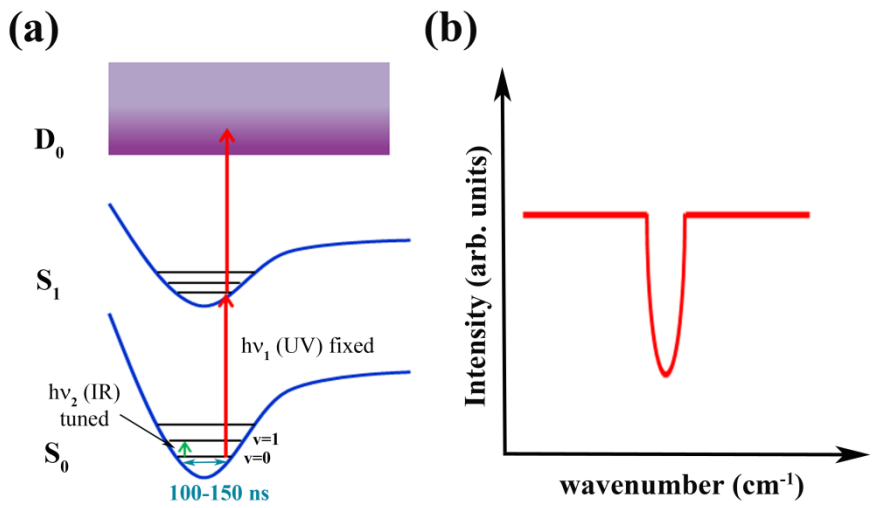

Figure 2.9: A schematic diagram of (a) RIDIRS and (b) IR spectrum

IR laser is fired 100-150 ns before UV laser. In this technique, the UV laser is fixed at a particular transition in the electronic spectrum, and IR laser is scanned. This technique measures the depletion in the ion signal due to UV laser in the presence of the IR laser. When IR frequency matches with any vibrational transition of the molecule or complex in the ground electronic state, molecules get vibrationally excited, and depletion in ion signal is observed.

2.1.6.3 IR-UV double resonance spectroscopy

IR-UV double resonance spectroscopy[128] is used to determine the number of conformers present in the electronic spectrum of molecule or complex. Figure 2.10 shows the schematic diagram of the IR-UV double resonance spectroscopy. This technique is also called IR-UV

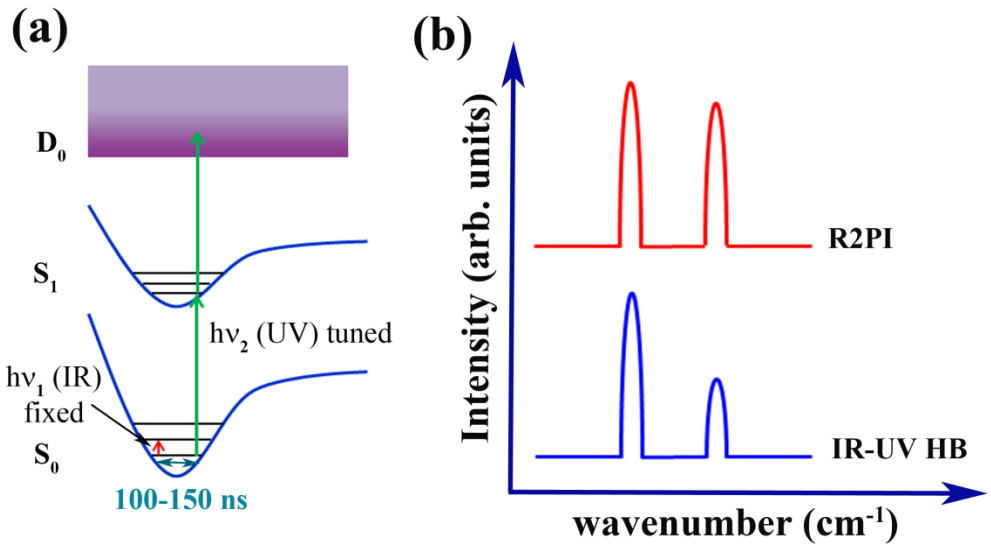

Figure 2.10: A schematic representation of (a) IR-UV hole burn spectroscopy and (b) IR-UV hole burn spectrum.

hole burn spectroscopy because IR laser burns the population from the ground vibrational state to vibrationally excited state. In this technique, IR laser is fixed at a particular vibrational frequency of the molecule or complex and UV laser is scanned throughout the whole electronic spectral region. The IR laser depletes the population of a particular conformer of the molecule or complex in the ground electronic state, and hence the intensity

of all the bands in the electronic spectrum belonging to that particular conformer gets reduced. The bands belonging to different conformer in the electronic spectrum remain unaffected. In this technique, IR laser is fired 100-150 ns prior to UV laser.

2.1.6.4 UV-UV double resonance spectroscopy

UV-UV double resonance spectroscopy is also used to determine the number of conformers present in the electronic spectrum of molecule or complex. Figure 2.10 shows the schematic

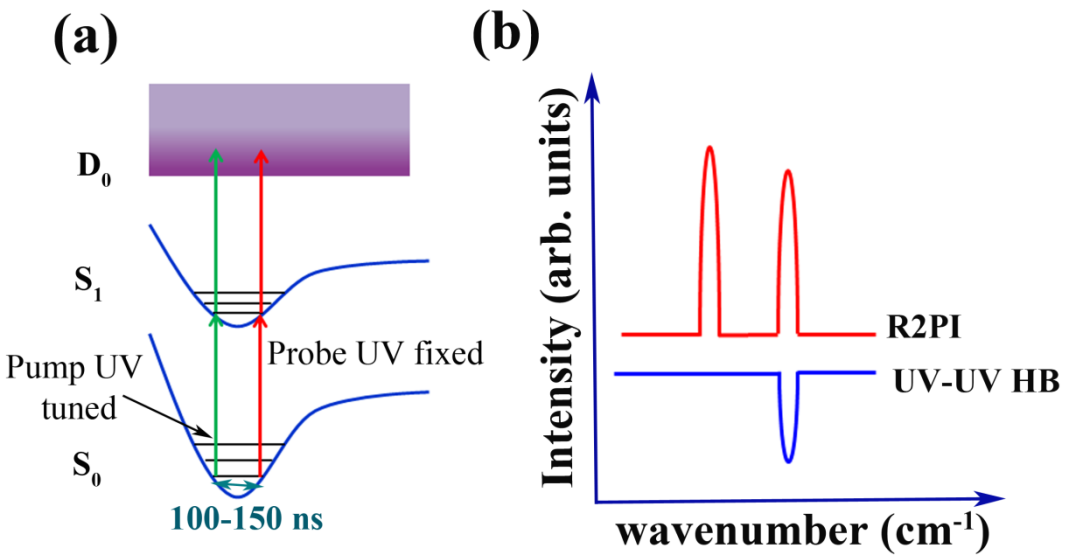

Figure 2.11: A schematic representation of (a) UV-UV hole burn spectroscopy and (b) UV-UV hole burn spectrum.

diagram of UV-UV double resonance spectroscopy. This technique is also called UV-UV hole burn spectroscopy. In this technique, probe UV laser having pulse energy 0.2-0.3 mJ is fixed at a particular transition in the electronic spectrum and pump UV laser having pulse energy 0.5-0.6 mJ is scanned throughout the whole electronic spectral region. The pump UV laser is fired 100 ns prior to the probe UV laser. If the signal due to pump laser and signal due to probe laser originate from the same ground state, depletion in the probe signal is observed whenever pump laser excites the molecule.

2.2 Computational Methods

To interpret our experimental data, we have performed detailed quantum chemical calculations. We have used Gaussian09, Gaussian16, QChem4.3, Psi4, NBO6.0 and GAMESS packages for quantum chemical calculations.

2.2.1 Geometry optimization and frequency calculation

We have used density functional theory (DFT) for ground state geometry optimization, and harmonic vibrational frequency calculations of molecules and weakly bound complexes studied in work. We have used dispersion-corrected DFT functionals, i.e., B97-D, ωB97X-D, M05-2X, M06-2X, etc. for most of our calculations.[129-133]We have employed both Pople type (i.e., 6-31+G(d), 6-311++G(d,p)), as well as Dunning's correlation consistent (i.e., aug-cc-pVDZ) basis, sets to perform geometry optimization as well as frequency calculation of the molecules and complexes. All the calculations are performed using "opt=tight" convergence criteria and "ultrafine" numerical integration grid to obtain reliable results. The binding energy (BE) of various isomers of the dimer, trimer and tetramer complexes is corrected for basis set superposition error (BSSE) and zero point energy (ZPE). BSSE correction has been done using the counterpoise method proposed by Boys and Bernardi.[134] All the geometry optimization, frequency calculation, and BSSE calculation was performed by Gaussian09 and Gaussian16 program packages.[135,136]

The structures of various isomers of complexes obtained in the experiment were determined by comparing their scaled theoretical vibrational frequencies with the experimentally observed frequency values. The scaling factor was determined by either taking the ratio of the experimental frequency with corresponding theoretical frequency or by the linear fit method. All the scaling factors are discussed in details in different chapters.

2.2.2 Binding energy calculation with BSSE and Zero Point Energy (ZPE) correction

The binding energy of a complex AB can be given as

$$\Delta E_{bind}(AB) = E_{AB}^{AB}(AB) - E_{A}^{A}(A) - E_{B}^{B}(B) \quad .....(2.10)$$

Where A and B are monomers infinitely separated from each other and AB is the complex molecule. $E_{AB}^{AB}(AB)$ represents the energy of the complex AB calculated on the geometry of the complex and in the dimer basis set which is the union of basis sets of monomers A and B. Similarly, $E_{A}^{A}(A)$ and $E_{B}^{B}(B)$ are the energy of monomers A and B calculated on their geometry and their own basis set.

During the complex formation, the monomers approach towards each other. Hence, each monomer uses the basis functions of other monomers to some extent which provides additional stabilization to the complex. The extra stabilization to the complex is termed as basis set superposition error (BSSE).

The BSSE corrected binding energy is calculated as

$$\Delta E_{bind}^{CP}(AB) = E_{AB}^{AB}(AB) - E_{A}^{AB}(A) - E_{B}^{AB}(B) \quad ..... \qquad (2.11)$$

Where $\Delta E_{bind}^{CP}(AB)$ is the counterpoise (CP) corrected binding energy of the complex, $E_{A}^{AB}(A)$ and $E_{B}^{AB}(B)$ are the energy of monomers calculated at dimer basis set.

2.2.3 Energy Decomposition Analysis (EDA)

We have used various EDA methods to decompose the binding energy of the complexes into different components. Localized Molecular Orbital- Energy Decomposition Analysis (LMO-EDA) method developed by Su and Li,[137] implemented in GAMESS[138] decomposes the total interaction energy (ΔE_{Total}) into electrostatic (ΔE_{ES}), exchange (ΔE_{EX}), polarization (ΔE_{POL}), repulsion (ΔE_{REP}) and dispersion (ΔE_{DISP})components.

$$\Delta E_{Total} = \Delta E_{ES} + \Delta E_{EX} + \Delta E_{POL} + \Delta E_{REP} + \Delta E_{DISP} \quad ..... \qquad (2.12)$$

Absolutely Localized Molecular Orbital-Energy Decomposition Analysis (ALMO-EDA)

method developed by Khaliullin *et al.*[139] and implemented in Q-Chem[140] decomposes the total interaction energy into frozen density, polarization and charge transfer components.

$$\Delta E_{Total} = \Delta E_{FRZ} + \Delta E_{POL} + \Delta E_{CT} \quad ..... \qquad (2.13)$$

The frozen density is defined as the energy change that corresponds to bringing two infinitely separated fragments into the complex geometry without any relaxation of the molecular orbitals (MO) of the fragments. The frozen density component in ALMO-EDA calculation consists of electrostatic (ΔE_{ES}), dispersion (ΔE_{DISP}) and repulsion (ΔE_{REP}) components.

$$\Delta E_{FRZ} = \Delta E_{ES} + \Delta E_{DISP} + \Delta E_{REP} \quad ..... \qquad (2.14)$$

Reduced Variational Space-Energy Decomposition Analysis (RVS-EDA)[141,142] method implemented in GAMESS decomposes the total interaction energy (ΔE_{Total}) into Coulomb/exchange (ΔE_{ESX}), polarization (ΔE_{POL}) and charge transfer (ΔE_{CT}) components.

$$\Delta E_{Total} = \Delta E_{ESX} + \Delta E_{POL} + \Delta E_{CT} \quad ..... \qquad (2.15)$$

Where the Coulomb/exchange (ΔE_{ESX}) term is the sum of electrostatic (ΔE_{ES}) and exchange (ΔE_{EX}) components.

$$\Delta E_{ESX} = \Delta E_{ES} + \Delta E_{EX} \quad ..... \qquad (2.16)$$

Symmetry-Adapted Perturbation Theory-Energy Decomposition Analysis (SAPT-EDA) is a perturbation-based energy decomposition analysis scheme.

2.2.4 Natural Bond Orbital (NBO) analysis

NBO6.0 program developed by Weinhold and co-workers[143,144] and implemented in Gaussian09 has been used to determine the strength of the hydrogen bond interaction present in the molecular complexes. The NBO6.0 program transforms the delocalized MOs into localized natural bond orbitals (NBOs). These NBOs are localized on one center, two centers or three centers. The mathematical algorithm of NBO suite converts the input atomic orbital

basis functions into natural atomic orbitals (NAOs). These NAOs give rise to natural hybrid orbitals (NHOs) through linear combination which in turn give rise to natural bond orbitals (NBOs) through linear combination. For a diatomic molecule AB, the linear combination of NHOs gives rise to two NBOs. One is bonding NBO (Lewis type), and another is antibonding NBO (non-Lewis type). The bonding NBO, also known as donor orbital is occupied with electrons and antibonding orbital, also known as acceptor orbital has less occupancy.

Hydrogen bonding involves delocalization of electrons from filled (donor) NBOs to antibonding (acceptor) NBOs. The strength of the hydrogen bonding interaction according to the NBO formalism is measured by second-order perturbation energy $\left(E^{(2)}_{i\rightarrow j^*}\right)$, Where i and j* are the lone pair orbital of hydrogen bond acceptor atom and X-H antibonding orbital, respectively. X is the hydrogen bond donor atom. It measures the extent of overlap between the donor (i) bonding NBO and acceptor (j*) antibonding NBO and hence the strength of the interaction. Due to the overlap between donor and acceptor orbitals, there is a donation of electron density from donor NBO to acceptor NBO. It is referred to as delocalization. For each donor NBO (i) and acceptor NBO (j*), the donor-acceptor stabilization energy $E^{(2)}$ associated with $i\rightarrow$ j* delocalization is given as

$$E^{(2)}_{i\rightarrow j^*} = q_i \frac{F(i,j)^2}{\varepsilon_j - \varepsilon_i} \quad \text{.....} \qquad (2.17)$$

Where q_i is the occupancy of donor orbital, F(i,j) is the off-diagonal NBO Fock matrix element. ε_i and ε_j are diagonal elements (orbital energies). Greater will be overlap between donor and acceptor orbitals; more will be the second-order perturbation energy value and hence stronger will be the hydrogen bond.

Chapter 3

The nature and strength of selenium hydrogen bonding interaction

3.1 Introduction

We have discussed in Chapter 1 that hydrogen bonding is the most important non-covalent interactions present in almost every sphere of life. Since the discovery of the concept of the hydrogen-bond, many scientists have contributed significantly to understand the strength and nature of this fascinating intermolecular interaction. Huggins[145,146], Pimmentel[147], McClellen, Pauling, Jeffrey are a few notable names along with others who have made a seminal contribution towards the more profound understanding of the physical nature of the hydrogen bond. Pauling introduced the idea that hydrogen bond must be electrostatic, but later it was found through NMR and Compton scattering experiments that it has some covalent character. However, it is still not straightforward to explain the origin of the strength of the hydrogen bonds having various types of unconventional hydrogen-bond donor or acceptor atoms.

After the recent re-definition of the hydrogen-bonding by the IUPAC committee, there has been a growing search for finding the presence of this ever interesting non-covalent interaction between a hydrogen atom in an X–H group and any other atom in the periodic table. One of the most suitable techniques to obtain a molecular-level understanding of any unexplored hydrogen-bonding interaction is isolated gas phase IR spectroscopy in combination with quantum chemistry calculations.

The most extensively studied unconventional hydrogen bonding interaction using a less electronegative atom as a hydrogen bond acceptor is sulfur-centered hydrogen bonding.[103,112,113] Oxygen (O), sulfur (S) and selenium (Se) belong to the same group of the periodic table. Interestingly, the electronegativity of S (2.58) and Se (2.55) is much less compared to that of O (3.44). At the same time, both S (180 pm) and Se (190 pm) are much larger in size than O (152 pm). Thus, the charge density of S and Se is much less compared to that of O. It will be interesting to have detailed quantitative understanding of both S and Se centered hydrogen bonding as both of these interactions involving the S and Se containing

amino acid residues contribute to the stability of proteins. However, gas phase spectroscopic study of Se hydrogen-bonding interaction is sparse in the literature except the one reported recently by Biswal and co-workers.[104] Surprisingly, it has been observed that S and Se form hydrogen bond of similar strength as compared to O. Both S and Se hydrogen bonds are described as dispersion stabilized hydrogen bonds as the contribution of the electrostatic interaction to the total stabilization energy of these hydrogen-bonds are relatively less compared to the conventional strong hydrogen bonds. However, a better understanding of the origin of the pronounced IR red-shift observed in the X-H stretching frequency of the S and Se hydrogen bonds demands further experimental and theoretical investigation of these intriguing non-covalent interactions.

In this work, the intrinsic nature of selenium hydrogen bonding has been investigated by studying gas phase electronic and IR spectroscopy as well as detailed quantum chemistry calculations of indole…dimethyl selenide (Ind…Me_2Se) and phenol…dimethyl selenide (Ph…Me_2Se) complexes. The results have been compared with the literature data of indole…dimethyl sulfide (Ind…Me_2S) and phenol…dimethyl sulfide (Ph…Me_2S) complexes.[113,115] For the sake of completeness of the comparison among O, S, and Se hydrogen bonding interactions, indole…dimethyl ether (Ind…Me_2O) and phenol…dimethyl ether (Ph…Me_2O) complexes are studied only computationally. Our results indicate that the S and Se centered hydrogen bonded complexes in comparison to the O centered hydrogen-bonded complexes are conformationally rich. We have found through various energy decomposition analysis (EDA) methods and natural bond orbital (NBO) calculations that the significant IR red-shift of the S and Se hydrogen bond cannot be explained only by electrostatic interaction rather charge transfer interaction plays a significant role for the strength of these types of hydrogen bonds.

3.2 Results and discussion

3.2.1 Time of Flight (TOF) Mass spectra of dimeric complexes

Figure 3.1a and 3.1b shows the mass spectra of Ind…Me_2Se and Ph…Me_2Se dimeric complexes, respectively, measured by fixing the excitation laser at 35066 cm^{-1} and 36349 cm^{-1}, respectively. Figure 3.1a shows several other peaks of higher masses compared to Ind…Me_2Se complex peak.

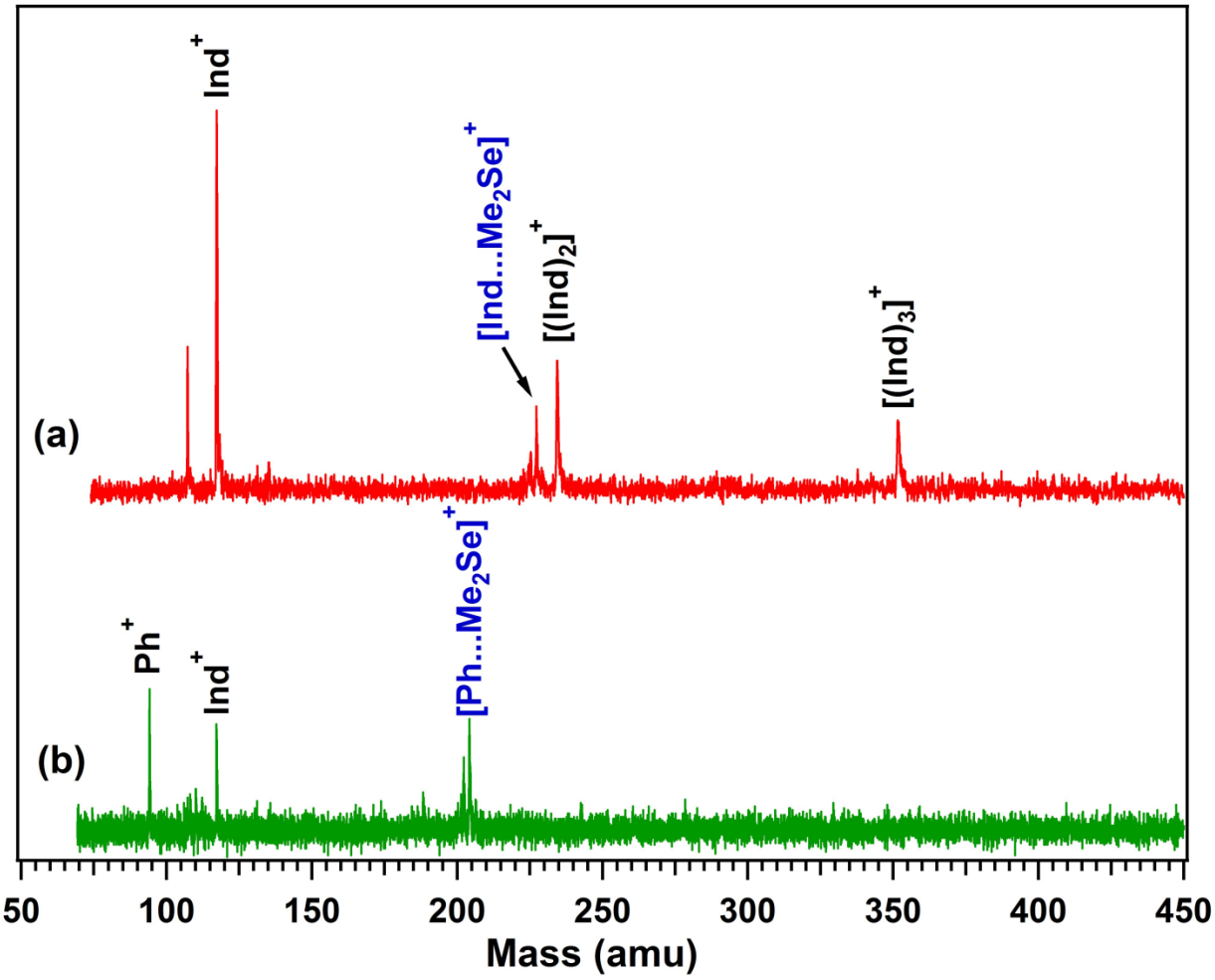

Figure 3.1: Time of flight mass spectra of (a) indole (Ind) in the presence of Me_2Se and (b) phenol (Ph) in the presence of Me_2Se by fixing the laser wavelength at 35066 cm^{-1} and 36349 cm^{-1}, respectively.

These peaks are due to higher clusters of indole monomer. Indole…dimethyl selenide (Ind…Me_2Se) and phenol…dimethyl selenide (Ph…Me_2Se) dimeric complexes were

synthesized in a supersonic expansion of mixed vapor of indole (heated at 75 °C) or phenol (heated at 40 °C) and dimethyl selenide (cooled at -78 °C) seeded in a 55 psig gas mixture of 70% Ne/30% He through a pulsed nozzle (0.5 mm dia, 10 Hz) into a high vacuum chamber.

3.2.2 Electronic spectra of the dimeric complexes

Figure 3.2b and 3.2e show the mass-selected electronic spectra of Ind…Me_2Se and Ph…Me_2Se dimeric complexes, respectively, measured by 2C-R2PI spectroscopy. Figure 3.2a and 3.2d show the mass-selected electronic spectra of the indole and phenol monomers. The origin bands of the indole and phenol monomers appear at 35240 cm^{-1} and 36349 cm^{-1} respectively which match very well with previously reported one.[148,149] The electronic spectra shown in Figure 3.2 are presented in a relative wavenumber scale with respect to the 0_0^0 band (origin transition) of the individual complex. The origin transition for Ind…Me_2Se (Figure 3.2b) appears at 35066 cm^{-1} while the same for Ph…Me_2Se (Figure 3.2e) is observed at 36039 cm^{-1}.

A few sharp bands are observed in the blue side of the 0_0^0 bands of both of the complexes. To determine whether all the electronic bands in the spectra (Figure 3.2b and 3.2e) originate due to a single conformer or multiple conformers of the complex, an IR-UV hole-burning experiment has been performed by probing the N-H/O-H stretching frequency corresponding to the origin band of the complexes. Figure 3.2c and 3.2f display IR-UV hole-burning spectra by probing the N-H stretching frequency (3371 cm^{-1}) of Ind…Me_2Se and O-H stretching frequency (3414 cm^{-1}) of Ph…Me_2Se, respectively. The IR-UV hole-burning spectra of both the complexes show depletion in the ion signal of all the electronic bands confirming the presence of only one conformer of these complexes in the experiment. Thus the low-frequency vibronic

bands observed in the electronic spectra (Figure 3.2b and 3.2e) are due to intermolecular vibrations of the dimeric complexes. The IR spectra of the complexes are presented in the next section.

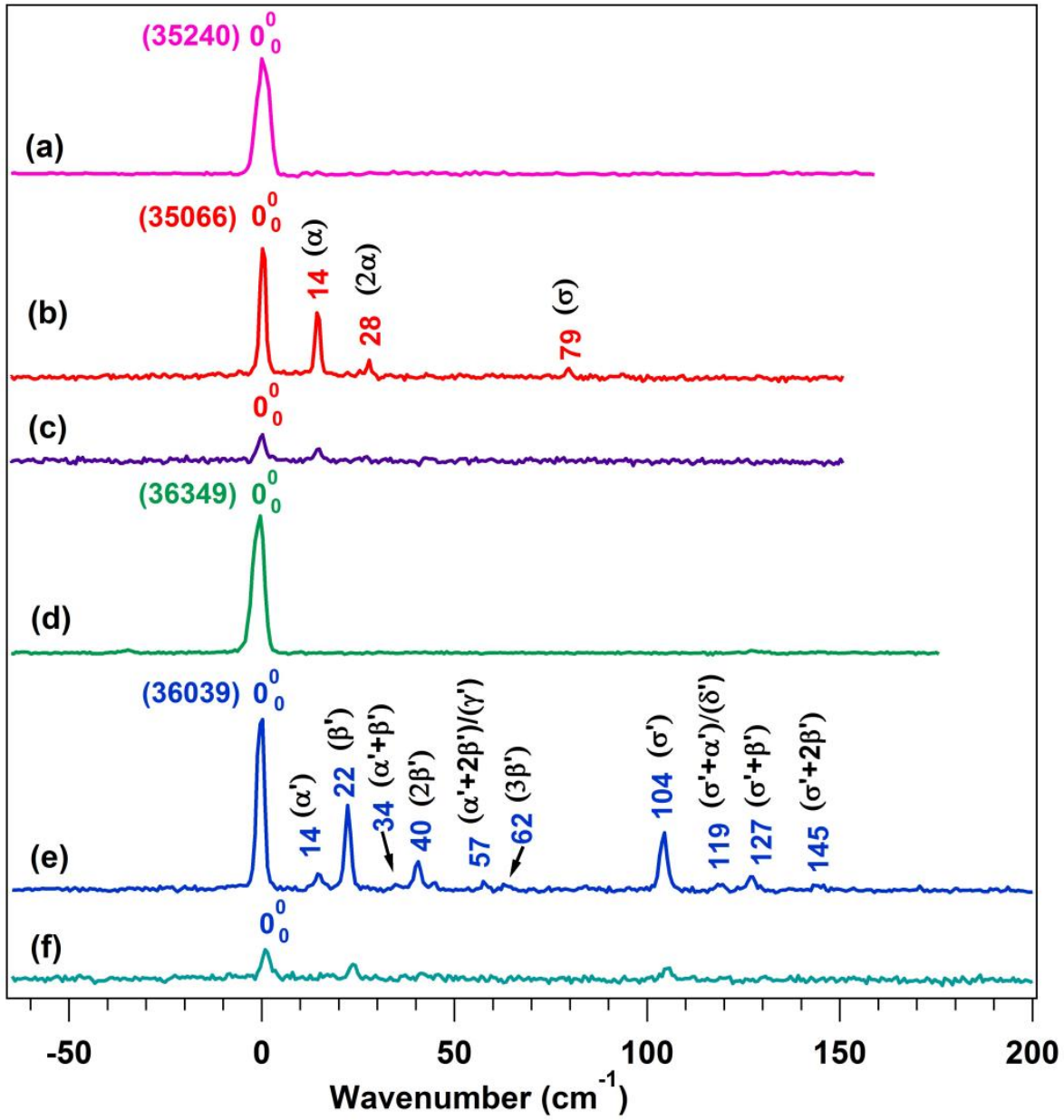

Figure 3.2: Electronic spectra of (a) indole monomer (b) Ind…Me_2Se complex (d) phenol monomer and (e) Ph…Me_2Se complex measured using 2C-R2PI spectroscopy. Parts (c) and (f) show IR-UV hole-burning spectra of Ind…Me_2Se and Ph…Me_2Se complexes. Tentative assignment of the bands in the electronic spectra of the complexes is done through their vibrational frequency calculation. The spectra of monomers and complexes have been presented in a relative wavenumber scale with respect to the individual 0_0^0 band.

Theoretically, there are 6 intermolecular modes in a dimer. However one might not see all the modes in the experiment. An S_1 state frequency calculation of Ind…Me_2Se complex at the TD-B3LYP/6-31G(d) level (Table 3.1) shows that the low-frequency vibronic bands in Figure 3.2b are due to an intermolecular hydrogen-bond (N-H…Se) stretching mode σ (79 cm^{-1}) and a progression of another 14 cm^{-1} mode denoted by α. Similarly, we have compared the low-frequency vibronic bands present in Figure 3.2e with the calculated intermolecular vibrational modes of the Ph…Me_2Se complex

Table 3.1 Observed and calculated low frequency intermolecular vibrational modes of Ind…Me_2Se and Ph…Me_2Se complexes. The S_1 state intermolecular vibrational modes for Ind…Me_2Se are calculated at the TD-B3LYP/6-31G(d) level of theory. The S_0 state low-frequency vibrational modes for Ph…Me_2Se are calculated at the B97-D/6-311++G(d,p) level of theory.

Ind…Me_2Se			Ph…Me_2Se		
Observed (cm^{-1})	Calculated (S_1) (cm^{-1})	Assignments	Observed (cm^{-1})	Calculated[a] (S_0) (cm^{-1})	Assignments
14	20	α	14	17	α'
28	-	2α	22	28	β'
	36		34		α' + β'
	48		40		2β'
	70		57	59	(α'+2β')/(γ')
79	85	σ	62		3β'
	110			72	
			104	86	σ'
			119	113	(σ'+ α')/(δ')
			127		σ'+ β'
			145		σ'+2β'

[a]Observed low-frequency vibronic bands of Ph…Me_2Se complex is compared with the vibrational frequency calculated at the S_0 state as the S_1 state calculation was not successful.

(Table 3.1). The band at 104 cm^{-1} is assigned to the intermolecular O-H…Se hydrogen bond stretch (σ') while the 14, 22, 57, and 119 cm^{-1} bands are four other intermolecular modes denoted as α', β', γ', and δ' respectively. The remaining vibronic

bands are due to overtones or combinations of bands of these modes only. Low-frequency intermolecular vibrations of Ph…Me_2Se could not be calculated at the S_1 state as there was a problem in optimizing the geometry of the complex due to the breaking of the Se-CH_3 bond. However, the low-frequency vibrations calculated at the S_0 level match pretty well with those observed in the experiment.

3.2.3 IR spectra of the complexes

The most important part of the present work is the determination of the structures of the observed conformers of Ind…Me_2Se and Ph…Me_2Se complexes as well as the nature of the selenium hydrogen bonding interaction by performing IR spectroscopy and quantum chemistry calculations. IR spectra of the indole monomer, Ind…Me_2Se complex, phenol monomer, and Ph…Me_2Se complex measured by RIDIR spectroscopy have been provided in Figure3.3a, b, c, and d, respectively. The free N-H stretching vibration (3525 cm^{-1}) of indole and the free O-H stretching vibration (3654 cm^{-1}) of phenol shown in Figure3.3a and c were reported earlier.[149,150] The N-H stretching frequency in Ind…Me_2Se is red-shifted by 154 cm^{-1} with respect to that in the indole monomer while the red-shift observed in the O-H stretching frequency in Ph…Me_2Se with respect to that in the phenol monomer is 240 cm^{-1}. The observed red-shifts in the N-H and O-H stretching frequencies in these two complexes prove the presence of selenium hydrogen bonding (N-H…Se and O-H…Se) interactions.

Stronger selenium hydrogen bonding in the case of O-H…Se compared to N-H…Se is quite evident as the O-H group is a better hydrogen bond donor in comparison to the N-H group. The results of the detailed calculations on various conformers of Ind…Me_2Se and Ph…Me_2Se complexes are discussed in the next section. However, the theoretical IR spectra of only the conformer of each of these two complexes which match well with the experimental IR spectra are provided in Figure 3.3.

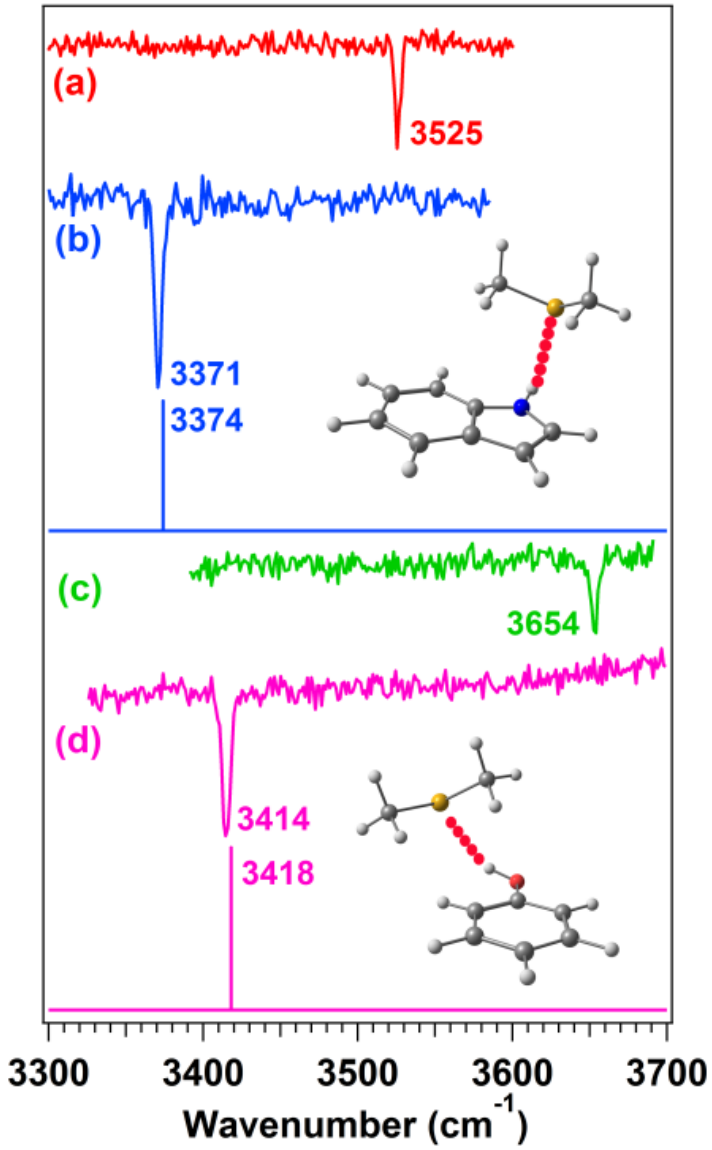

Figure 3.3: IR spectra of (a) indole, (b) Ind…Me_2Se complex, (c) phenol and (d) Ph…Me_2Se complex measured by probing the origin bands of indole (35240 cm^{-1}), Ind…Me_2Se complex (35066 cm^{-1}), phenol (36349 cm^{-1}) and Ph…Me_2Se complex (36039 cm^{-1}), respectively, using RIDIR spectroscopy. Theoretical IR spectra and structures of the Ind…Me_2Se(A) conformer of Ind…Me_2Se and Ph…Me_2Se(A) conformer of Ph…Me_2Se obtained at the B97-D/6-311++G(d,p) level of theory are provided with (b) and (d) , respectively.

The stick spectra presented with Figure 3.3b and d are theoretical IR spectra of Ind…Me_2Se(A) conformer of Ind…Me_2Se complex and Ph…Me_2Se(A) conformer of the Ph…Me_2Se complex, respectively, calculated at the B97-D/6-311++G(d,p)level of theory. The calculated harmonic frequencies reported here are scaled with respect to

the experimental N-H and O-H stretching frequencies of indole and phenol monomers, respectively. To determine the structures of the observed conformers of the complexes in the experiment, theoretical IR spectra of various conformers were compared with the experimental IR spectra of the complexes. As the vibrational frequencies were calculated according to harmonic approximation, the calculated frequencies (N-H and O-H) were corrected using a scaling factor. The scaling factor was obtained from the ratio of experimental N-H/O-H stretching frequency of monomer (indole/phenol) and calculated harmonic N-H/O-H stretching frequency of monomer (indole/phenol) obtained at a particular level of theory and basis set. The agreement between experimental and theoretical IR spectra of both experimental and theoretical IR spectra of both the complexes is excellent.

It could be mentioned here that Biswal and co-workers observed a red-shift of 91 and 262 cm^{-1} in the N-H stretching frequency of the N-H…Se hydrogen bonded complexes of N-phenylacetamide…Me_2Se and 2-pyridone…Me_2Se, respectively.[104] However, further detailed study of this unconventional hydrogen-bonding interaction is essential to obtain in-depth physical insight behind the large amount of red-shift observed in the IR stretching frequency for the Se or S centered-hydrogen bond.

3.2.4 Quantum chemistry calculations of the different structures of the complexes

Computational studies on Se, S, and O centered hydrogen-bonding, and a comparison of these data with the corresponding experimental results indicate that the strength of the hydrogen-bonding with Se or S depends on the structural aspects of the multiple possible conformations of the complexes containing Se or S hydrogen-bonding. Figure 3.4 shows optimized structures (hydrogen bonded) as well as binding energies and N-H/O-H stretching frequencies of various conformers of Ind…Me_2Se, Ind…Me_2S, and Ind…Me_2O complexes as well as Ph…Me_2Se, Ph…Me_2S, and Ph…Me_2O complexes calculated at the B97-D/6-311++G(d,p) level of theory. The most striking feature of

this result is that the O-centered hydrogen-bonded complex provides only one conformation while the Se or S-centered hydrogen bonded complexes show multiple low energy conformations. The single structure of Ind…Me_2O or Ph…Me_2O is dominated by strong hydrogen bonding interaction (N-H…O or O-H…O). On the other hand, each of Ind…Me_2Se, Ind…Me_2S, Ph…Me_2Se, and Ph…Me_2S complexes show two types of structure. One of the conformers of these complexes, for instance, Ind…Me_2Se(B), Ind…Me_2S(B), Ph…Me_2Se(B) and Ph…Me_2S(B), is dominated by a strong hydrogen- bonding interaction. However, the other class of conformer, namely, Ind…Me_2Se(A), Ind…Me_2S(A), Ph…Me_2Se(A), and Ph…Me_2S(A), is stabilized by a delicate balance between relatively weaker hydrogen-bonding and dispersion interactions. A similar observation was reported recently by Kjaergaard and co-workers by studying dimethylamine (Me_2NH)…Me_2O and dimethylamine (Me_2NH)…Me_2S complexes with gas phase FTIR spectroscopy.[151] They found two conformers of Me_2NH…Me_2S complex where the N-H…S hydrogen bond in one of the conformers is stronger than that in the other conformer. On the other hand, the N-H…O hydrogen bond of the two conformers of the Me_2NH…Me_2O complex is of similar strength.

A comparison of the experimental N-H and O-H stretching frequencies of the indole and phenol complexes with those obtained from the B97-D/6-311++G(d,p) calculations (Figure 3.4) reveals that the observed structure for Se and S complexes is the one which is stabilized by a subtle interplay between the relatively weaker hydrogen bond and dispersion interaction. The S complexes of indole and phenol have been reported earlier and the experimental vibrational frequencies of Ind…Me_2S (ν_{N-H}=3367 cm^{-1}), Ph…Me_2S (ν_{O-H}=3527 cm^{-1}) and Ind…Me_2O (ν_{N-H}=3381, 3345, 3278 cm^{-1}) obtained from the literature are given in Figure 3.4.[113,115,152]

In the case of the indole complexes, the observed structures (Ind…Me_2Se(A)) and Ind…Me_2S(A)) are the most stable conformers while the observed structures (Ph…Me_2Se(A)) and Ph…Me_2S(A)) for phenol complexes are higher in energy by 0.1-0.5 kcal/mol from the most stable structures. The calculation has also been performed at the B97-D/6-31+G(d), B97-D/cc-pVTZ, B97-D/aug-cc-pVTZ, and CCSD/6-311++G(d,p) levels of theory but the trend in the zero point energy corrected relative binding energies of all the conformers of the complexes remain same (Table 3.2). Moreover, we have calculated the Gibbs free energies (Δ*G*)of various conformers of the complexes as these determine the abundance of the conformers more accurately. Comparison of the binding energies (Δ*E*) and Gibbs free energies (Δ*G*) of all the complexes is provided in Table 3.2.

Table 3.2 Comparison of binding energies (Δ*E*, in kcal/mol) calculated at various levels of theory. Gibbs free energies (Δ*G*, in kcal/mol) of various conformers of hydrogen-bonded complexes of indole and phenol are calculated at the B97-D/6-311++G(d,p) level of theory. Δ*G* has been calculated at 10 K and 50 K.

	Complexes	ΔE B97-D/6-31+G(d,p)	ΔE B97-D/cc-pVTZ	ΔE B97-D/aug-cc-pVTZ	ΔE CCSD/6-311++G (d,p)	ΔG (10 K) B97-D/6-311++G (d,p)	ΔG (50 K) B97-D/6-311++G (d,p)
Complexes of Indole	Ind…Me_2Se(A)	-6.83	-5.75	-5.77	-4.47	-6.05	-5.58
	Ind…Me_2Se(B)	-6.00	-5.53	-5.50	-4.26	-5.81	-5.56
	Ind…Me_2S(A)	-5.77	-5.49	-5.47	-5.05	-6.12	-5.92
	Ind…Me_2S(B)	-5.03	-5.27	-5.20	-4.23	-5.48	-5.32
	Ind…Me_2O	-6.87	-5.51	-5.63	-5.70	-6.51	-6.14
Complexes of Phenol	Ph…Me_2Se(A)	-7.02	-5.96	-6.02	-4.54	-6.44	-5.98
	Ph…Me_2Se(B)	-7.40	-6.16	-6.27	-4.87	-6.72	-6.35
	Ph…Me_2S(A)	-5.52	-5.68	-5.75	-4.98	-6.16	-5.91
	Ph…Me_2S(B)	-6.36	-6.04	-6.13	-5.23	-6.29	-5.87
	Ph…Me_2O	-6.54	-6.29	-6.46	-6.51	-7.40	-7.23

It has been found that the order in the binding energies and Gibb free energies (calculated at 10 K and 50 K) of the conformers of the complexes is similar. However,

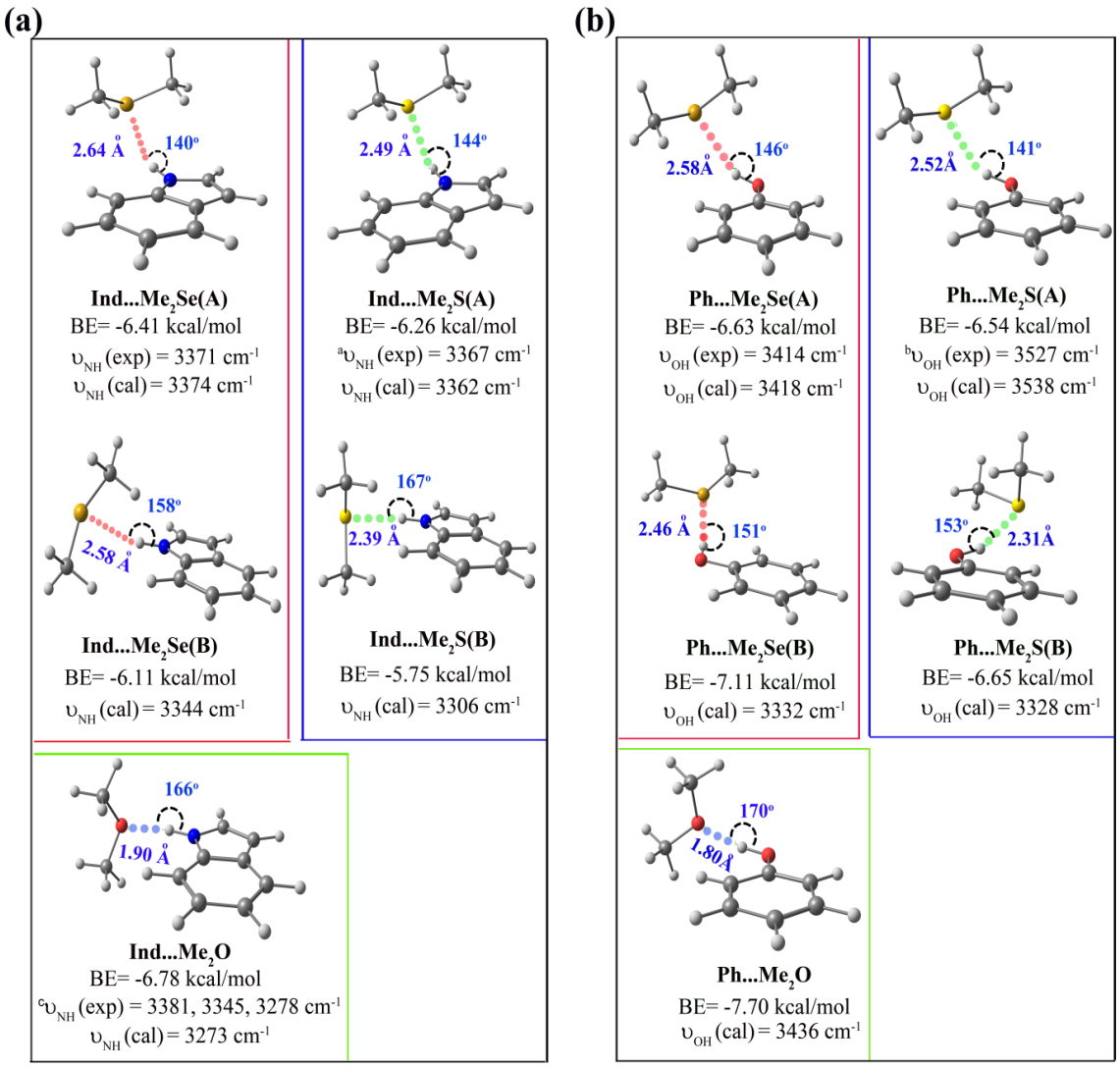

Figure 3.4: Structures of various conformers of (a) indole and (b) phenol complexes with dimethyl selenide (Me_2Se), dimethyl sulfide (Me_2S) and dimethyl ether (Me_2O) optimized at the B97-D/6-311++G(d,p) level of theory. BE represents the BSSE and zero point energy corrected binding energies of the complexes. $^{a}\nu_{NH}$(exp) = 3367 cm^{-1} (Experimental N-H stretching frequency of Ind…Me_2S), $^{b}\nu_{OH}$(exp) = 3527 cm^{-1} (Experimental O-H stretching frequency of Ph…Me_2S) and $^{c}\nu_{NH}$(exp) = 3381, 3345, 3278 cm^{-1} (Experimental N-H stretching frequency of the three conformers of Ind…Me_2O) are taken from references 113, 115 and 152 respectively. Theoretical harmonic N-H stretching frequencies [ν_{NH}(cal)] of the indole complexes and O-H stretching [ν_{OH}(cal)] frequencies of the phenol complexes provided with the structures in the figure are scaled using factors of 0.9588 and 0.9609, respectively.

since the computational methods employed (DFT or CCSD) are correct to about 0.5-1 kcal/mol, this is not a proof that we observe the less stable structures in the case of phenol complexes. The reason behind not observing the near isoenergetic conformers

in the experiment could be interconversion of the higher energy one to the global minimum through a shallow potential energy barrier. However, the most interesting point here is that moving in the chalcogen group from O to S and Se provides conformational abundance within the framework of S and Se hydrogen bonding.

3.2.5 Physical Origin of the strength of Se/S hydrogen bond

It turns out that S and Se being quite less electronegative and more polarizable (diffused electron density) compared to O, show the possibility of multiple conformations through small variation of the strength of the hydrogen bond. Du et al. have also reported that there is a subtle difference between the O-H...O and O-H...S hydrogen bonds.[153] The electron density in the sulfur-hydrogen bond is weaker the secondary interaction present there is quite significant. It could be pointed out here that S and Se neither form weaker nor stronger hydrogen bonds than O does. Rather multiple conformations of S and Se complexes with different hydrogen bond strength but similar binding energies are found from the theoretical calculations. In the case of Se and S complexes of indole as well as phenol, the conformers with a stronger hydrogen bond (those are not observed in the experiment) have red-shifts in the N-H or O-H stretching frequency which is closer to or even more than that in Ind…Me_2O and Ph…Me_2O complexes.

3.2.5 Physical Origin of the strength of Se/S hydrogen bond

3.2.5.1 Symmetry-Adapted Perturbation Theory (SAPT) energy decomposition analysis (SAPT-EDA)

To understand the origin of the unusual strength of the Se and S centered hydrogen bonds, the interaction energies of the various conformers of the three types (O, S, and Se) of the complexes of indole and phenol have been decomposed using symmetry-

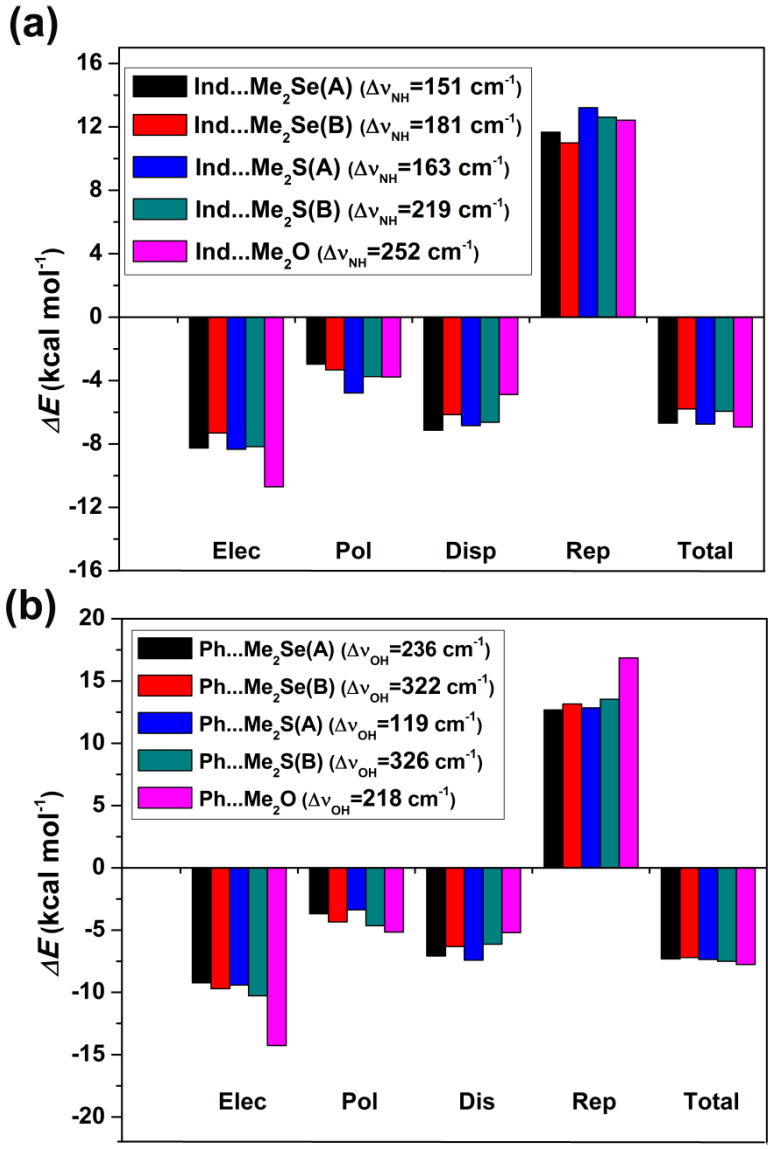

Figure 3.5: SAPT2/aug-cc-pVDZ decomposition of interaction energies of different conformers of the complexes of (a) indole and (b) phenol. The red-shift in the N-H/O-H stretching frequency ($\Delta\nu_{N\text{-}H}$ or $\Delta\nu_{O\text{-}H}$) of the complexes has been provided in the annotation of the figure. Different components of the total interaction energy in SAPT2 method are Electrostatics (Ele), Polarization (Pol), Dispersion (Disp), and Repulsion (Rep).

adapted perturbation theory (SAPT). Different components of the interaction energies in the complexes of indole and phenol obtained from the SAPT2/aug-cc-pVDZ calculation have been shown as a bar graph in Figure3.5a and 3.5b, respectively. In the SAPT2 method, the total interaction energy (ΔE_{Total}) of the complexes is partitioned

into electrostatics (ΔE_{Ele}), polarization (ΔE_{Pol}), dispersion (ΔE_{Disp}), and repulsion (ΔE_{Rep}) components. It is noticed that the electrostatic component is much smaller in all the conformers of the Se and S complexes compared to that in the O-centered hydrogen-bonded complexes. On the other hand, the polarization component in all the complexes is not very much different. However, the red-shift in the N-H/O-H stretching frequency (see the box in Figure 3.5a and 3.5b) of the various conformers of the Se/S complexes is not appreciably different and even higher in some cases compared to that in the O-centered hydrogen-bonded complexes. Thus electrostatic/polarization interaction alone cannot explain the red-shift in the IR stretching frequency or strength of the hydrogen bond when the hydrogen bond acceptors are Se or S, which are very poor in electronegativity.

3.2.5.2 Absolutely Localized Molecular Orbital Energy Decomposition Analysis (ALMO-EDA)

In order to find out the contribution of the charge transfer interaction energy to the red-shift in the X-H stretching frequency of the S/Se centered hydrogen-bonded complexes, we have performed an ALMO-EDA calculation. This energy decomposition method has been demonstrated to be very useful in determining the charge transfer/covalent contribution in the hydrogen bonded complexes.[154-156] Recently, Ahlquist and co-workers have reported from ALMO-EDA calculation that charge transfer interaction plays a major role in the stabilization of platinum (Pt) centered hydrogen bonds where Pt is an electropositive element.[155] In the ALMO-EDA method, the total interaction energy (ΔE_{Total}) is decomposed into the frozen density energy (ΔE_{Frz}), the polarization energy (ΔE_{Pol}) and the charge transfer energy(ΔE_{CT}). The ΔE_{Frz} term is composed of electrostatics, Pauli repulsion, and dispersion. Figure 3.6 shows a bar diagram of the different components of the

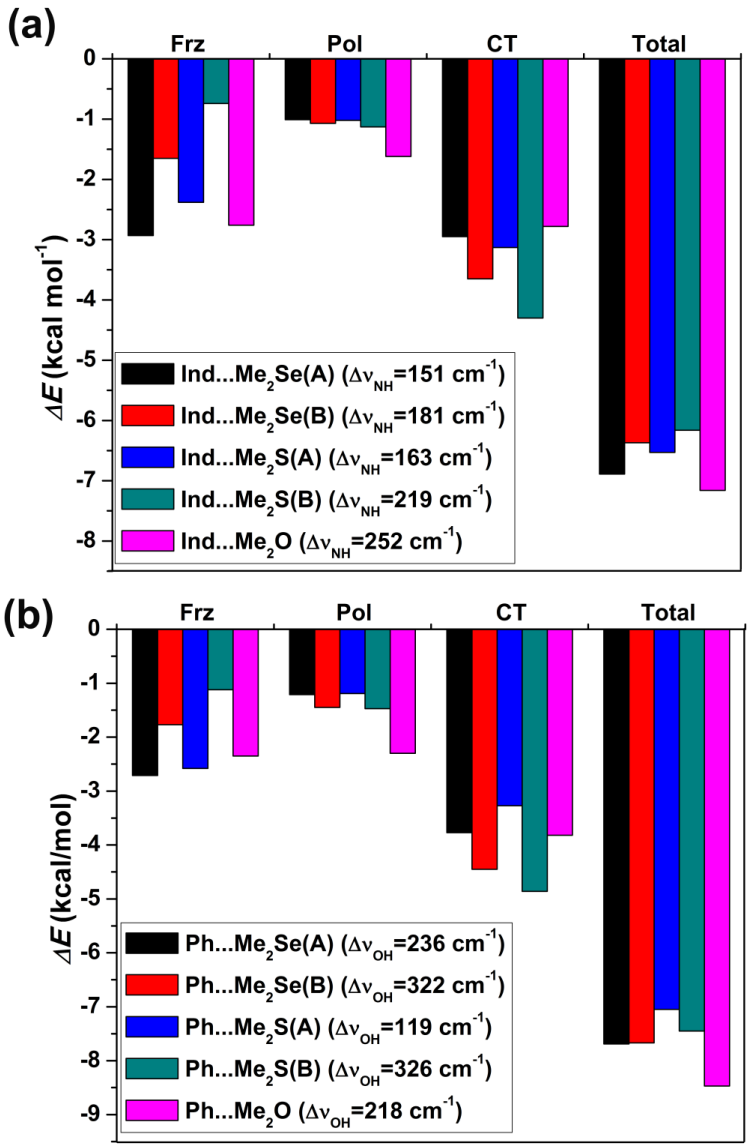

Figure 3.6: Decomposition of the interaction energies of the different conformers of the complexes of (a) indole and (b) phenol obtained at the B97-D/6-311++G(d,p) level of theory using the ALMO-EDA method. The red-shift in the N-H/O-H stretching frequency ($\Delta\nu_{N\text{-}H}$ or $\Delta\nu_{O\text{-}H}$) of the complexes has been provided in the box in the figure. Different components of the interaction energies in the ALMO-EDA method are Frozen density interaction (Frz), Polarization (Pol), and Charge transfer (CT).

interaction energy in all the conformers of Se, S, and O centered hydrogen bonded complexes of indole and phenol obtained from the ALMO-EDA method using the B97-D/6-31+G(d,p) level of theory. The ALMO-EDA results show that the charge transfer (ΔE_{CT}) interaction in most of the conformers of Se and S complexes is not

only a significant component of the total interaction energy but also higher than that in the O-centered hydrogen-bonded complexes.

Indeed, Tomoda and co-workers reported that covalent interaction plays a paramount role in the stabilization of C-H…Se hydrogen bond.[78] They obtained first spectroscopic proof of the Se hydrogen bonding by studying the structure of diselenocin using X-ray crystallography, low temp NMR spectroscopy, solid state FTIR, and ab initio calculations. Later, Madzhidov et al. have performed quantum chemistry calculations of hydrogen-bonded complexes of a few organoselenium compounds and reported that significant stabilization of the Se hydrogen bonding arises from the charge transfer (CT) contribution.[118] They have concluded from NBO CT calculation that the CT values in the Se hydrogen bonding are more in comparison to those in the conventional hydrogen bonding, i.e., N or O centered hydrogen bonds. It should be pointed out here that the authors have looked at the charge density shift from the hydrogen bond acceptor to the hydrogen bond donor. The CT in a molecular system is defined as the difference between the sum of all the natural charges over individual atom in the complex and the sum of all the charges over individual atom in the monomers.

3.2.5.3 NBO CT analysis

We have computed the CT (charge density shift) values in all the conformers of the Se, S, and O centered hydrogen bonded complexes of indole and phenol by performing NBO analysis at the B97-D/6-311++G(d,p) level of theory. The CT values along with the IR red-shift in all the complexes are provided in Table 3.3. It has been found that there is a systematic trend in increasing the CT contribution with the increase of the red-shift in the N-H/O-H stretching frequency of indole/phenol in the various conformers of the S and Se complexes.

Table 3.3 NBO charge transfer (CT) values in the various conformers of the hydrogen-bonded complexes of indole and phenol with Me_2Se, Me_2S and Me_2O along with the change in the occupancy of the s and p-type lone pair orbitals ($\Delta\eta_s$ and $\Delta\eta_p$) of the hydrogen bond acceptor atoms (Se/S/O) and antibonding orbital ($\Delta\sigma^*_{N\text{-}H/O\text{-}H}$) of the N-H/O-H bond upon complex formation obtained at the B97-D/6-311++G(d,p) level of theory.

	Complexes	$\Delta\nu_{cal}$[a]	CT	$\Delta\eta_s$	$\Delta\eta_p$	$\Delta\sigma^*_{N\text{-}H/O\text{-}H}$
Complexes of Indole	Ind…Me_2Se(A)	151	0.0332	-0.0008	-0.0290	0.0279
	Ind…Me_2Se(B)	181	0.0381	-0.0016	-0.0325	0.0322
	Ind…Me_2S(A)	163	0.0353	-0.0007	-0.0248	0.0288
	Ind…Me_2S(B)	219	0.0434	-0.0013	-0.0323	0.0368
	Ind…Me_2O	252	0.0308	-0.0066	-0.0011	0.0249
Complexes of Phenol	Ph…Me_2Se(A)	236	0.0372	-0.0008	-0.0295	0.0305
	Ph…Me_2Se(B)	322	0.0485	-0.0004	-0.0404	0.0415
	Ph…Me_2S(A)	119	0.0311	-0.0012	-0.0202	0.0233
	Ph…Me_2S(B)	326	0.0527	-0.0010	-0.0392	0.0449
	Ph…Me_2O	218	0.0400	-0.0092	-0.0039	0.0348

[a]Theoretical red-shift ($\Delta\nu_{cal}$) in cm^{-1} in the N-H/O-H stretching frequency in the complexes with respect to that in indole/phenol monomer

On the other hand, the CT contribution in Ind…Me_2O/Ph…Me_2O is not significant in proportion to the IR red-shift values. Furthermore, we notice that the changes in the NBO occupation of the s and p-type lone pair ($\Delta\eta_s$ and $\Delta\eta_p$) and the N-H/O-H antibonding orbitals ($\Delta\eta_{\sigma^*}$) in the case of the Se and S centered hydrogen bonding are indeed much larger than those in the case of the O centered hydrogen bond. A careful inspection of Table 3.3 reveals that the CT values in the case of the Ind…Me_2O and Ph…Me_2O complexes are close to those in some of the Se and S complexes. However, it is intriguing to note that the total changes in the NBO occupation of the lone pair orbitals ($\Delta\eta_s + \Delta\eta_p$)on oxygen atom are insignificant compared to those on Se and

S atoms.

Efficient CT in the Se and S hydrogen bonds with respect to that in the O hydrogen bond is expected due to the higher polarizability and diffused orbitals/electron density of the former two atoms compared to the latter one. Very recently, Stone has reported that the CT component of the interaction energy calculated from the NBO analysis suffers from the basis set superposition error.[157] However, the relative values of the CT of the complexes could be compared.

Table 3.4 NBO charge transfer values (CT) in various conformers of Ind…Me_2Se, Ind…Me_2S, and Ind…Me_2O complexes calculated at the B97-D/6-311++G(d,p) level of theory using various basis sets. Change in the occupancy of s and p-type lone pair orbitals ($\Delta\eta_s$ and $\Delta\eta_p$) of the hydrogen bond acceptor atoms (Se/S/O) and antibonding orbital ($\Delta\sigma^*_{N-H}$) of the N-H bond upon complex formation are also shown.

Complexes	Methods	CT	$\Delta\eta_s$ [a]	$\Delta\eta_p$ [b]	$\Delta\sigma^*_{N-H}$
Ind…Me_2Se(A)	B97-D/6-31+G(d)	0.0348	-0.0011	-0.0357	0.0331
	B97-D/6311++G(d,p)	0.0332	-0.0008	-0.0290	0.0279
	B97-D/cc-pVTZ	0.0304	-0.0010	-0.0262	0.0251
Ind…Me_2Se(B)	B97-D/6-31+G(d)	0.0408	-0.0017	-0.0391	0.0368
	B97-D/6311++G(d,p)	0.0381	-0.0016	-0.0325	0.0322
	B97-D/cc-pVTZ	0.0358	-0.0017	-0.0301	0.0295
Ind…Me_2S(A)	B97-D/6-31+G(d)	0.0358	-0.0012	-0.0400	0.0306
	B97-D/6311++G(d,p)	0.0353	-0.0007	-0.0248	0.0288
	B97-D/cc-pVTZ	0.0296	-0.0007	-0.0201	0.0244
Ind…Me_2S(B)	B97-D/6-31+G(d)	0.0430	-0.0013	-0.0366	0.0391
	B97-D/6311++G(d,p)	0.0434	-0.0013	-0.0323	0.0368
	B97-D/cc-pVTZ	0.0376	-0.0014	-0.0266	0.0315
Ind…Me_2O	B97-D/6-31+G(d)	0.0363	-0.0084	-0.0074	0.0319
	B97-D/6311++G(d,p)	0.0308	-0.0066	-0.0011	0.0249
	B97-D/cc-pVTZ	0.0242	-0.0035	0.0038	0.0200

The NBO CT analysis of the indole and phenol complexes (Tables 3.4 and Table 3.5)

has also been performed using different basis sets, i.e., 6-31+G(d) and cc-pVTZ at the B97-D level of theory and a similar correlation between the red-shift in the X-H stretching frequency, and CT values have been obtained.

Table 3.5 NBO charge transfer values (CT) in all the possible conformers of phdmse, phdms, and phdmo complexes calculated at the B97-D/6-311++G(d,p) level of theory using various basis sets. Change in the occupancy of s and p-type lone pair orbitals ($\Delta\eta_s$ and $\Delta\eta_p$) of the hydrogen bond acceptor atoms (Se/S/O) and antibonding orbital ($\Delta\sigma^*_{O\text{-}H}$) of the O-H bond upon complex formation are also shown.

Complexes	Methods	CT	$\Delta\eta_s$ [a]	$\Delta\eta_p$ [b]	$\Delta\sigma^*_{O\text{-}H}$
Ph…Me_2Se(A)	B97-D/6-31+G(d)	0.0422	-0.0012	-0.0388	0.0372
	B97-D/6-311++G(d,p)	0.0372	-0.0008	-0.0295	0.0305
	B97-D/cc-pVTZ	0.0362	-0.0012	-0.0284	0.0307
Ph…Me_2Se(B)	B97-D/6-31+G(d)	0.0528	-0.0004	-0.0490	0.0470
	B97-D/6-311++G(d,p)	0.0485	-0.0004	-0.0404	0.0415
	B97-D/cc-pVTZ	0.0467	-0.0006	-0.0390	0.0412
Ph…Me_2S(A)	B97-D/6-31+G(d)	0.0329	-0.0018	-0.0260	0.0283
	B97-D/6-311++G(d,p)	0.0311	-0.0012	-0.0202	0.0233
	B97-D/cc-pVTZ	0.0267	-0.0013	-0.0164	0.0216
Ph…Me_2S(B)	B97-D/6-31+G(d)	0.0543	-0.0012	-0.0450	0.0485
	B97-D/6-311++G(d,p)	0.0527	-0.0010	-0.0392	0.0449
	B97-D/cc-pVTZ	0.0465	-0.0012	-0.0346	0.0418
Ph…Me_2O	B97-D/6-31+G(d)	0.0443	-0.0119	-0.0104	0.0417
	B97-D/6-311++G(d,p)	0.0400	-0.0092	-0.0039	0.0348
	B97-D/cc-pVTZ	0.0322	-0.0066	0.0020	0.0310

Therefore, based on both the ALMO-EDA and NBO calculations we find that along with electrostatics and polarization, charge transfer interactions are important to nderstand H-bonding, and it is a delicate balance between the various interactions that play the crucial role rather than a single component of the interaction energy

3.3 Conclusion

In conclusion, we have investigated the nature of Se hydrogen bonding interaction (N-H...Se and O-H...Se) by studying the complexes of dimethyl selenide (Me_2Se) with indole as well as phenol using R2PI, IR-UV double resonance spectroscopy and quantum chemistry calculations. The results have been compared with the data on the sulfur and oxygen-centered hydrogen bonds of indole and phenol. It has been found that the hydrogen-bonded complexes of indole and phenol with dimethyl ether (Me_2O) show only one conformation dominated by a strong hydrogen bond (N-H…O or O-H…O) while the Se/S centered hydrogen bonded complexes provide at least two conformations having binding energies close to each other. One of the conformers of the Se/S complexes is dominated by a stronger hydrogen bond (N-H…Se, N-H…S or O-H…Se, O-H…S) while the other conformer is stabilized by a subtle balance between a relatively weaker hydrogen bond (N-H…Se, N-H…S or O-H…Se, O-H…S) and dispersion interaction. Interestingly, the experimentally observed conformer of the Se/S complexes is the one which is stabilized by the relatively weaker hydrogen bond and dispersion interaction. However, the other conformer of the Se/S complexes, which has a hydrogen bond (N-H…Se, N-H…S or O-H…Se, O-H…S) of similar or higher strength to the N-H…O/O-H…O, is not observed in the experiment, is almost isoenergetic with the experimentally observed conformer. Thus the Se/S hydrogen bonding interaction is neither weaker nor stronger compared to the O-centered hydrogen bonding interaction.

The strength of the Se/S hydrogen bonding interaction varies depending on the orientation of this atom with respect to the hydrogen bond donor group by balancing other intermolecular interactions, i.e., the repulsion between Se/S with H atom of X-H group and dispersion interaction between methyl groups and phenyl group in the complex. We have shown through

the ALMO-EDA, SAPT-EDA and NBO CT calculations that the CT interaction plays a role for the strength of the Se/S hydrogen bond interaction, along with the already acknowledged electrostatics and polarization components. The Larger polarizability of Se and S atoms leads to an enhanced CT interaction in these complexes. The finding from the present work is extremely important as it will be able to explain the strength of the hydrogen bond having a hydrogen bond acceptor atom of poor electronegativity.

Chapter 4

Water-mediated selenium hydrogen bonding interactions in proteins: PDB analysis and gas phase spectroscopy and Quantum Chemical calculation

4.1 Introduction

So far we have discussed selenium hydrogen-bonding interaction between two amino acid residues in proteins. We have shown through various spectroscopy experiments as well as quantum chemical calculations that Se forms hydrogen bond of similar strength as compared to S and O. It has been found that charge transfer component in the total interaction energy plays a pivotal role along with the electrostatics and polarization components to provide significant IR red-shift in the stretching frequency of the S and Se centered hydrogen bond donors. We have also discussed the biological importance of selenium in chapter 1. Selenomethionine is the selenium analog of methionine in which sulfur is replaced by selenium. Selenomethionine can be incorporated into proteins without affecting their structures and functions. This provides a mechanism for reversible Se storage in organs and tissues. This free Se is incorporated into selenocysteine which is found in more than thirty selenoproteins including glutathione peroxidases (GPx) enzyme.[158]

In general, the subtle interplay between various types of non-covalent interactions in the backbone and side-chain of amino acid residues plays a significant role for protein folding, protein-protein as well as protein-ligand interactions.[2,4,7,159,160] Water molecules also contribute significantly to the folding of proteins and biomolecular recognition processes through hydrophobic interactions.[161-164] However, water molecules specifically present in the cavity of proteins and at the interface of proteins and ligands in protein-ligand complexes can play a crucial role in their stability.[119,165-175] It has been found from high-resolution X-ray crystallography and 2D NMR studies that water-mediated hydrogen bonding interactions bridging two or more amino acid residues contribute to the stability of proteins and protein-ligand complexes.[119,167,170,171,175-179]

A few examples describing water-mediated hydrogen-bonding interactions contributing to the stability of the protein structures can be mentioned here briefly. Takano et al. reported that

one or two water molecules in the cavity forming multiple strong hydrogen-bonds with neighboring residues contribute significantly to the stability of proteins.[119]Wang et al. have studied water molecules bound at the interface of the complex of HIV-1 protease and an inhibitor using X-ray crystallography and NMR spectroscopy.[170] The observation of cross peaks between the protons of water molecules and proteins as well as long residence time (1 ns or greater) of water molecules in the cavity measured by Nuclear Overhauser Effect (NOE) and Rotating-frame Overhauser Enhancement (ROE) relaxation rates confirms that water-mediated hydrogen-bonding interactions contribute to the stability of protein-inhibitor complexes. The longer residence time (ns to ms) of water molecules in protein cavity has been reported by many other groups using high-resolution NMR spectroscopy.[176,180] Helms et al. performed molecular dynamics simulation of protein-ligand complexes and concluded that a water molecule in the cavity stabilizes the complexes only if it forms more than one hydrogen bond with the ligand and neighboring residues of the protein.[171]

Although water-mediated conventional strong hydrogen-bonding interactions present in the cavity contributing to the stability of proteins are reported in the literature, there is surprisingly no study on water-mediated unconventional hydrogen-bonding interactions leading to the stability of proteins. It is also important to verify the stabilizing nature of this water-mediated non-covalent interaction present in the PDB structures through quantum chemistry calculations.

In this work, we have investigated water-mediated selenium (Se) hydrogen-bonding interactions between amino acid residues in proteins through extensive PDB analysis and quantum chemical calculations. To better understand the nature, strength, and binding motif of this interaction, conformation-specific IR spectroscopy of a model complex consisting of indole (Ind), dimethyl selenide (Me_2Se) and H_2O mimicking water-mediated Se hydrogen-

bonding has been studied further in an isolated condition. The present work establishes that water-mediated Se hydrogen bonding interactions are also present in proteins and these interactions can contribute significantly to the stability of proteins.

4.2 Results and Discussion

4.2.1 Analysis of PDB structures

9175 PDB files that contained Selenomethionine (MSE) were downloaded from the RCSB website.[181] On filtering these PDBs with sequence identity less than 30% and X-ray resolution of ≤ 2.5 Å using PISCES[182], we got 5186 structures that were used for further analysis. Hydrogen atoms were added to the amino acid residues in the protein structures using REDUCE software.[183] In this data, there were 4334 direct Se hydrogen bonding interactions between MSE and other amino acid residues.[69] However, the search of single water-mediated Se hydrogen bonding interactions from PDB analysis is not documented in the literature. In the water bridged interactions, Se of MSE is always the hydrogen bond acceptor with water as its donor. However, the residues that are bridged by the water could either have atoms that donate or accept hydrogen from water (Figure 4.1). The distance ($d_{O...Se}$) cut-off considered between Se atom of MSE and O atom of water is ≥2.5 Å and ≤4.5 Å while the distance ($d_{D/A\cdots O}$) criterion between O atom of water and hydrogen bond donor or acceptor atom (D/A) of any other amino acid residue is ≥2.0 Å and ≤3.5 Å. The minimum and maximum distances ($d_{D/A...Se}$) between Se atom and hydrogen bond donor or acceptor atom (D/A) of amino acid residues are 3.8 and 8 Å, respectively. The search criterion used for the angle (∠D…O…Se) comprising of Se, O atom of water and hydrogen bond donor atom (D) of amino acid residues is 40°-180° while the same consideration for the angle (∠A…O…Se) consisting of Se, O atom of water and hydrogen bond acceptor atom (A) of amino acid residues is 75°-135° (see Figure 4.1).

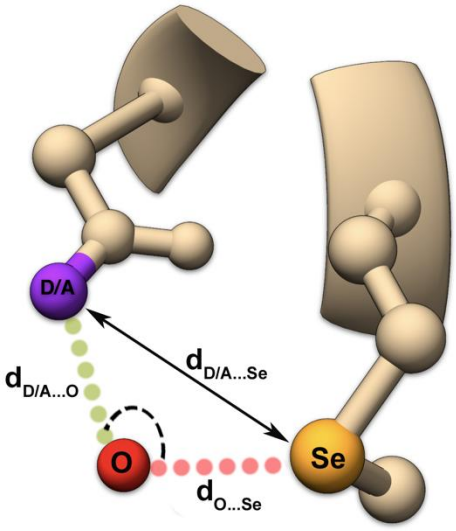

Figure 4.1: A schematic showing the features of the Se…H_2O…amino acid hydrogen- bond network in PDB structures.The selenium, oxygen of the water and the donor (D) or acceptor (A) atom from another amino acid are shown in orange, red and purple ball representation, respectively and labeled accordingly. The two hydrogen bond distances ($d_{D/A}…_O$ and $d_{O...Se}$) as well as the ∠D/A…O…Se and $d_{D/A...Se}$ are also labeled in the figure.

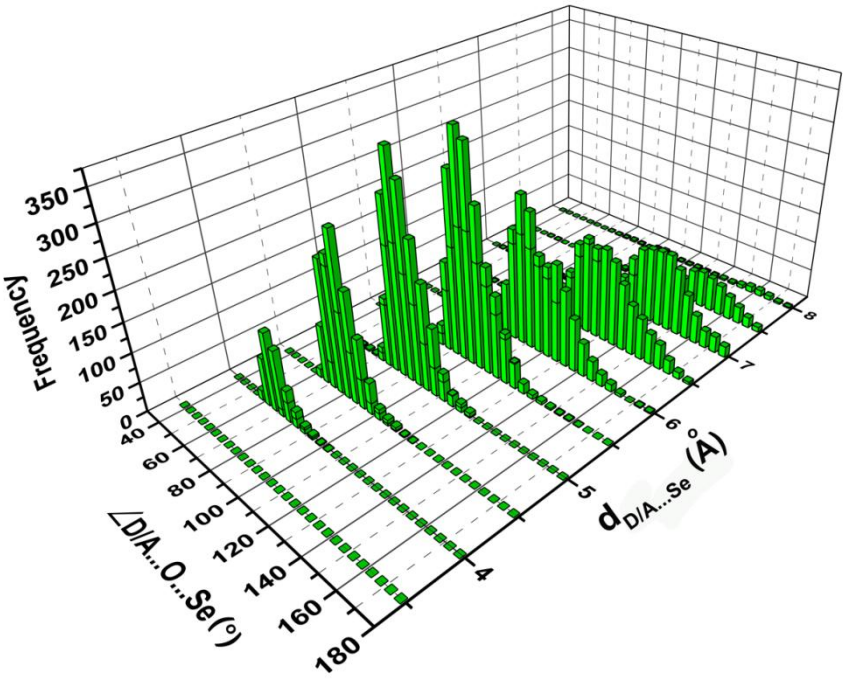

Figure 4.2: A 3D plot showing frequency of single water mediated Se hydrogen bonding interactions screened from PDB as a function of ∠D/A…O…Se (°) and $d_{D/A...Se}$ distance (Å), where D/A is a hydrogen bond donor/acceptor atom of any amino acid residue except MSE (See Figure 4.1). Note that the distances ($d_{D/A...Se}$) are binned at an interval of 0.5 Å for representation purposes.

We observed 4017 and 3509 single water-mediated Se hydrogen bonding (water bridges) considering interactions of H_2O with hydrogen bond donors (D) or acceptors (A) of the amino acids residues, respectively (see Figure 4.1). Thus, we have a non-redundant set of 7526 single water-mediated Se hydrogen bonding interactions from 2978 different PDB entries.

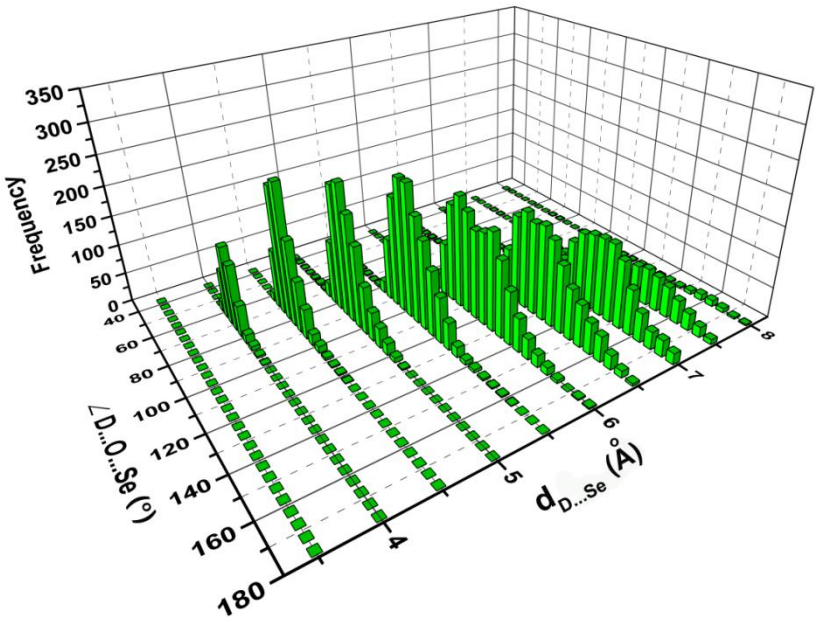

Figure 4.3: 3D histogram showing frequency of single water mediated Se hydrogen bonding interactions retrieved from PDB as a function of ∠D…O…Se (°) and D…Se distance (Å), where D is a hydrogen bond donor atom of any amino acid residue except MSE (See Figure 4.1). Note that the distances ($d_{D/A...Se}$) are binned at an interval of 0.5 Å for representation purposes.

It is interesting that the number of single water-mediated Se hydrogen bonding interactions observed in the PDB is almost twice than that of the direct Se hydrogen bonding interactions. Figure 4.2 shows a 3D plot representing the frequency of single water-mediated Se hydrogen bonding interactions or water bridges observed in the PDB as a function of ∠D/A…O…Se and D/A…Se distance ($d_{D/A...Se}$), where D/A is a hydrogen bond donor/acceptor atom of any amino acid residue except MSE (See Figure 4.1). The plot shows that the occurrence of

single water-mediated Se hydrogen bonding interactions is maximum at $d_{D/A...Se}$ = 5-5.5 Å and ∠D/A…O…Se = 80°-90°.

Figure 4.3 shows a 3D plot representing the frequency of single water-mediated Se hydrogen bonding interactions or water bridges observed in the PDB as a function of ∠D …O…Se and D …Se distance ($d_{D ...Se}$), where D is a hydrogen bond donor atom of any amino acid residue except MSE (See Figure 4.1). The plot shows that the occurrence of single water-mediated Se hydrogen bonding interactions is maximum at $d_{D...Se}$ = 5-5.5 Å and ∠D…O…Se = 80° - 90°. We observed 4017 interactions of this kind.

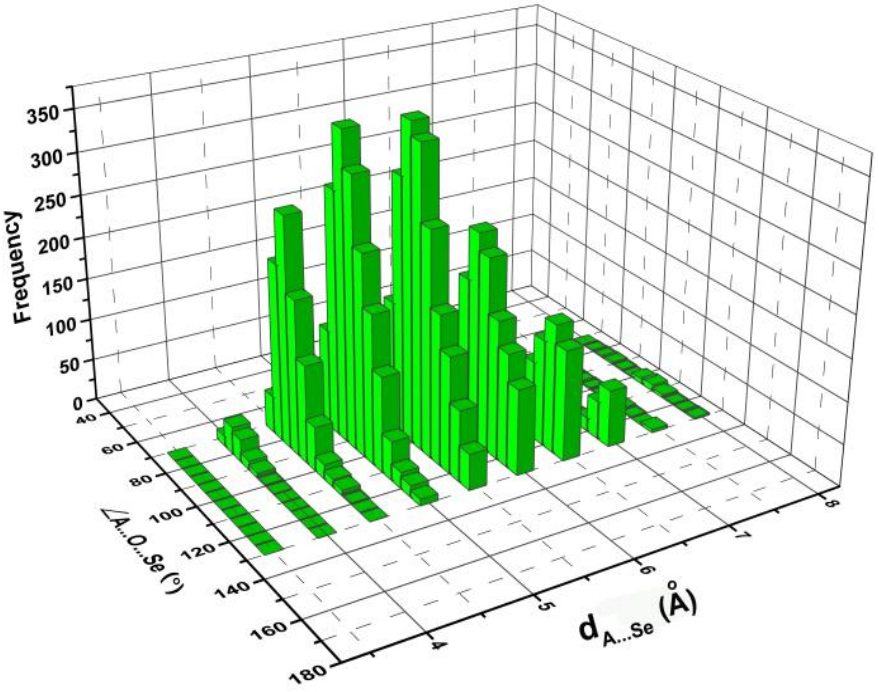

Figure 4.4: 3D plot showing frequency of single water mediated Se hydrogen bonding interactions screened from PDB as a function of ∠A…O…Se (°) and $d_{A...Se}$ distance (Å), where A is a hydrogen bond acceptor atom of any amino acid residue except MSE (See Figure 4.1). Note that the distances ($d_{A...Se}$) are binned at an interval of 0.5 Å for representation purposes.

Figure 4.4 shows a 3D plot representing the frequency of single water-mediated Se hydrogen bonding interactions or water bridges observed in the PDB as a function of ∠A …O…Se and A …Se distance ($d_{A ...Se}$), where A is a hydrogen bond acceptor atom of any amino acid

residue except MSE (See Figure 4.1). The plot shows that the occurrence of single water-mediated Se hydrogen bonding interactions is maximum at $d_{A...Se}$ = 5-5.5 Å and ∠A…O…Se = 80° - 90°. We observed 3509 interactions of this kind.

Two representative examples of single water-mediated Se hydrogen bonding interactions with neighboring residues extracted from PDB are shown in Figure 4.3. Hydrogen bond distances are shown between the heavy atoms, i.e., Se atom of MSE and oxygen atom of water as well as hydrogen bond donor/acceptor atom of any other residue and the oxygen atom of water as it is quite challenging to determine the exact position of hydrogen atoms of free water in protein from X-ray crystallography. It should be noted that a single water molecule in a cavity can make more than two hydrogen bonding interactions with multiple neighboring residues.

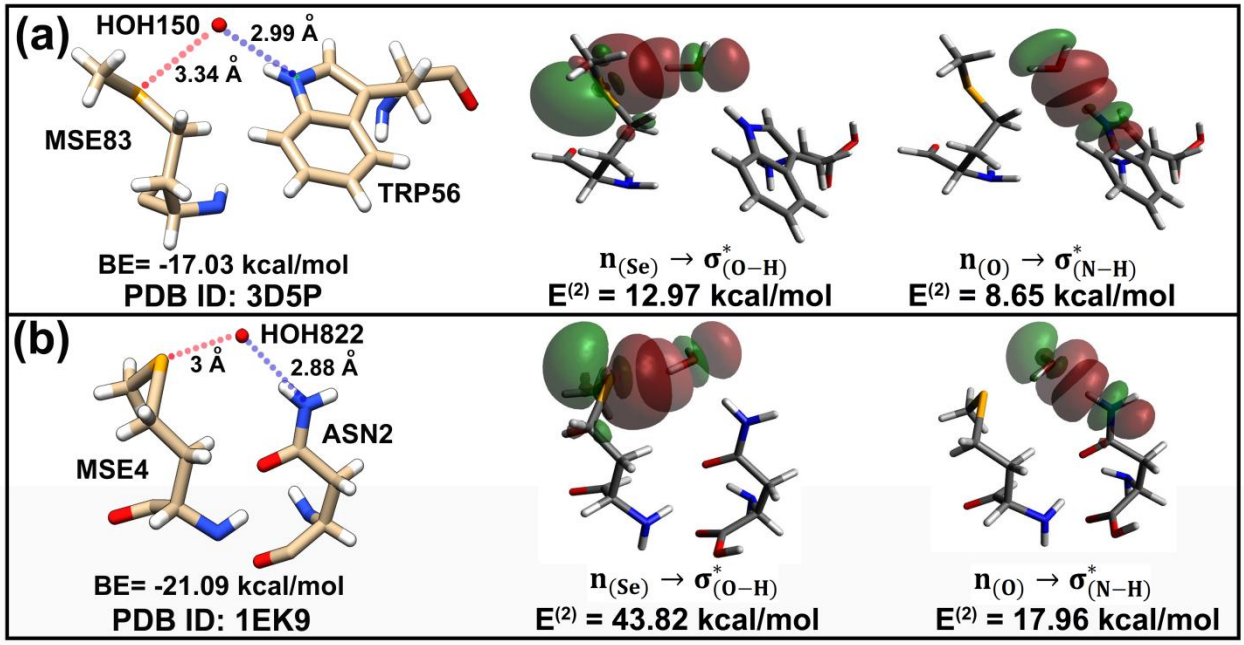

Figure 4.5: Two examples of single water mediated Se hydrogen bonding interactions between (a) selenomethionine (MSE) and tryptophan (TRP) residues in PDB ID 3D5P (b) selenomethionine (MSE) and asparagine (ASN) residues in PDB ID 1EK9. Binding energy (BE) and NBO plots showing individual hydrogen bond interaction between the residues in the PDB structures are also shown in the Figure. $E^{(2)}$ stands for NBO 2nd order perturbation energy.

The distances depicted between water oxygen and neighboring hydrogen bond donor/acceptor atoms indicate the presence of water-mediated hydrogen bonding interactions. The van der Walls (vdW) radii of Se, H, O, and N are 1.9 Å, 1.2 Å, 1.52 Å, and 1.55 Å, respectively.[184] We have also calculated the binding energies, natural bond orbital (NBO) energies and atoms in molecules (AIM) electron density topology of the peptide residues interacting with water in the two selected PDB structures provided in Figure 4.5. For the binding energy, NBO and AIM calculations of the PDB structures, we have put H atoms on the amino acid residues through REDUCE software while H atoms on water oxygen atoms using pymol software.[185]

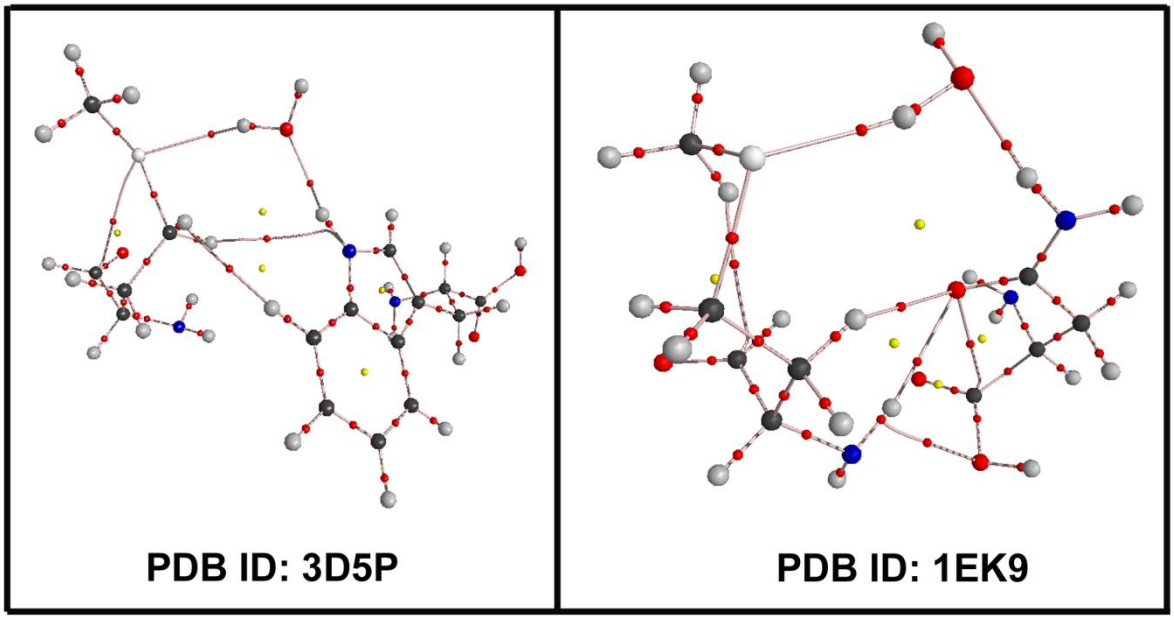

Figure 4.6: Electron density topology obtained from AIM calculation indicating water-mediated Se hydrogen bonding interactions between the residues in the selected PDB structures.

We have performed partial optimization of all the hydrogen atoms keeping all other coordinates of the PDB structures fixed. The binding energies (BE) of the interacting residues of the PDBs and NBO 2nd order perturbation energies ($E^{(2)}$) of the hydrogen bond interactions

present there are provided in Figure 4.5 while electron density topology obtained from AIM calculation has been provided in Figure 4.6.

The BE, NBO and AIM results point out that single water-mediated Se hydrogen bonding interactions between amino acid residues can contribute to the stability of protein structures. We have also analyzed the PDB structures to obtain the frequency distribution of the amino acid residues involved in water-mediated Se hydrogen bonding interactions (Figure 4.7). It has been found that Argentine (ARG) residue dominates over all other residues to have interactions with Se through a water bridge. Further, we did not find any instance of Se hydrogen-bonding interactions with amino acids mediated by two water molecules (using the distance and angle criteria mentioned above).

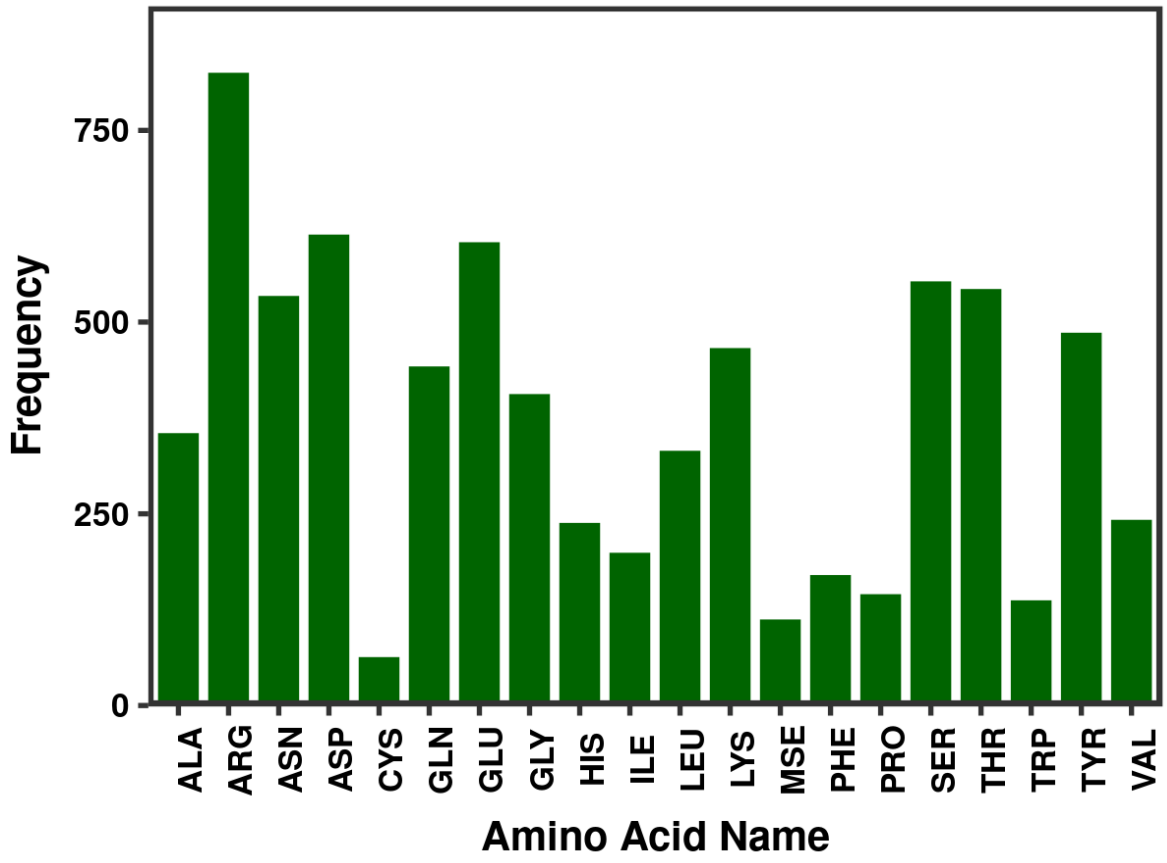

Figure 4.7: Histogram showing the frequency distribution of the amino acid residues involved in single water-mediated Se hydrogen bonding interactions.

Both Figures 4.2 and 4.5 reveal that there is a large variation in the Se…O, N…O and O…O distances involving water-mediated Se H-bonding interactions in the PDB due to the constraint of the optimum arrangement of other surrounding residues of the proteins. However, the Se H-bonding interactions through a water bridge observed in the crystal structures can be mimicked by studying a non-covalently bonded model complex, consisting of two amino acid residues including MSE and a water molecule, in an isolated condition. Study of this model complex is extremely important to have a quantitative understanding of the nature, stability and structural motif of this water-mediated Se H-bonding interaction.

4.2.2 Gas phase laser spectroscopy

4.2.2.1 Time of flight mass spectrometry

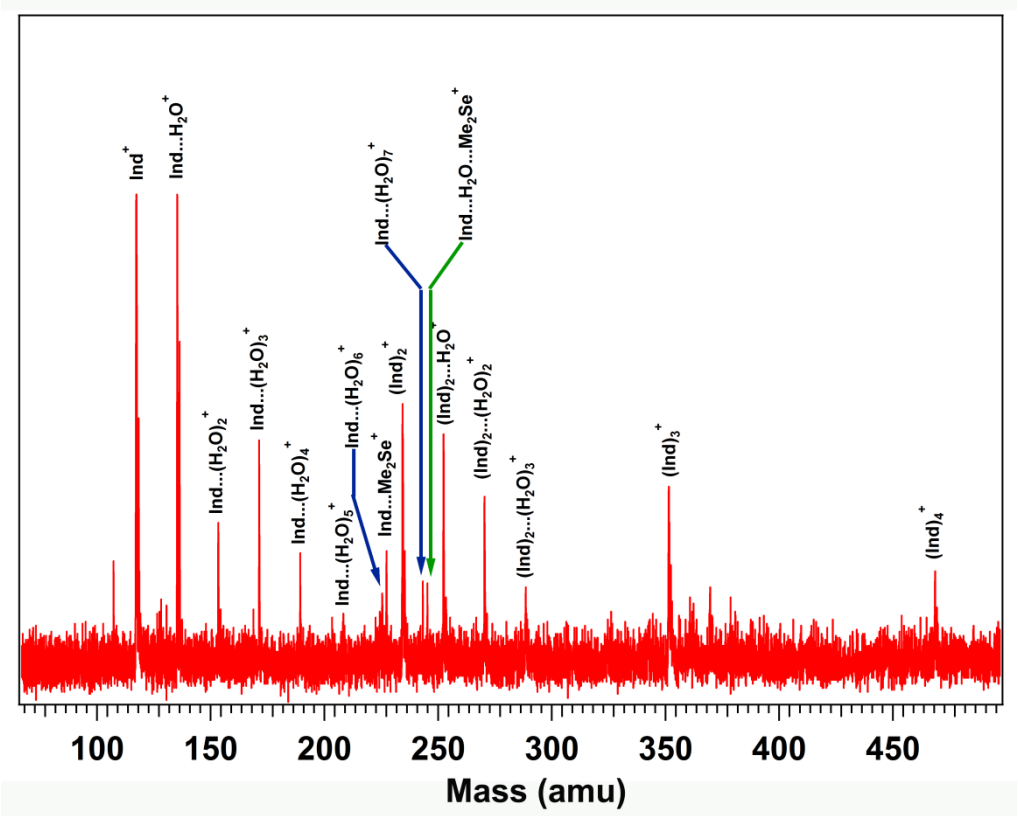

Figure 4.8: Time of flight (TOF) mass spectrum of indole in presence of water and dimethyl selenide (Me_2Se) by fixing the laser wavelength at 35118 cm^{-1}.

Figure 4.8 shows the mass spectrum of Ind…H_2O…Me_2Se trimeric complex, measured by fixing the excitation laser at 35118 cm^{-1}. The mass spectrum shows several other peaks apart from the trimeric complex peak. These peaks are due to complexes of indole with water or complexes of indole with dimethyl selenide. We observed several peaks in the mass spectrum which evolve due to the interaction of several water molecules with indole. We observed dimer, trimer, and tetramer of indole also. Ind…H_2O…Me_2Se complex was synthesized by supersonic expansion of mixed vapor of Indole (Ind), H_2O, and Me_2Se seeded in a He-Ne (30:70) carrier gas through a pulsed valve (General Valve, series 9, 10 Hz, 0.5 mm diameter) into a high vacuum chamber. The carrier gas (55 psig) mixed with Me_2Se (90+%, Alfa Aesar) and H_2O maintained at -78°C and 5°C, respectively, was passed through Indole (99%, Sigma Aldrich) heated at 75°C before the expansion through the orifice.

4.2.2.2 Electronic spectroscopy

A weakly bound 1:1:1 model complex of indole, dimethyl selenide, and water has been studied in the isolated gas phase using UV and IR laser-based spectroscopic techniques. Here, indole (Ind) and dimethyl selenide (Me_2Se) represents tryptophan (TRP) and selenomethionine (MSE) residues of the protein, respectively. Figure 4.9(a) shows an electronic spectrum measured in the mass channel of Ind…H_2O…Me_2Se complex employing 2C-R2PI spectroscopy. The electronic spectrum consists of several sharp but weak bands in the 35040-35200 cm^{-1} spectral region.

UV-UV hole-burning spectrum depicted in Figure 4.9 (b) has been recorded by probing the 35126 cm^{-1} band marked by a green asterisk in Figure 4.9 (a). The hole-burning spectrum shown in Figure 4.9 (b) indicates that all the electronic bands of Figure 4.9 (a) except the35118 cm^{-1} peak marked by a red asterisk belong to a single conformer of Ind…H_2O…Me_2Se complex. The UV-UV hole-burning spectrum presented in Figure 4.9 (c)

by probing the 35118 cm^{-1} band shows only its own depletion. Thus the 35118 cm^{-1}band presents in the electronic spectrum of Ind…H_2O…Me_2Se complex either belong to its

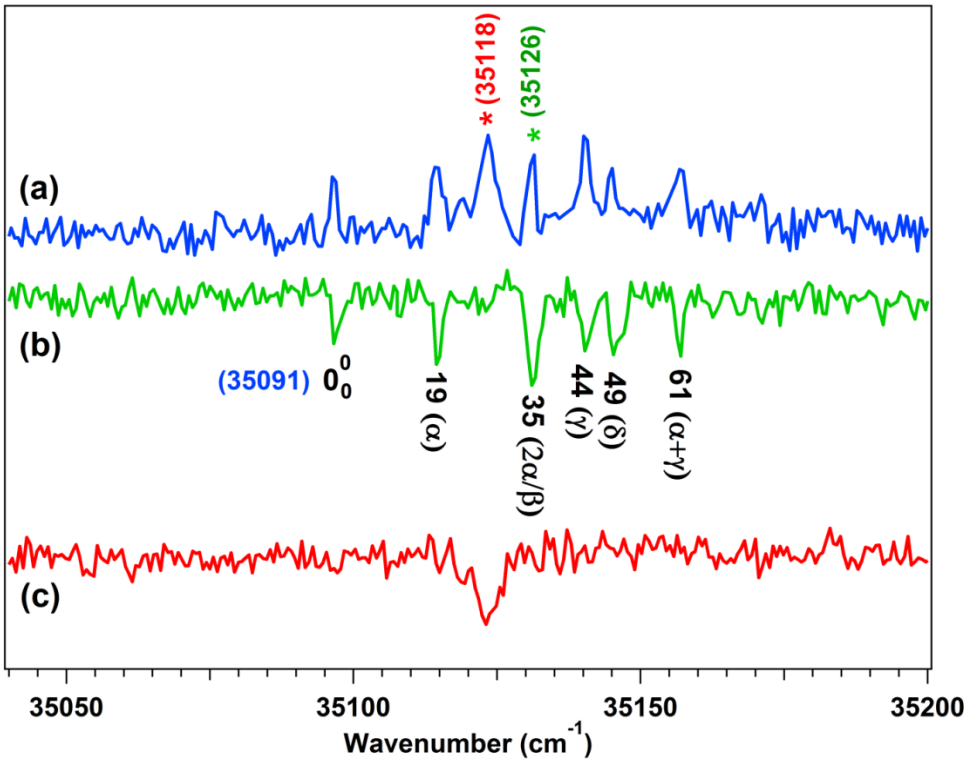

Figure 4.9: (a) Electronic spectrum measured in the Ind…H_2O…Me_2Se mass channel using 2C-R2PI spectroscopy. (b)-(c) UV-UV hole-burning spectra by fixing the probe UV laser at 35126 and 35118 cm^{-1} bands, respectively, marked by asterisks in the electronic spectrum shown in part (a). The low frequency bands riding on the origin band of Ind…H_2O…Me_2Se in Figure 4.7(b) are intermolecular vibration of the complex.

different conformer or higher order cluster fragmented into the trimer mass channel. Measurement of the IR spectra by probing one of the electronic bands of Ind…H_2O…Me_2Se and the 35118 cm^{-1} band in combination with quantum chemistry calculations can reveal the source of the single band observed in the hole-burning spectrum displayed in Figure 4.9 (c), and this has been discussed in the latter section. It should be noted that the electronic origin band for the $S_1 \leftarrow S_0$ transition of Ind…H_2O…Me_2Se trimeric complex (Figure 4.9 (b)), which appears at 35091 cm^{-1}, is red-shifted compared to that of the indole monomer and indole…H_2O complex by 132 and 150 cm^{-1}, respectively.[150] The low-frequency vibronic bands riding on the origin band of the trimeric complex (Figure 4.9 (b)) can be explained

tentatively in terms of fundamental, overtone and combination modes of intermolecular vibrations denoted as α, β, γ, and δ.

4.2.2.3 Conformational landscape of Ind…H_2O…Me_2Se and Ind…$(H_2O)_2$…Me_2Se complexes.

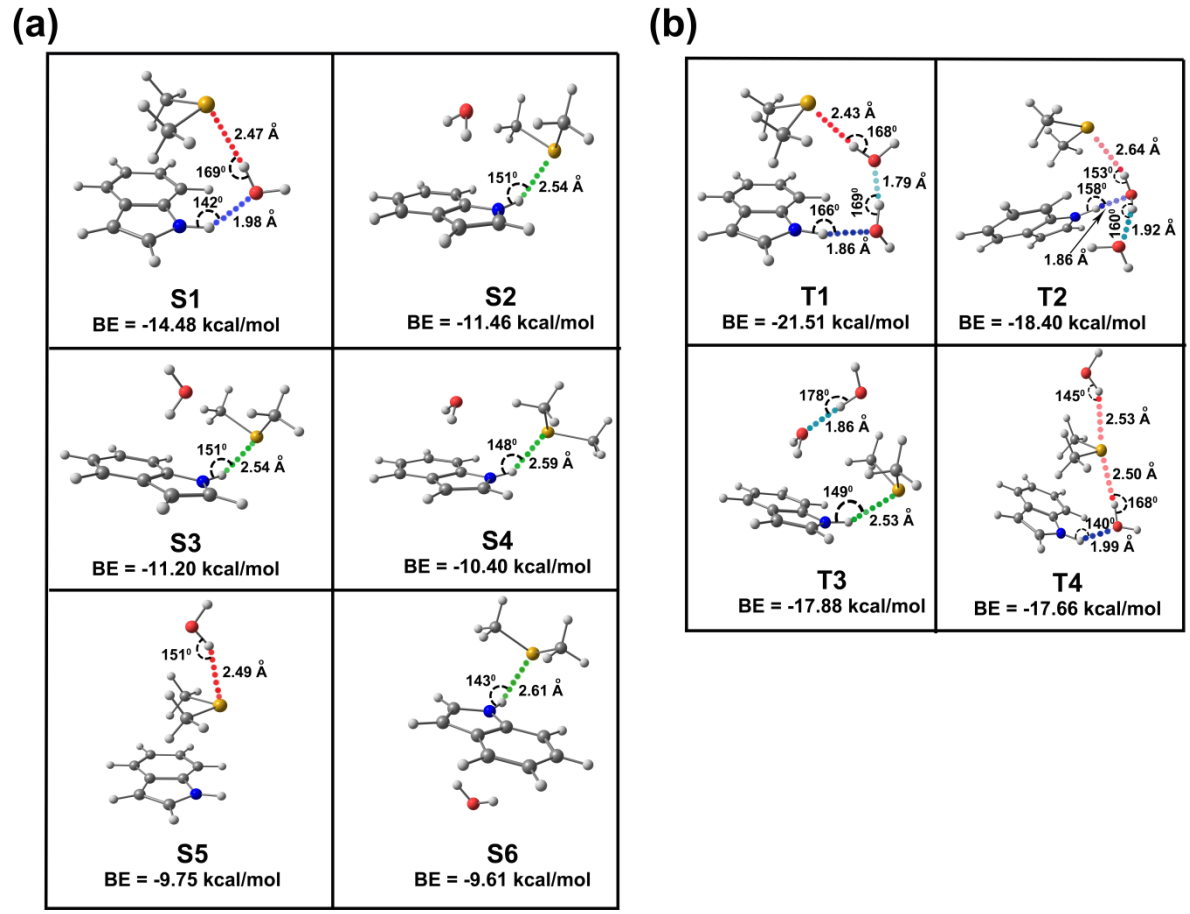

Figure 4.10: Various low energy conformers of (a) indole…H_2O…Me_2Se and (b) indole…$(H_2O)_2$…Me_2Se complexes optimized at the ωB97X-D/6-311++G(d,p) level of theory. Binding energy (BE) values are BSSE and zero point energy corrected.

Figure 4.10(a) and 4.10(b) shows various low energy conformers of Ind…H_2O…Me_2Se and Ind…$(H_2O)_2$…Me_2Se, respectively, optimized at the ωB97X-D/6-311++G(d,p) level of theory. BSSE and ZPE corrected binding energies, as well as selected hydrogen bond parameters of different conformers of these two complexes, are listed with the structures. Six low energy structures of Ind…H_2O…Me_2Se are reported in Figure 4.10(a). Interestingly, it

has been found that the most stable trimeric structure S1 mimics the single water bridge mediated Se hydrogen bonded structural motif observed in protein crystal structures. In the S1 structure, water acts as a hydrogen bond donor to Se as well as a hydrogen bond acceptor to the NH group of indole. The S1 structure of Ind…H_2O…Me_2Se resembles specifically the structural motif of single water bridge mediated hydrogen bonding interactions between MSE (residue number 83) and TRP (residue number 56) via H_2O (residue number 150) in a protein (PDB 3d5p, Figure 4.5(a)) named putative glucan synthesis regulator of SMI1/KNR4 family. It can be noted that Se…O, N…O distances and ∠N…O…Se in the PDB 3d5p (Figure 4.5(a)) are 3.34 Å, 2.99 Å, and 108.47°, respectively, while the same parameters in the S1 structure of Ind…H_2O…Me_2Se are 3.43 Å, 2.98 Å, and 105°, respectively. Thus the structural motif and hydrogen bond parameters for single water-mediated Se hydrogen bonding interaction in the trimeric model structure (S1) and the PDB 3d5p has a close resemblance.

Table 4.1 BSSE and ZPE corrected Binding energies (BE) of different conformers of the Ind…H_2O…Me_2Se complex calculated with different DFT functionals using the same basis set

Complexes	BE (kcal/mol)	
	ωB97X-D/6-311++G(d,p)	M06-2X/6-311++G(d,p)
S1	-14.48	-14.58
S2	-11.46	-11.56
S3[a]	-11.20	-11.55
S4	-10.40	-10.15
S5	-9.75	-9.86
S6	-9.61	-9.48

[a]S3 conformer converges to S2 after geometry optimization at the M06-2X/6-311++G(d,p) level of theory. Thus binding energy values are the same for S2 and S3 conformers at the M06-2X/6-311++G(d,p) level of theory.

The other higher energy structures (S2, S3, S4, S5, and S6) of Ind…H_2O…Me_2Se are not stabilized through a water bridge, and there is a direct interaction between indole and Me_2Se. Four low energy structures of Ind…$(H_2O)_2$… Me_2Se complex is listed in Figure 4.10(b). The most stable tetrameric structure is double water-bridge mediated Se hydrogen bonded structure denoted as T1 where indole and Me_2Se interact with each other through a double water bridge. Binding energy calculations of different conformers of the Ind…H_2O…Me_2Se and Ind…$(H_2O)_2$…Me_2Se complexes have been performed with different functionals as well as basis sets and a similar trend in the stability of various conformers has been observed (Table 4.1 and Table 4.2).

Table 4.2 BSSE and ZPE corrected Binding energies (BE) of different conformers of Ind…$(H_2O)_2$…Me_2Se complex calculated with different DFT functionals using the same basis set

Complexes	BE (kcal/mol)	
	ωB97X-D/6-311++G(d,p)	M06-2X/6-311++G(d,p)
T1	-21.51	-20.95
T2	-18.40	-18.52
T3	-17.88	-18.47
T4	-17.66	-18.19

4.2.2.4 IR spectroscopy of the complexes.

Figure 4.11(b) and 4.11(d) show IR spectra in the N-H and O-H stretching region by probing the 35126 cm^{-1} band (0-0 + 35 cm^{-1}) of the Ind…H_2O…Me_2Se complex and the 35118 cm^{-1} band, respectively, observed in the electronic spectrum presented in Figure 4.11(a). The two IR spectra are entirely different in terms of the number of bands, and this observation confirms that the 35118 cm^{-1} band cannot be due to a conformer of Ind…H_2O…Me_2Se trimer. The 35118 cm^{-1} band could be somewhat due to a higher order cluster. The IR

spectrum of indole monomer[186] in the N-H stretching region has been provided in Figure4.11(a) to compare the N-H stretching frequency of the complexes with the free N-H stretching frequency.

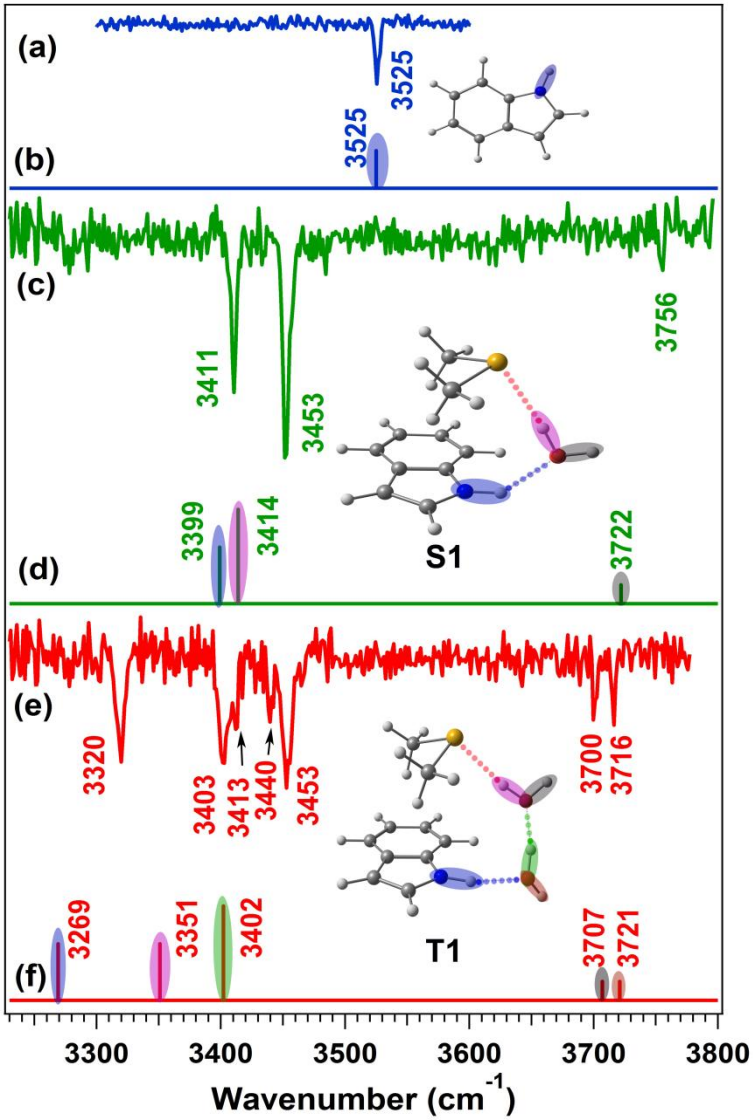

Figure 4.11: IR spectra of (a) indole (c) Ind…H_2O…Me_2Se and (e) Ind…$(H_2O)_2$…Me_2Se complexes measured using Resonant Ion Dip Infrared (RIDIR) spectroscopy. (b), (d) and (f) Theoretical scaled IR stick spectra of indole monomer, Ind…H_2O…Me_2Se (S1) and Ind…$(H_2O)_2$…Me_2Se (T1) complexes, respectively, calculated at the ωB97X-D/6-311++G(d,p) level of theory. Scaling factors of 0.9463 and 0.9378 have been used to correct the harmonic NH and OH stretching frequencies, respectively (see the computational method section). Assignment of the IR bands is shown through color code provided in the theoretical IR spectra as well as the optimized structures.

Figure 4.11(d) and 4.11(f) shows theoretical harmonic scaled IR spectra of the most stable structures of the Ind…H_2O…Me_2Se (S1) and Ind…$(H_2O)_2$…Me_2Se (T1) complexes, respectively, obtained at the ωB97X-D/6-311++G(d,p) level of theory. The global minimum structures of the Ind…H_2O…Me_2Se (S1) and Ind…$(H_2O)_2$…Me_2Se (T1) complexes are provided with the theoretical IR spectra in Figure 4.11(d) and 4.11(f), respectively. The N-H and O-H groups in the structures of the complexes and the corresponding theoretical IR bands are marked with specific colors for a clear understanding of the assignment of the experimental IR bands of the complexes. There is a reasonably good agreement of the experimental IR spectra presented in Figure 4.11(c) and 4.11(e) with the theoretical IR spectra of Ind…H_2O…Me_2Se (S1) and Ind…$(H_2O)_2$…Me_2Se (T1) complexes, respectively, shown in Figure 4.11(d) and 4.11(f).

A comparison of the experimental IR spectra of Ind…H_2O…Me_2Se and Ind…$(H_2O)_2$…Me_2Se with the theoretical scaled IR spectra of their various structures is shown in Figures 4.12 and 4.13, respectively. It is quite clear from the Figures 4.12 and 4.13 that the theoretical IR spectra of only the S1 structure of Ind…H_2O…Me_2Se and the T1 structure of Ind…$(H_2O)_2$ …Me_2Se corroborate with the experimental IR spectra. IR spectra of all the structures of the trimeric and tetrameric complexes are also calculated at the M06-2X/6-311++G(d,p) level of theory. Figures 4.14 and 4.15 show a comparison of the experimental IR spectra of the Ind…H_2O…Me_2Se and Ind…$(H_2O)_2$ …Me_2Se complexes, respectively, with the theoretical scaled IR spectra of all the structures calculated at the ωB97X-D/6-311++G(d,p) and M06-2X/6-311++G(d,p) levels of theory. Interestingly, there is a similar trend in the calculated frequencies obtained at both the levels of theory and thus the assignment of the observed trimeric and tetrameric complexes to the S1 and T1 structures, respectively, is unequivocal.

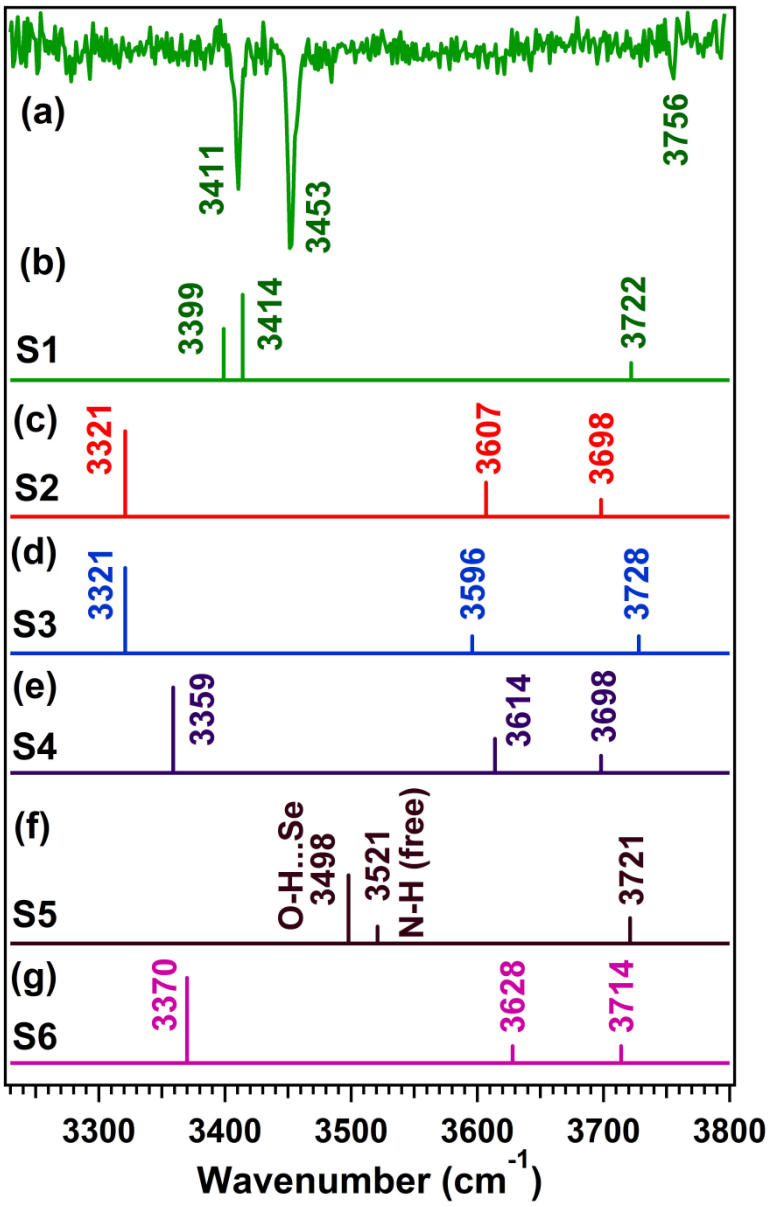

Figure 4.12: Comparison of experimental IR spectrum of Ind…H_2O…Me_2Se complex with ωB97X-D/6-311++G(d,p) level calculated scaled IR spectra of different structures (S1, S2, S3, S4, S5, S6) of Ind…H_2O…Me_2Se. Scaling factors of 0.9463 and 0.9378 have been used to correct the harmonic NH and OH stretching frequencies, respectively (see the computational method section). The harmonic NH stretching frequency in the complex is scaled with respect to the experimental NH stretching frequency (3525 cm^{-1}) of bare indole[150] while the harmonic OH stretching frequency in the complex is scaled with respect to the experimental symmetric OH stretching frequency (3657 cm^{-1}) of bare water[149].

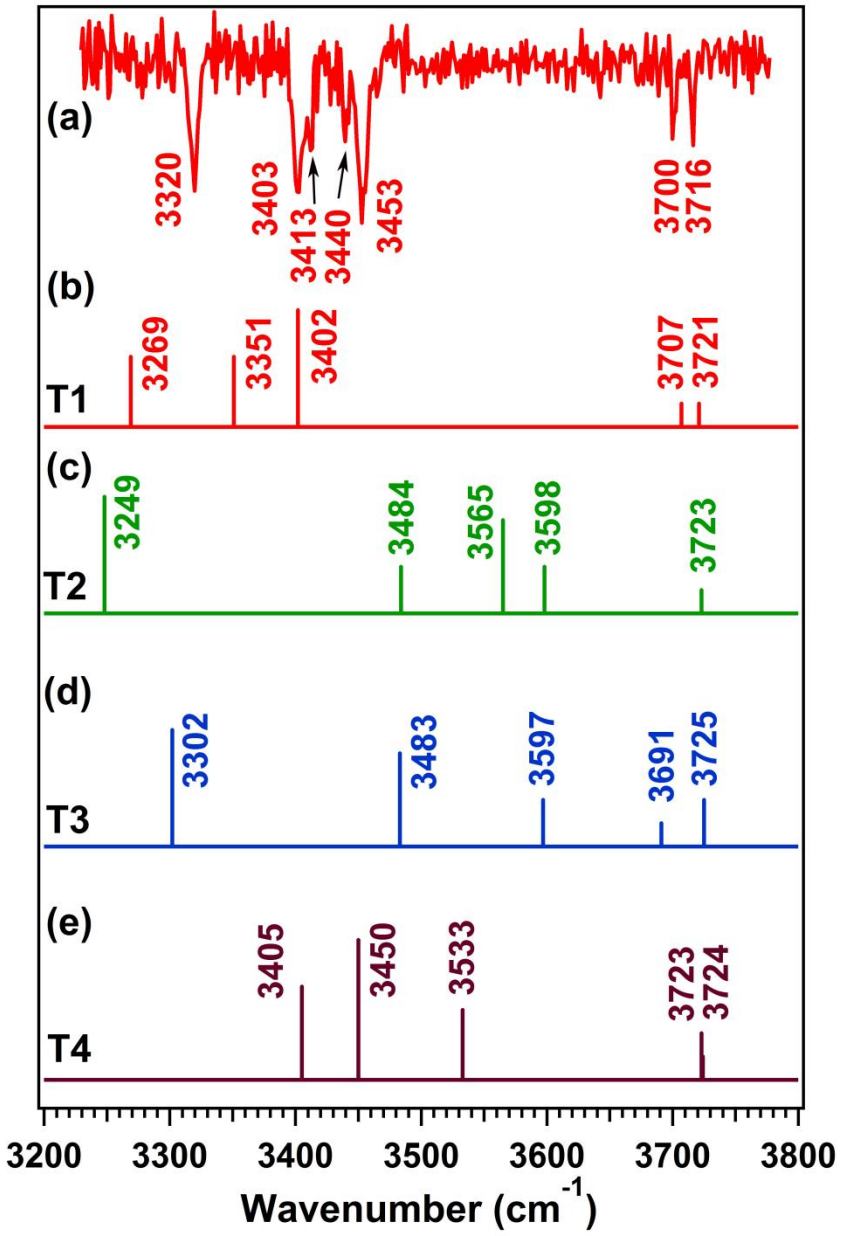

Figure 4.13: Comparison of experimental IR spectrum of Ind…$(H_2O)_2$…Me_2Se complex with ωB97X-D/6-311++G(d,p) level calculated scaled IR spectra of different structures (T1, T2, T3, T4) of Ind…$(H_2O)_2$…Me_2Se. Scaling factors of 0.9463 and 0.9378 have been used to correct the harmonic NH and OH stretching frequencies, respectively (see the computational method section). The harmonic NH stretching frequency in the complex is scaled with respect to the experimental NH stretching frequency (3525 cm^{-1}) of bare indole[1] while the harmonic OH stretching frequency in the complex is scaled with respect to the experimental symmetric OH stretching frequency (3657 cm^{-1}) of bare water[2].

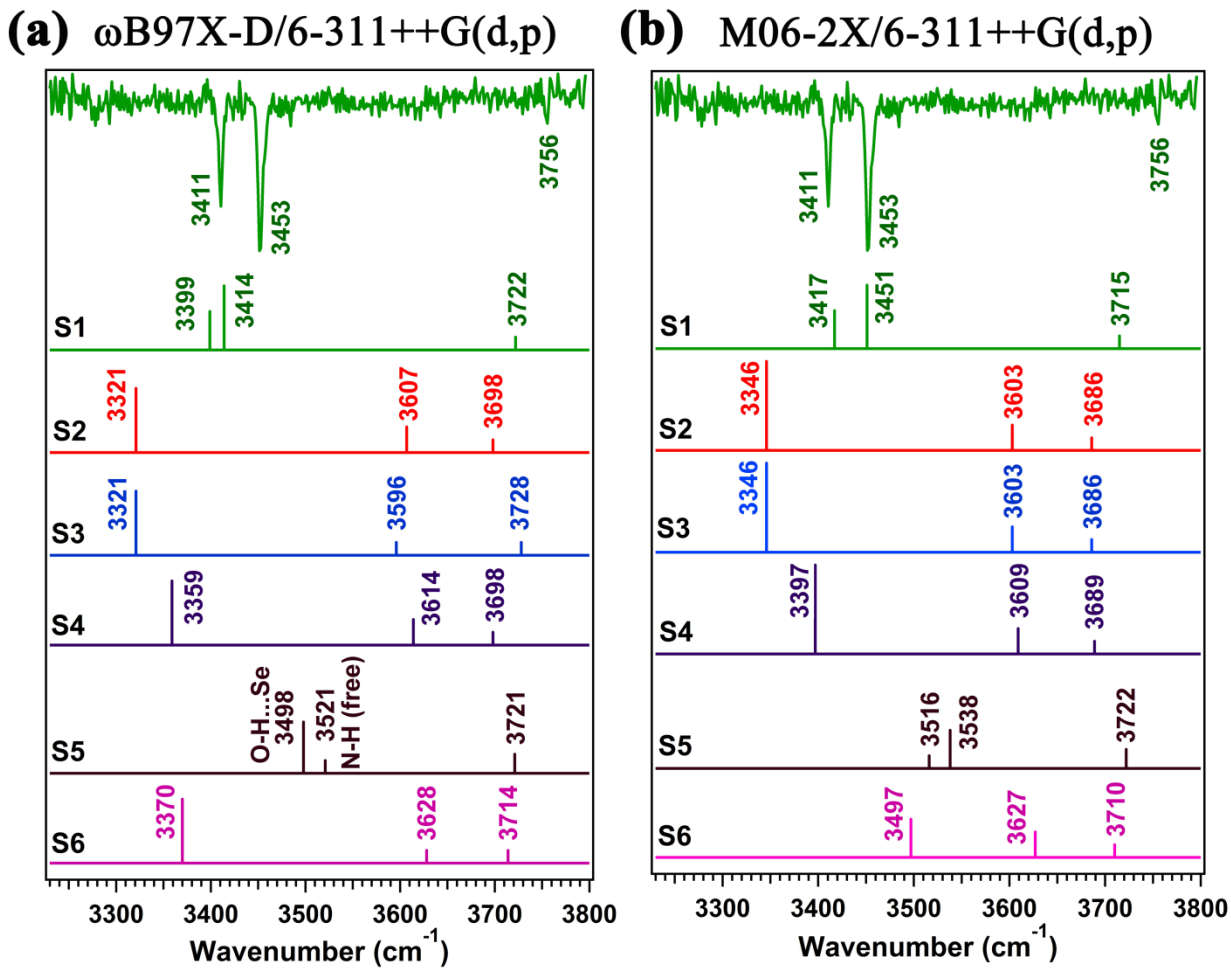

Figure 4.14: Comparison of the experimental IR spectrum of the Ind…H_2O…Me_2Se complex with the theoretical scaled IR spectra of its different structures calculated at the (a) ωB97X-D/6-311++G(d,p) and (b) M06-2X/6-311++G(d,p) levels of theory. Scaling factors of 0.9463 and 0.9378 have been used to correct the harmonic NH and OH stretching frequencies, respectively, at the ωB97X-D/6-311++G(d,p) level of theory. Scaling factors used for the harmonic NH and OH stretching frequencies at the M06-2X/6-311++G(d,p) level of theory are 0.9503 and 0.9398, respectively.

In Figure 4.11(b), the 3756 cm^{-1} band is assigned to the free O-H freq of H_2O of Ind…H_2O…Me_2Se complex while the 3453 cm^{-1} and 3409 cm^{-1} bands are assigned to hydrogen bonded OH (O-H…Se) of H_2O and N-H (N-H…O) of indole, respectively. A red-shift of 303 cm^{-1} in the O-H stretch frequency of the O-H…Se hydrogen bond with respect to that of the free O-H indicates the presence of a very strong hydrogen bond interaction there. The N-H stretch frequency of indole in this trimeric complex is red-shifted by 114 cm^{-1}

compared to that of the indole monomer while the red-shift in the N-H stretch frequency in indole…H_2O complex[150] is reported to be 89 cm^{-1}. The stronger N-H…O interaction in the

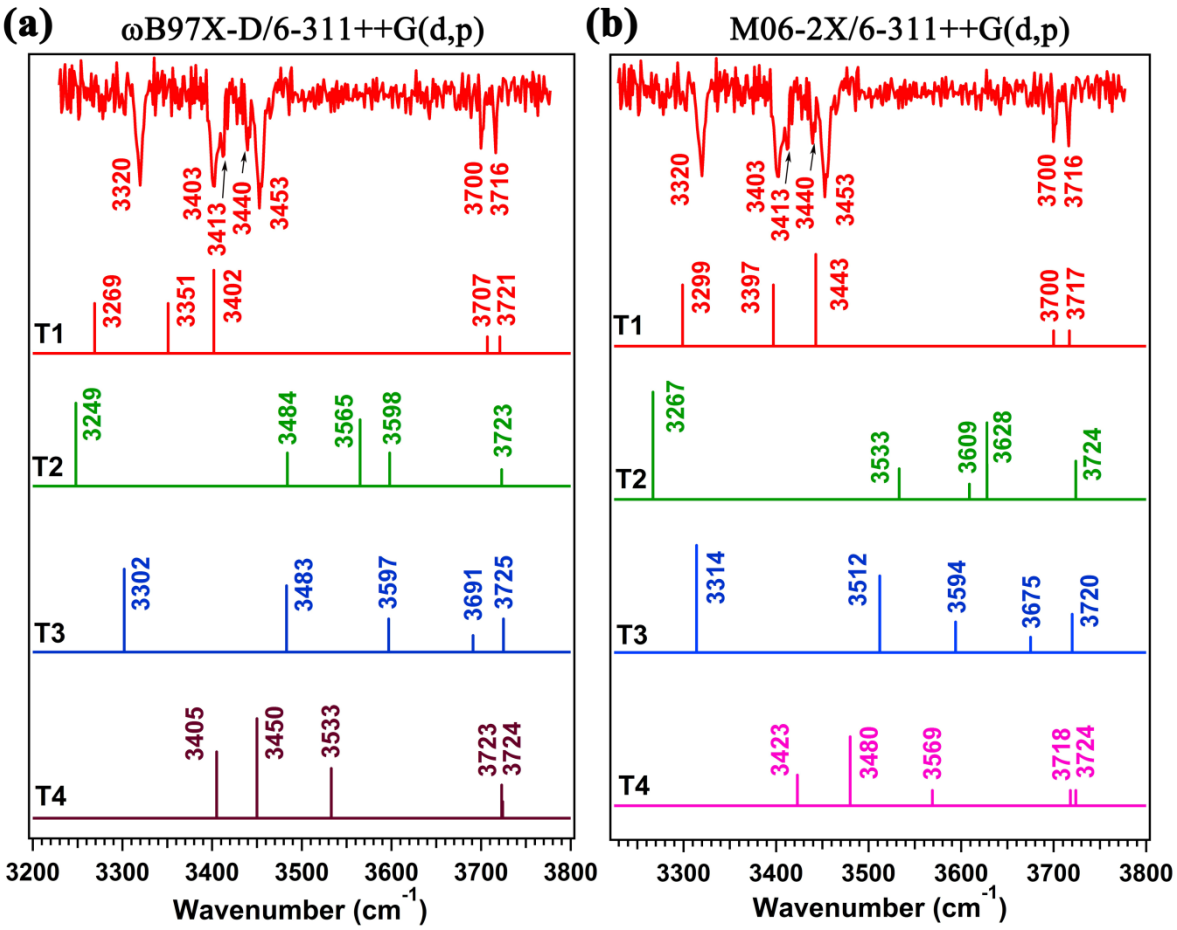

Figure 4.15: Comparison of the experimental IR spectrum of the Ind…H_2O…Me_2Se complex with the theoretical scaled IR spectra of its different structures calculated at the (a) ωB97X-D/6-311++G(d,p) and (b) M06-2X/6-311++G(d,p) levels of theory. Scaling factors of 0.9463 and 0.9378 have been used to correct the harmonic NH and OH stretching frequencies, respectively, at the ωB97X-D/6-311++G(d,p) level of theory. Scaling factors used for the harmonic NH and OH stretching frequencies at the M06-2X/6-311++G(d,p) level of theory are 0.9503 and 0.9398, respectively.

Ind…H_2O…Me_2Se complex compared to that in the indole…H_2O complex could be due to co-operative nature of the hydrogen bond interaction as the water molecule in Ind…H_2O…Me_2Se is engaged in hydrogen bonding interaction with both indole and Me_2Se. In the case of Ind…$(H_2O)_2$…Me_2Se, two free OH groups of the two water molecules appear at 3716 (asymmetric stretch- free OH of indole bound water) and 3700 cm^{-1} (asymmetric

stretch free OH of Me_2Se bound water). On the other hand, stretching frequencies of the two hydrogen-bonded bridged OH groups (O-H…Se and O-H…O) of two water molecules are strongly coupled with each other and appear at 3403 and 3453 cm^{-1}, respectively.

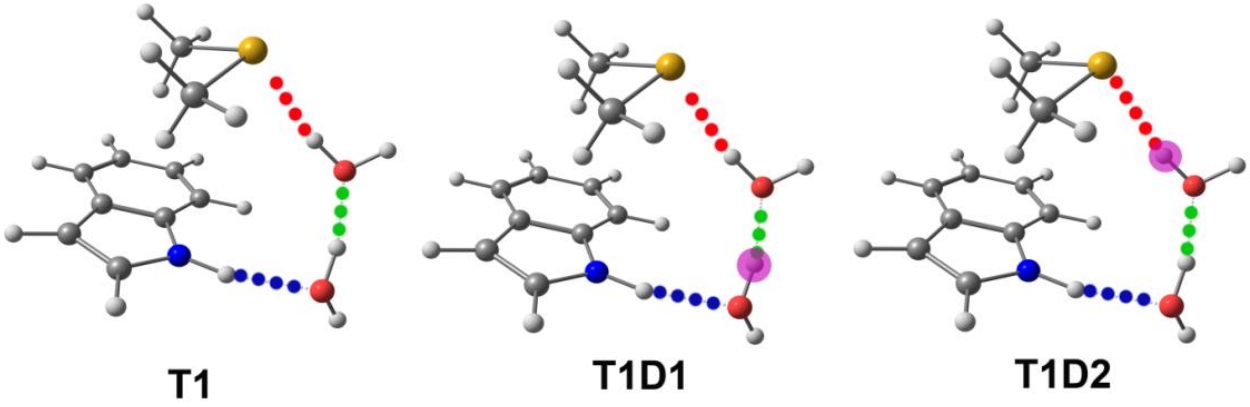

Figure 4.16: ωB97X-D/6-311++G(d,p) level optimized geometries of T1, T1D1 and T1D2 structures of Ind…$(H_2O)_2$…Me_2Se. Hydrogen atom of water molecule marked by pink circle is replaced by deuterium in T1D1 and T1D2. All other geometrical parameters of T1D1 and T1D2 are same as of T1.

Assignment of these two O-H groups held together by a strongly hydrogen bonded bridge is performed by theoretical calculation of deuterated complexes by replacing at a time one of the bridging hydrogens of the two water molecules in the T1 structure of Ind…$(H_2O)_2$…Me_2Se complex (Figure 4.16, Table 4.5 and Figure 4.17). Broadening of the two bands at 3403 and 3453 cm^{-1} and appearance of additional two weak bands at 3413 and 3440 cm^{-1} could be due to strong coupling of the hydrogen-bonded bridged OH vibrations which are close in frequencies.[187,188]

Both the experimental and the theoretical IR spectra as well as the energetics of different conformers of Ind…H_2O…Me_2Se and Ind…$(H_2O)_2$…Me_2Se confirm the observation of S1 and T1structures, respectively, in the experiment. Our spectroscopic studies on model complex Ind…H_2O…Me_2Se demonstrate the finding of single water-mediated Se hydrogen-bonded structural motif (S1 structure) which is abundant in the PDB.

Table 4.3 Unscaled theoretical N-H and O-H stretching frequency values in T1, T1D1 and T1D2 geometries of Ind…$(H_2O)_2$…Me_2Se. The values in parentheses against each vibrational frequency indicate the intensity (Int) of that particular vibration. Frequency values are in cm^{-1} whereas intensity values are in km/mol.

Parameters	T1 Frequency(Int)	T1D1 Frequency(Int)	T1D2 Frequency(Int)
ν_{N-H}	3455 (599)	3461 (692)	3456 (705)
ν_{O-H} (OH…Se)	3573 (1119)	3590 (814)	-
ν_{O-H} (OH…O)	3628 (317)	-	3611 (540)
ν_{O-H} (free) (Me_2Se bound water)	3953 (95)	3952 (97)	3949 (67)
ν_{O-H} (free) (Indole bound water)	3968 (85)	3963 (53)	3968 (88)
ν_{O-D} (OD…Se)	-	-	2613 (425)
ν_{O-D} (OD…O)	-	2626 (294)	-

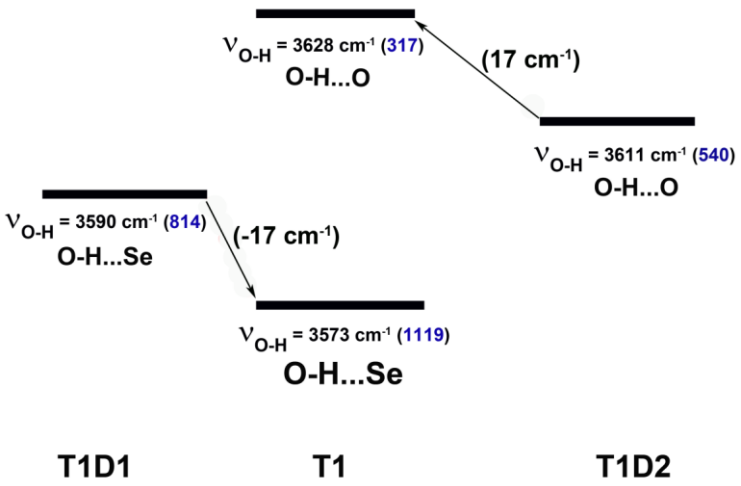

Figure 4.17: Unscaled theoretical ν_{O-H} (O-H…Se) in T1D1 (leftmost) and ν_{O-H} (O-H…O) in T1D2 (rightmost). Due to coupling of these two O-H vibrations in T1, ν_{O-H} (O-H…Se) is decreased by 17 cm^{-1} whereas ν_{O-H} (O-H…O) is increased by 17 cm^{-1}. The value in parenthesis against each vibrational frequency indicates the intensity of that particular vibration. Intensity values are in km/mol. Note that after coupling, intensity of ν_{O-H} (O-H…Se) increases whereas intensity of ν_{O-H} (O-H…O) decreases.

4.2.2.5 Natural Bond Orbital (NBO) analysis

NBO 2nd order perturbation energy ($E^{(2)}$) between the lone pair orbitals of the hydrogen bond acceptor atom (Y) and antibonding sigma orbital of the hydrogen bond donor group X-H) is a measure of the strength of an X-H…Y hydrogen bond. Figure 4.18 shows the ωB97X-D/6-311++G(d,p) level calculated $E^{(2)}$values of the hydrogen bonds present in the S1 structure of

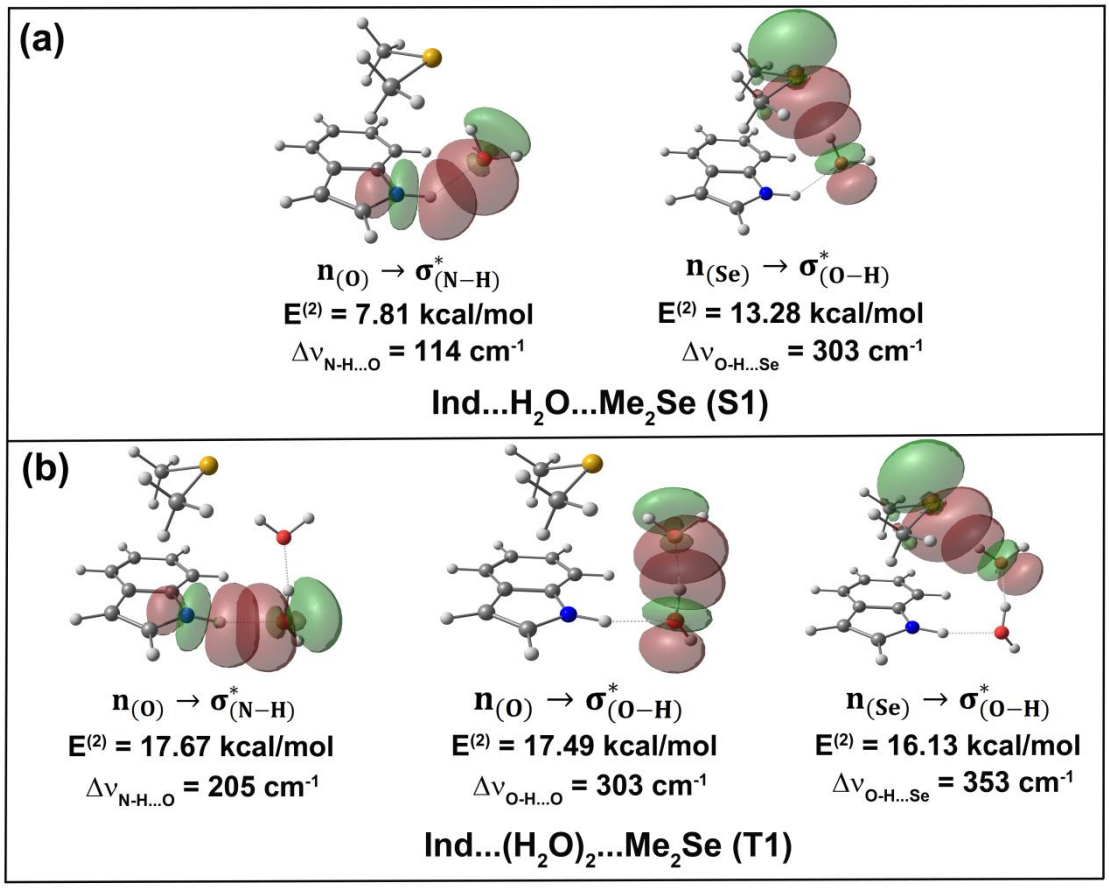

Figure 4.18: NBO views for the hydrogen bonds present in the (a) S1 structure of Ind…H_2O…Me_2Se (N-H…O, O-H…Se) and (b) T1 structure of Ind…$(H_2O)_2$…Me_2Se (N-H…O, O-H…O, O-H…Se) complexes calculated at the ωB97X-D/6-311++G(d,p) level of theory. Red-shift values in the X-H stretching frequency ($\Delta\nu_{X-H}$) of the hydrogen bonds present in the trimer and the tetramer are also provided in the figure.

Ind…H_2O…Me_2Se (N-H…O, O-H…Se) and the T1 structure of Ind…$(H_2O)_2$…Me_2Se (N-H…O, O-H…O, O-H…Se) complexes. The red-shift ($\Delta\nu_{X-H}$) values in the X-H stretching frequencies of all the hydrogen bond interactions present in the trimer and tetramer

complexes are provided with corresponding $E^{(2)}$values. Both $\Delta\nu_{X\text{-}H}$ and $E^{(2)}$ values demonstrate that Se-centered hydrogen bond is of similar strength to O-centered hydrogen bond. It is intriguing to note that the $E^{(2)}$ values for the O-H…Se and N-H…O hydrogen bonds in the S1 structure of Ind…H_2O…Me_2Se complex and the PDB structure (ID: 3D5P, Figure 4.5) of a putative glucan synthesis regulator protein is similar.

4.2.2.6 Energy decomposition analysis (EDA)

EDA of the S1 structure of Ind…H_2O…Me_2Se and T1 structure of Ind…$(H_2O)_2$…Me_2Se is performed to find out different components of the total interaction energies which contribute to the stability of these complexes. EDA calculations have been performed using LMO and RVS methods. In the LMO-EDA method, total interaction energy ($\Delta E_{\mathrm{TOTAL}}$) is decomposed according to the following equation: $\Delta E_{TOTAL} = \Delta E_{ES} + \Delta E_{EX} + \Delta E_{REP} + \Delta E_{POL} + \Delta E_{DISP}$, where ΔE_{ES}, ΔE_{EX}, ΔE_{REP}, ΔE_{POL}, and ΔE_{DISP} stand for electrostatic, exchange, repulsion, polarization and dispersion interactions, respectively. [189] On the other hand, the form of the RVS-EDA interaction energy ($\Delta E_{\mathrm{TOTAL}}$) partitioning is: $\Delta E_{TOTAL} = \Delta E_{ESX} + \Delta E_{POL} + \Delta E_{CT} + \Delta E_{MIX}$, where ΔE_{ESX} term is equal to the sum of the electrostatic and exchange terms.[190] A number of other schemes apply this reduction of terms, including the ALMO and BLW EDA schemes.[191] ΔE_{POL} and ΔE_{CT} are the polarization and charge transfer components, respectively. The mixing component, ΔE_{MIX}, of the RVS-EDA, is the residual energy due to counterpoise (CP) correction. As RVS-EDA is performed at the HF level, it does not include any dispersion component of the interaction energy.

EDA calculation is also useful to underpin the origin of the strength of the hydrogen bond,i.e., the red-shift in the X-H stretch frequency of an X-H…Y hydrogen bond. As we have found from IR spectroscopy and NBO analysis that Se-centered hydrogen bond is as strong as any conventional hydrogen bond, we have compared the components of the

interaction energies of the most stable conformer of Ind…H_2O…Me_2X as well as Ind…$(H_2O)_2$…Me_2X by varying X from O to S and Se. The components of the total interaction energies of these complexes obtained from the LMO-EDA method are provided in Table 1. It is found for both the trimeric and tetrameric complexes that the electrostatic component (ΔE_{ES}) is significantly smaller in the complexes of Me_2S and Me_2Se compared to that in the complex of Me_2O. However, the percentage of the polarization component (%POL) of the total interaction energy increases appreciably as we move from the complexes of Me_2O to Me_2S and Me_2Se (Table 1). It is also evident from Table 1 that the percentage of the dispersion component (% DISP) of the total interaction energy is higher in the Me_2S and Me_2Se complexes compared to that in the Me_2O complexes

Table 4.4 Decomposition of the total interaction energies (kcal/mol) of the most stable conformer of Ind…H_2O…Me_2X as well as Ind…$(H_2O)_2$…Me_2X (X=O, S, Se) using LMO-EDA method at the B3LYP/6-31G level of theory.

Complexes	ΔE_{ES}	ΔE_{EX}	ΔE_{REP}	ΔE_{POL}	ΔE_{DISP}	ΔE_{TOTAL}	% POL[a]	% DISP[a]
Ind…H_2O…Me_2O	-30.83	-14.70	53.09	-11.40	-10.69	-14.52	78.51	73.62
Ind…H_2O…Me_2S	-25.41	-12.86	46.83	-9.88	-9.87	-11.20	88.21	88.12
Ind…H_2O…Me_2Se	-24.62	-12.79	46.58	-9.83	-9.82	-10.52	93.44	93.35
Ind…$(H_2O)_2$…Me_2O	-55.22	-27.26	92.44	-23.38	-15.67	-29.09	80.37	53.86
Ind…$(H_2O)_2$…Me_2S	-47.74	-24.03	81.80	-20.17	-14.44	-24.58	82.05	58.76
Ind…$(H_2O)_2$…Me_2Se	-46.76	-23.84	81.17	-20.00	-14.32	-23.76	84.17	60.26

[a]%POL and %DISP represent the percentage contribution of the polarization and dispersion components, respectively, in total interaction energy.

To know about the contribution of the CT component to the total interaction energies of the complexes, RVS-EDA has been performed. Table 2 shows the components of the interaction energies of the complexes obtained by RVS-EDA method. It is intriguing to note that moving from the complexes of Me_2O to Me_2S and Me_2Se, the percentage contribution of

coulomb/exchange (%ESX) in total interaction energy decreases while percentage contribution of charge transfer (%CT) increases significantly. Thus LMO-EDA and RVS-EDA calculations demonstrate that the strength of the S- and Se- centered hydrogen bonds in terms of the IR red-shift in the stretching frequency of the hydrogen bond donor could be due to the significant contribution of the charge transfer component apart from the electrostatic and polarization interactions present there. A similar explanation has been provided for the strong Se hydrogen bond in indole…Me_2Se and phenol…Me_2Se complexes reported in the literature.[192] Dey and co-workers have also reported that the IR red-shift in the stretching frequency of the hydrogen bond donor is governed by electrostatic, polarization and charge transfer components of the interaction energy while the overall stability of the complexes is controlled by the dispersion energy.[117]

Table 4.5 Decomposition of the interaction energies (kcal/mol) of the most stable conformer of Ind…H_2O…Me_2X as well as Ind…$(H_2O)_2$…Me_2X (X=O, S, Se) obtained with 6-31G basis set using RVS-EDA method

Complexes	ΔE_{ESX}	ΔE_{POL}	ΔE_{CT}	ΔE_{TOTAL}	% ESX[a]	% POL[a]	% CT[a]
Ind…H_2O…Me_2O	-5.14	-4.38	-4.72	-14.96	34.36	29.28	31.95
Ind…H_2O…Me_2S	-1.33	-3.12	-4.44	-9.49	14.01	32.88	46.79
Ind…H_2O…Me_2Se	-0.47	-2.92	-4.63	-8.62	5.45	33.87	53.71
Ind…$(H_2O)_2$…Me_2O	-9.20	-8.62	-8.60	-27.80	33.09	31.01	30.94
Ind…$(H_2O)_2$…Me_2S	-5.57	-6.58	-7.94	-21.21	26.26	31.02	37.44
Ind…$(H_2O)_2$…Me_2Se	-4.64	-6.30	-8.09	-20.15	23.03	31.26	40.15

[a]%ESX, %POL, and %CT represent percentage contribution of the Coulomb/exchange, polarization and charge transfer components, respectively, in total interaction energy.

4.3 Conclusion

Single water-mediated Se hydrogen bonding interactions in proteins have been investigated by PDB analysis and gas phase spectroscopy coupled with the quantum chemical calculation

of model complexes consisting of indole, dimethyl selenide, and H_2O. In an analysis of protein structures deposited in the PDB, Se hydrogen bonding between two or more amino acid residues through water bridges is found in abundance, ~2.5 bridged interaction per PDB entry on average. Binding energy and NBO calculations of the water-bridged amino acid residues of a few PDB structures demonstrate that single water-mediated Se hydrogen bonding interactions can contribute significantly to the stability of the proteins. Mass-selected electronic and IR spectroscopy of the model complex indole…H_2O…dimethyl selenide qualitatively mimics the nature, motif, and energetics of single water-mediated Se hydrogen bonding interactions present in protein structures. Interestingly, the number of Se-hydrogen bonds involving water bridges is more abundant than direct Se-amino acid hydrogen bonds in the PDB. Various energy decomposition analysis methods of the total interaction energy of the complexes demonstrate that charge transfer interaction plays a significant role in the strength of the S and Se centered hydrogen bonds in terms of the IR red-shift in the stretching frequency of the hydrogen bond donor. The present work, for the first time, reports a systematic PDB analysis of this water-mediated Se hydrogen bonding interactions in proteins and understanding this interaction through the spectroscopic study of a model complex.

Chapter 5

Observation of strong hydrogen-bond involving unconventional hydrogen bond donor as well as acceptor atoms

5.1 Introduction

We have already discussed in the previous chapters that hydrogen bond is one of the most important non-covalent interactions which governs the structures and functions of biomolecules.[1,2,4,7] Hydrogen-bond is generally denoted as X-H…Y, where X-H is a hydrogen bond donor and Y, is a hydrogen bond acceptor. Despite being a century old concept,[44] it is still the most enthralling topic of research among the scientific community. It is well known that O, N, and F act as conventional strong hydrogen-bond donors and acceptors due to their small size and high electronegativity. The nature and strength of O-H…O, N-H…O, N-H…N, O-H…N hydrogen bonds have been studied and documented very well in the literature. Later, it has been observed that apart from these highly electronegative atoms, less electronegative atoms can also act as hydrogen bond donors and acceptors which are denoted as unconventional ones. It has also been reported and documented in the literature that π-electron cloud can also act as a hydrogen bond acceptor. Unconventional hydrogen-bonds such as C-H…O, C-H…N, O-H…π, N-H…π and C-H…π are widely present in biomolecules and materials.

Following the recent re-definition of the hydrogen-bond by the IUPAC committee,[111] there is a growing interest in the scientific committee to search for a further different type of atoms, in the periodic table, which can form a hydrogen-bond. As per the recent re-definition of the hydrogen-bond X-H…Y, X should be more electronegative than H while Y could be any other atom in the periodic table.[111] Biswal and co-workers have extensively studied S-centered hydrogen-bond through isolated gas phase experiment and reported that S forms hydrogen bond of similar strength as compared to O when it is used as a hydrogen-bond acceptor.[113-115,185] Kjaergard and co-workers have also reported from gas phase FTIR spectroscopy study that N-H…S and N-H…O are of similar strength.[116] Kjaergaard, and co-workers also reported that positively charged phosphorus (P) can act as a potential hydrogen-

bond acceptor although both hydrogen and phosphorus have similar electronegativity.[105] Very recently, Biswal and co-workers[104], as well as Das and co-workers194, have reported that selenium (Se) centered hydrogen bond with Se as a hydrogen-bond acceptor is as strong as S and O centered hydrogen bonds.

Most of the unconventional hydrogen bonds reported in the literature deal with unconventional hydrogen bond acceptor atoms while the hydrogen bond donor is the conventional one, i.e., N-H, O-H, etc. Hydrogen-bond involving unconventional hydrogen-bond donor is mostly limited to C-H…Y hydrogen-bond where Y is generally a conventional hydrogen bond acceptor. However, the spectroscopic study of unconventional hydrogen-bond involving unconventional hydrogen-bond donor as well as acceptor atoms is sparse in the literature. Biswal and co-workers reported that S-H…π interaction is as strong as O-H…π interaction.[193] Bhattacherjee and co-workers[194] studied S-H…S hydrogen bond in H_2S dimer using VUV ionization detected IR pre-dissociation spectroscopy method. They observed 31 cm^{-1} red-shift in the S-H…S bound S-H stretching frequency compared to the free S-H stretching frequency in H_2S dimer. They further reported a red-shift of 46 cm^{-1} in the S-H stretching frequency in 1:1 complex of H_2S and diethyl ether.[19] Robertson and co-workers[195] showed that S can act as a hydrogen bond donor. They studied the complexes of 2-phenylethanethiol (PET) with water and diethyl ether (DEE) and observed a red-shift of 9 cm^{-1} in the PET…H_2O complex and 24 cm^{-1} in the PET…DEE complex. They reported that S is a weak hydrogen bond donor as compared to O because the former one is less electronegative than the latter one. Very recently, Arunan and co-workers[196] reported from microwave study that H_2S dimer is hydrogen bonded and its geometry is similar to that of the H_2O dimer. Interestingly, S-H...S hydrogen bonding has been observed in protein crystal structures.[197,198] It has been found that cysteine acts as a hydrogen bond donor and form S-H...S hydrogen bond with methionine and cysteine.

In this work, we have studied unconventional hydrogen bonds (S-H…S and S-H…Se) having both unconventional hydrogen bond donor and acceptor atoms using isolated gas phase and quantum chemistry calculations. More specifically, we have investigated hydrogen-bond interaction in 1:1 complex of 2-chlorothiophenol (2-CTP) with dimethyl sulfide (Me_2S) and dimethyl selenide (Me_2Se) employing R2PI, UV-UV hole-burning, and RIDIR spectroscopy. We could not perform the experiment with thiophenol (TP) as it has extremely short lifetime in the excited state.[199-201] According to common wisdom, the hydrogen-bond interaction should be quite weak when both hydrogen bond donor and acceptor atoms are weakly electronegative. However, it is quite surprising that both S-H…S and S-H…Se hydrogen-bond interactions observed in our experiment are as strong as O-H…S and N-H...S interactions or even any conventional hydrogen bond, i.e., N-H...N, N-H...O, etc.

5.2 Results and discussion

5.2.1 Time of Flight (TOF) mass spectra of 2-CTP...Me_2S and 2-CTP…Me_2Se complexes

2-CTP…Me_2S and 2-CTP…Me_2Se complexes were synthesized by the supersonic expansion of mixed vapor of 2-CTP, and Me_2S/Me_2Se seeded in He (30%)-Ne (70%) carrier gas of 50 Psig. 2-CTP was heated to 65^0 C to generate sufficient vapor pressure while Me_2S and Me_2Se were cooled to -78^0Cby keeping them in dry ice. Figure 5.1a shows a mass spectrum of the 2-CTP…Me_2S complex measured by 1C-R2PI spectroscopy by fixing the laser wavelength at 34529 cm^{-1}, which is the electronic origin band of the complex. The mass peak at 124 a.m.u. is due to the dimer complex of dimethyl sulfide whereas the 260 a.m.u. mass peak belongs to 2-CTP…$(Me_2S)_2$ trimer. The mass peak at 208 a.m.u. corresponds to the 2-CTP…Me_2S complex formed in the supersonic jet.

Figure 5.1b shows the mass spectrum of 2-CTP…Me_2Se complex. The mass spectrum shows

multiple peaks. The peak at 110 a.m.u. is designated to either Me_2Se or thiophenol (TP) which can be formed due to fragmentation of 2-CTP. The peak at 144 a.m.u. belongs to 2-CTP whereas the peak at 288 a.m.u. is due to a dimer of 2-CTP, i.e., $(2\text{-CTP})_2$. The small peak at 208 is due to 2-CTP…Me_2S complex because of the presence of Me_2S in the system. The peak at 220 a.m.u. is due to a dimer of Me_2Se or thiophenol. The peak at 94 a.m.u. marked with a green asterisk in the mass spectrum could not be assigned. The peak at 254 a.m.u. corresponds to 2-CTP…Me_2Se complex formed in the supersonic jet. There are multiple peaks in the 2-CTP…Me_2Se complex mass channel which arises because selenium has multiple isotopes. The most intense peak at 254 a.m.u. corresponds to Se-80 which has a maximum abundance (~ 50 %). The mass spectrum is recorded at the 0-0 excitation wavelength of the 2-CTP…Me_2Se complex (34516 cm^{-1}).

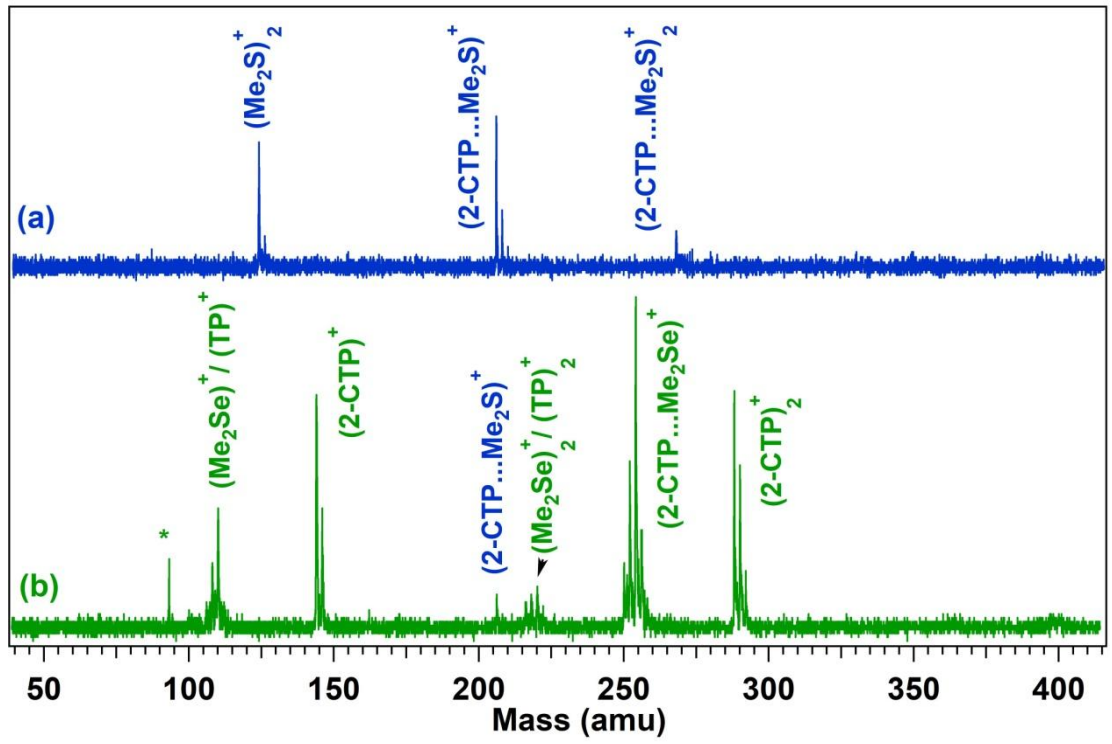

Figure 5.1: TOF Mass spectra of (a) 2-chlorothiophenol…dimethyl sulfide (2-CTP…Me_2S) and (b) 2-chlorothiophenol…dimethyl selenide (2-CTP…Me_2Se) complexes.

5.2.2 Electronic spectra

5.2.2.1 Electronic spectrum of 2-chlorothiophenol monomer

Electronic spectrum of 2-chlorothiophenol-d_1 (C_6H_4Cl-SD) has been reported earlier.[202] It shows multiple bands in the 0_0^0+2400 cm^{-1} cm^{-1} region with origin band at 34620 cm^{-1} as reported earlier by kim and co-workers. The electronic spectrum contains higher intensity peaks upto 500 cm^{-1} from the origin band. There are peaks of very low intensity from 0_0^0+500 cm^{-1} to 0_0^0+1200 cm^{-1}. There are no significant peaks after 0_0^0+1200 cm^{-1} in the electronic spectrum. We obtained origin band of 2-CTP at 34628 cm^{-1} (Figure 5.3a) which matches very well with the previous report.[202]

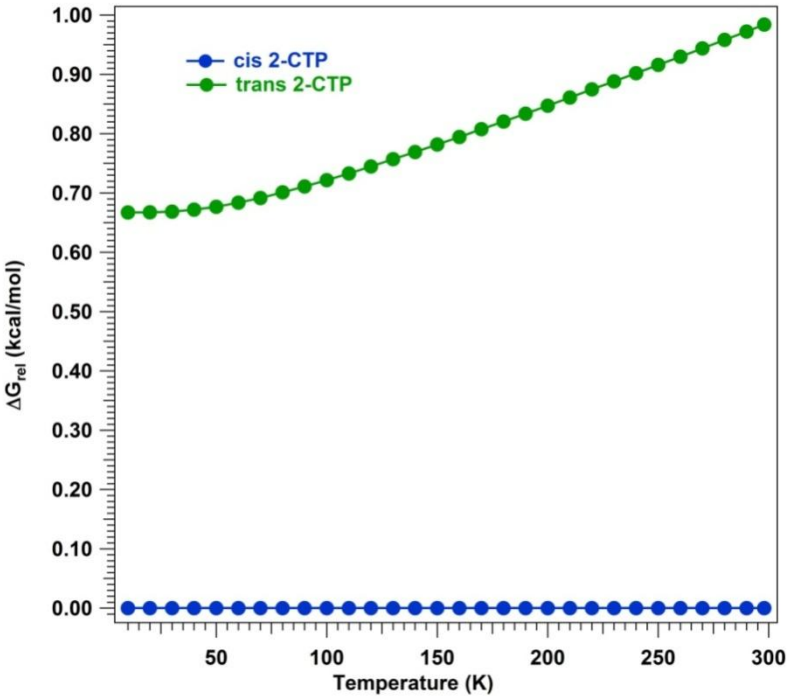

Figure 5.2: Relative Gibbs free energy (ΔG_{rel}) of cis-2-chlorothiophenol (cis-2-CTP) and trans-2-chlorothiphenol (trans-2-CTP) calculated at B97-D/6-311++G(d,p) level of theory

2-CTP can have two conformers depending on orientation of chlorine (Cl) with respect to S-H in 2-CTP. One conformer is cis-2-CTP where both Cl and S-H are oriented towards the same side of the phenyl ring whereas in trans-2-CTP, both Cl and S-H are oriented opposite

to each other (figure 5.7a). Our theoretical calculations at various levels of theory suggest that cis-2-CTP is more stable than trans-2-CTP by approx. 0.7 kcal/mol. Gibbs free energy calculation at various temperatures calculated at B97-D/6-311++G(d,p) level of theory also reveals that cis-2-CTP is more stable than trans-2-CTP (Figure 5.2). Thus, based on all these theoretical evidences, we can ascertain that the electronic spectrum of 2-CTP monomer is due to cis-2-CTP. Kim and co-workers have also reported through Franck-Condon simulation that all the vibronic bands in the electronic spectrum of 2-chlorothiophelol-d_1 are due to most stable cis-2-CTP-d_1. trans-2-CTP is not observed either due to conformational relaxation or due to its extremely short lifetime.[203]

5.2.2.2 Electronic spectrum of 2-CTP...Me_2S complex

Figure 5.3a shows the origin band of 2-chlorothiophenol (2-CTP). Electronic spectrum measured in the mass channel of 2-CTP…Me_2S dimeric complex is shown in Figure 5.3(b). The electronic spectrum of the 2-CTP…Me_2S complex shows multiple bands in the 34350-34700 cm^{-1} region. These bands could be due to different conformers of 2-CTP…Me_2S complex or vibronic bands of a single conformer. Figure 5.3(c) and 5.3(d) show UV-UV hole-burn spectra of 2-CTP…Me_2S complex by fixing the probe laser wavelength at 34529 cm^{-1} (denoted by a blue asterisk) and 34413 cm^{-1} (denoted by a green asterisk), respectively in the electronic spectrum. From UV-UV hole-burn spectra, it is confirmed that there are two conformers of 2-CTP…Me_2S complex.

The structural assignment of the two conformers is done by comparing their experimentally and theoretically obtained IR spectra, which are discussed later. Figures 5.3c-d are conformation-specific electronic spectra of cis-2-CTP…Me_2S and trans-2-CTP…Me_2S, respectively. The origin band of cis-2-CTP…Me_2S appears at 34513 cm^{-1} while the same for the trans-2-CTP…Me_2S is observed at 34388 cm^{-1}.

The bands in the electronic spectrum of the cis-2-CTP…Me_2S complex are much more

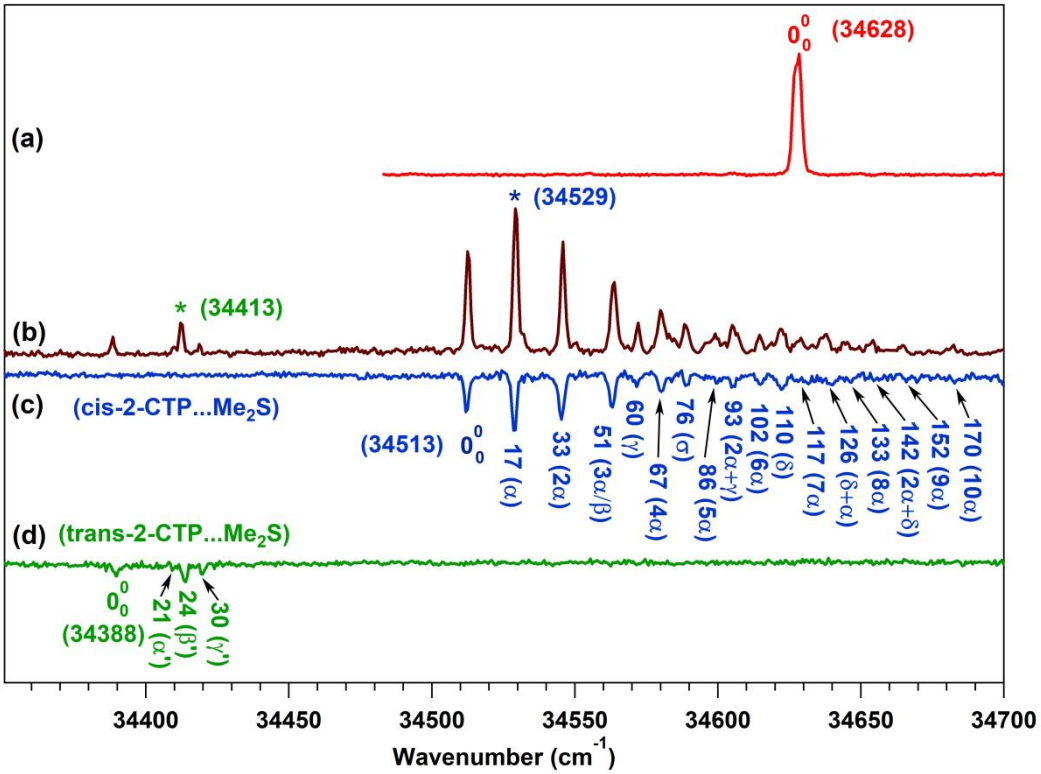

Figure 5.3: (a) Electronic spectrum showing the origin band of of 2-Chlorothiophenol (2-CTP). (b) Electronic spectrum of 2-Chlorothiophenol….Dimethyl Sulphide (2-CTP…Me_2S) complex. (c) and (d) are UV-UV hole burn spectra of 2-CTP…Me_2S complex, respectively. The peaks marked with asterisks in Figure 5.2b are probed for the UV-UV hole burn spectra

intense and rich in Franck-Condon activity than those of the trans-2-CTP…Me_2S complex. Theoretically, six low-frequency intermolecular modes are possible for any dimeric complex. A tentative assignment of all the vibronic bands in the electronic spectra of both the conformers of 2-CTP…Me_2S complex is shown in Figure 5.3 as well as Table 5.1.

The bands in the electronic spectrum of the cis-2-CTP…Me_2S complex is much more intense and rich in Franck-Condon activity than those of the trans-2-CTP…Me_2S complex. Theoretically, six low-frequency intermolecular modes are possible for any dimeric complex. A tentative assignment of all the vibronic bands in the electronic spectra of both the conformers of 2-CTP…Me_2S complex is shown in Figure 5.3 as well as Table 5.1.

The vibronic bands observed in the electronic spectra of the cis and trans conformers of 2-

Table 5.1 Observed (S_1) and calculated (S_0) low frequency intermolecular vibrational modes of cis-2-CTP...Me_2S and trans-2-CTP...Me_2S complexes. The S_0 state low-frequency vibrational modes are calculated at B97-D/6-311++G(d,p) level of theory.

cis-2-CTP…Me_2S			trans-2-CTP…Me_2S		
Observed[a] (S_1) (cm^{-1})	Calculated[b] (S_0)(cm^{-1})	Assignment	Observed[c] (S_1)(cm^{-1})	Calculated[d] (S_0)(cm^{-1})	Assignment
0_0^0 (34513)	-		0_0^0 (34388)		
17	15	α		10	
	27		21		α’
33		2α	24		β’
51	49	3α/ β	30	30	γ’
60	63	γ		45	
67		4α		6.0	
76	80	σ (stretch)		96	
86		5α		120	
96		2α+γ			
102		6α			
110	106	δ			
116		7α			
126	129	δ +α			
133		8α			
142		2α+δ			
152		9α			
170		10α			
188		11α			

[a]All the observed values are with respect to the origin band of cis-2-CTP...Me_2S complex (34513 cm^{-1})
[b]Excited state calculation of cis-2-CTP...Me_2S was not successful due to bond breaking between C and Cl in the excited state.
[c]All the observed values are with respect to the origin band of trans-2-CTP...Me_2S complex (34388 cm^{-1})
[d]Excited state calculation of trans-2-CTP...Me_2S was not successful due to bond breaking between C and Cl in the excited state.

CTP…Me_2S are compared with their low-frequency intermolecular modes obtained from the S_0 state theoretical calculations and provided in Table 5.1. We could not obtain the

vibrational frequencies of the complexes in the S_1 state as the C-Cl bond was breaking during optimization of the geometries in the excited state. Tentatively, the electronic spectrum of the cis-2-CTP…Me_2S complex is mostly dominated by overtones and combination bands of the αmode. In the case of the less populated trans-2-CTP…Me_2S complex, most likely three intermolecular modes denoted as α'(21 cm^{-1}), β' (24 cm^{-1}), andγ' (30 cm^{-1}) are observed in the experiment.

5.2.2.3 Electronic spectrum of 2-CTP...Me_2Se complex

Electronic spectrum of 2-chlorothiophenol…dimethyl selenide (2-CTP…Me_2Se) complex is shown in Figure 5.4a. The spectrum shows several sharp bands in the 34350-34650 cm^{-1} region. These bands could be originated due to different conformers or vibronic progressions of a single conformer. Figure 5.4b and c show UV-UV hole burn spectra of 2-CTP…Me_2Se complex measured by probing the bands at 34545 cm^{-1} (marked by a blue asterisk) and 34401 cm^{-1} (marked by green asterisks), respectively in the electronic spectrum shown in Figure 5.4a. From UV-UV hole burn spectra, it is confirmed that there are two conformers of 2-CTP…Me_2Se complex. The two conformers are assigned by comparing their experimentally and theoretically obtained IR spectra, which are discussed later. Figure 5.4b and 5.4c are conformation-specific electronic spectra of the cis-2-CTP…Me_2Se and trans-2-CTP…Me_2Se complexes, respectively. The origin band of cis-2-CTP…Me_2Se appears at 34516 cm^{-1} while the same for trans-2-CTP…Me_2Se is observed at 34401 cm^{-1}. The electronic bands in the case of cis-2-CTP…Me_2Se are more intense than those of trans-2-CTP…Me_2Se. Both cis-2-CTP…Me2Se and trans-2-CTP…Me2Se show large Franck-Condon activity in their electronic spectra. A tentative assignment of all the vibronic bands in the electronic spectra of both the conformers of 2-CTP…Me_2Se complex is shown in Figure 5.4b-c as well as in Table 5.2. The vibronic bands observed in both the conformers of the 2-CTP…Me_2Se complex

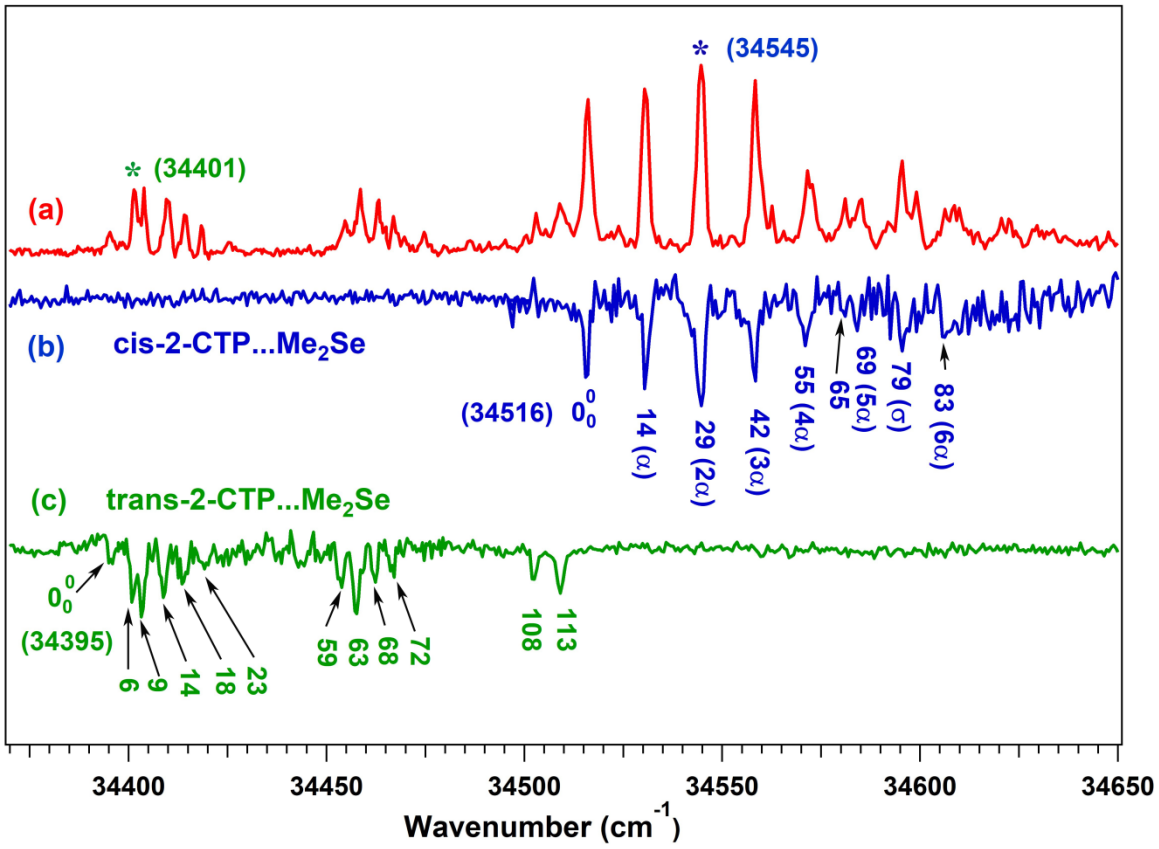

Figure 5.4: (a) Electronic spectrum of 2-chlorothiophenol….dimethyl selenide (2-CTP…Me_2Se) complex. (b) and (c) are UV-UV hole burn spectra of 2-CTP…Me_2Se complex. The bands marked with asterisks are probed for for UV-UV hole-burning spectra.

is compared with their low-frequency intermolecular vibrations obtained in the S_0 state theoretical calculation and are provided in table 5.2. Similar to the 2-CTP…Me_2S complex, vibrational frequencies of the two conformers of the 2-CTP…Me_2Se complex could not be calculated in the S_1 state. Tentatively, the electronic spectrum of cis-2-CTP…Me_2Se is dominated by overtones and combination of α modes while that of trans-2-CTP…Me_2Se is dominated by overtones and combination of α' and β' modes.

Table 5.2 Observed (S_1) and calculated (S_0) low frequency intermolecular vibrational modes of cis-2-CTP...Me_2Se and trans-2-CTP...Me_2Se complexes. The S_0 state low-frequency vibrational modes are calculated at B97-D/6-311++G (d, p) level of theory.

cis-2-CTP…Me_2Se			trans-2-CTP…Me_2Se		
Observed[a] (S_1) (cm^{-1})	Calculated[b] (S_0)(cm^{-1})	Assignment	Observed[c] (S_1)(cm^{-1})	Calculated[d] (S_0)(cm^{-1})	Assignment
0_0^0 (34516)	-	-	0_0^0 (34395)	-	-
14	15	α	6		α’
29	24	2α/β	9		β’
42	45	3α/γ	14	16	γ’
55	59	4α/δ	18		2β’
65		5α	23		4α’
69		5α/(α+ δ)		28	
79	75	σ (stretch)		45	
83		6α	59	54	4γ’/δ’
	111		63		7β’
			68		
			72		8β’
				83	
			108		12β’
			113	120	

[a]All the observed values are with respect to the origin band of cis-2-CTP...Me_2Se complex (34516 cm^{-1})
[b]Excited state calculation of cis-2-CTP...Me_2Se was not successful due to bond breaking between C and Cl in the excited state.
[c]All the observed values are with respect to the origin band of trans-2-CTP...Me_2Se complex (34395 cm^{-1})
[d]Excited state calculation of trans-2-CTP...Me_2Se was not successful due to bond breaking between C and Cl in the excited state.

5.2.3 IR spectroscopy

To determine the structures of the observed conformers of 2-CTP and the complexes of 2-CTP with Me_2S and Me_2Se, we performed IR spectroscopy combined with quantum chemical calculations. Figure 5.5a shows IR spectrum of bare 2-CTP measured by probing the

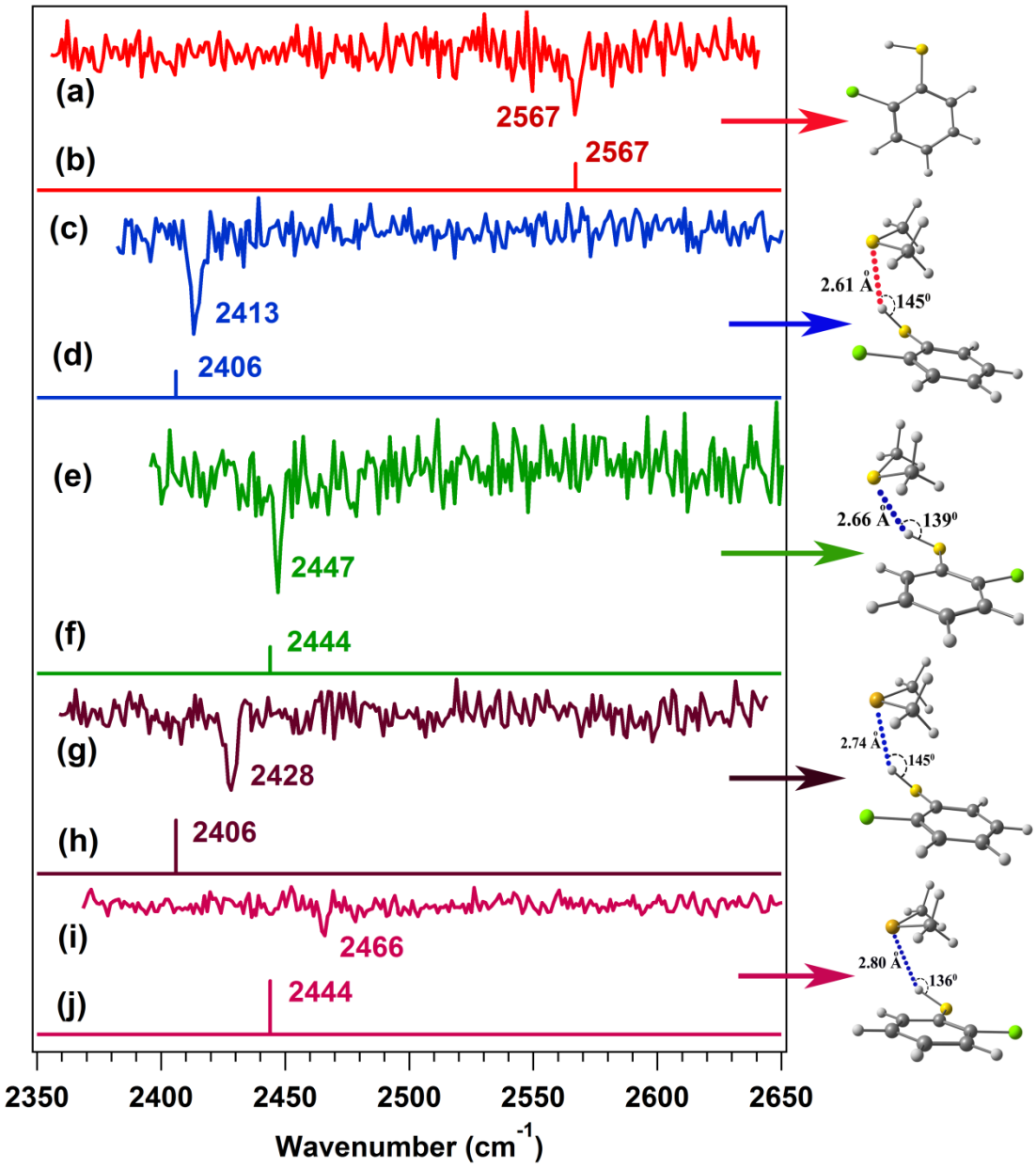

Figure 5.5: IR spectra of (a) cis-2-CTP (c) cis-2-CTP…Me_2S, (e) trans-2-CTP…Me_2S, (g)cis-2-CTP…Me_2Se and, (i) trans-2-CTP…Me_2Se by fixing the UV laser at (a) 34628 cm^{-1}, (c) 34529 cm^{-1}, (e) 34413 cm^{-1}, (g) 34545 cm^{-1}, and (i) 34401 cm^{-1} respectively. (b), (d), (f), (h) and (j) are theoretically scaled IR spectra of cis-2-CTP, cis-2-CTP…Me_2S, trans-2-CTP…Me_2S cis-2-CTP…Me_2Se and trans-2-CTP…Me_2Se respectively calculated at B97-D/6-311++G(d,p) level of theory. The scaling factor was obtained by the ratio of experimentally observed S-H stretching frequency and theoretically obtained S-H stretching frequency of cis-2-CTP calculated at the B97-D/6-311++G(d,p) level of theory.

electronic origin band of 2-CTP at 35628 cm^{-1} (Figure 5.3a) using RIDIR spectroscopy. The

S-H stretching frequency of 2-CTP occurs at 2567 cm^{-1}. A comparison of the experimental frequency with theoretically scaled frequency calculated at the B97-D/6-311++G(d,p) level of theory reveals that this S-H stretching frequency belongs to *cis*-2-CTP. We could not record the IR spectrum of trans-2-CTP.

Figure 5.5c shows IR spectrum of one of the conformers of 2-CTP…Me_2S by fixing the UV laser at 34529 cm^{-1} (marked with a blue asterisk in Figure 5.3b in the electronic spectrum of the complex) and scanning the IR laser in the S-H stretching frequency region. The S-H stretching frequency of this conformer is observed at 2411 cm^{-1}. By comparing this experimentally observed frequency with theoretically scaled frequency calculated at the B97-D/6-311++G(d,p) level of theory, we confirmed that this S-H stretching frequency is due to the cis-2-CTP…Me_2S complex. IR spectrum (Figure 5.5e) of another conformer of2-CTP…Me_2S complex measured by fixing the UV laser at 34413 cm^{-1} (marked with a green asterisk in Figure 5.3b in the electronic spectrum of the complex) shows the S-H stretching frequency at 2447 cm^{-1}. Again, a comparison of this experimentally observed frequency with theoretically scaled S-H stretching frequency calculated at the B97-D/6-311++G(d,p) level of theory tells that this S-H stretching frequency belongs to the trans-2-CTP…Me_2S complex. It has been found that the S-H stretching frequency in the cis-2-CTP…Me_2S complex is 154 cm^{-1}red-shifted compared to that in the cis 2-CTP monomer. The result is quite surprising as the red-shift observed in the S-H stretching frequency for the S-H...S hydrogen bond is similar to that observed for any conventional strong hydrogen bond. As we could not record the IR spectrum of trans-2-CTP, it is difficult to predict exact red-shift in the S-H stretching frequency of the trans-2-CTP…Me_2S complex.However, our theoretical calculations for both the cis and trans conformers of 2-CTP at the B97-D/6-311++G(d,p) level of theory suggest that there is not much difference in the S-H stretching frequency of both the conformers of 2-CTP monomer. The theoretically calculated and unscaled S-H stretching frequency for both

the conformers of 2-CTP is shown in Figure 5.5a. It should be noted that the red-shift in the S-H stretching frequency of cis-2-CTP…Me_2S is more than that of the trans-2-CTP…Me_2S complex. It will be intriguing to compare the red-shift observed in the S-H stretching frequency for the S-H...S hydrogen bond with that observed with any conventional strong hydrogen bond donor reported in the literature. Biswal and co-workers have reported 130 cm^{-1} red-shift in the O-H stretching frequency for the O-H...S hydrogen bond in phenol…dimethyl sulfide (Ph…Me_2S) complex.[112] We have observed 154 cm^{-1} red shift in S-H stretching frequency for the cis-2-CTP…Me_2S complex and 120 cm^{-1} red shift in S-H stretching frequency in the trans-2-CTP…Me_2S complex. Thus, it could be pointed out here that the red-shift reported in the case of the O-H...S interaction for the Ph…Me_2S complex is similar to that of the S-H...S interaction observed in the 2-CTP…Me_2S complex although S is less electronegative than O. This result indicates that S-H is as strong as O-H as a hydrogen bond donor. Further, the strength of the S-H...S hydrogen bond can be even compared with any conventional strong hydrogen bond with both hydrogen bond donor and acceptor atoms as strongly electronegative. As, the red-shift values in the X-H stretching frequency reported for N-H...O and O-H...O hydrogen bonds in indole...H_2O and phenol...H_2O are 89 and 133 cm^{-1}, respectively.[188,204] So, S-H...S is a quite strong hydrogen bond even if both hydrogen bond donor and acceptor atoms are very weak in electronegativity.

Similarly, IR spectra of the 2-CTP…Me_2Se complex has been measured by fixing the UV laser at one of the band positions of the electronic spectrum of each of the conformers and scanning the IR laser in the S-H stretching region. Figure 5.5g shows IR spectrum in the S-H frequency region by fixing the UV laser at 34545 cm^{-1} (marked with a blue asterisk in Figure 5.4a in the electronic spectrum of the complex). The spectrum shows the S-H stretching frequency of the complex at 2428 cm^{-1}. By comparing this experimentally observed frequency with theoretically scaled frequency calculated at B97-D/6-311++G(d,p) level of

Table 5.3 Unscaled harmonic S-H stretching frequency (ν_{S-H} in cm^{-1}) of different conformers of 2-CTP monomer and 2-CTP...Me_2S/Me_2Se complex calculated at B97-D level of theory and different basis sets.

Complex	ν_{S-H} (cm^{-1})		
	B97-D/6-31+G(d)	B97-D/6-311++G(d,p)	B97-D/aug-cc-pVDZ
cis-2-CTP	2653	2643	2634
trans-2-CTP	2633	2628	2622
cis-2-CTP…Me_2S	2495	2477	2417
trans-2-CTP…Me_2S	2509	2516	2452
cis-2-CTP…Me_2Se	2302	2476	2444
trans-2-CTP…Me_2Se	2418	2515	2469

Table 5.4 Unscaled harmonic S-H stretching frequency (ν_{S-H} in cm^{-1}) of different conformers of 2-CTP monomer and 2-CTP...Me_2S/Me_2Se complex calculated at different levels of theory and 6-311++G(d,p) basis sets.

Complex	ν_{S-H} (cm^{-1})	
	B97-D/6-311++G(d,p)	B3LYP-D3/6-311++G(d,p)
cis-2-CTP	2643	2686
trans-2-CTP	2628	2670
cis-2-CTP…Me_2S	2477	2511
trans-2-CTP…Me_2S	2516	2588
cis-2-CTP…Me_2Se	2476	2534
trans-2-CTP…Me_2Se	2515	2615

theory, we confirmed that this S-H stretching frequency is due to cis-2-CTP…Me_2Se complex. In another case, UV laser was fixed at 34401 cm^{-1} (marked with a green asterisk in Figure 5.5b in the electronic spectrum of the complex) and scanned IR laser throughout the S-H stretching region. In this case, we observed S-H stretching frequency at 2466 cm^{-1} as shown in figure 5.5i. A comparison of this experimentally observed frequency with theoretically scaled frequency calculated at B97-D/6-311++G(d,p) level of theory tells that

this S-H stretching frequency belongs to trans-2-CTP…Me_2S complex. cis-2-CTP…Me_2Se complex shows 139 cm^{-1} red shift in S-H stretching frequency. In this case also, cis-2-CTP…Me_2Se complex shows a more red shift in S-H stretching frequency than that in trans-2-CTP…Me_2Se complex. The assignment of the IR spectra of different conformers of the complexes has been reconfirmed by carrying out the geometry optimization and frequency calculation at different levels of theory (Table 5.3 and Table 5.4).

5.2.4 Quantum chemical calculations of different conformers of 2-CTP monomer and its dimeric complexes with Me_2S and Me_2Se

2-Chlorothiophenol (2-CTP) exists in two conformers. One is cis-2-CTP where S-H group and chlorine (Cl) are on the same side of the phenyl ring, and the other one is trans-2-CTP where S-H is in the opposite side of chlorine (Cl) as shown in Figure 5.7a. It has been found from B97-D/6-311++G(d,p) level of calculation that cis-2-CTP is more stable than trans-2-CTP by 0.67 kcal/mol. The main stability difference between the cis-2-CTP and trans-2-CTP is that the former one has a weak S-H...Cl interaction. Figure 5.7b-c shows the optimized structures as well as binding energies of cis and trans conformers of 2-CTP…Me_2S and 2-CTP…Me_2Se complexes calculated at the B97-D/6-311++G(d,p) level of theory. It has been found that the trans conformer is more stable than the cis conformer for both the 2-CTP…Me_2S and 2-CTP…Me_2Se complexes although the trend of stability is opposite in the case of the 2-CTP monomer. In the case of the complexes, the S-H...Cl bond, which is present in the monomer, is disrupted and the S-H bond becomes out of the plane. We have also calculated the binding energies of all the conformers of 2-CTP…Me_2S and 2-CTP…Me_2Se complexes at different levels of theory (Table 5.5) using different basis sets (Table 5.6) and the trend of the relative stability for all the conformers of 2-CTP…Me_2S and 2-CTP…Me_2Se complexes remain the same. Further, we have calculated the Gibbs free energy (ΔG) of all the conformers of the complexes at various temperatures (Table 5.7). The

Gibbs free energy of different conformers follows the same trend of relative stability, i.e., trans-2-CTP…Me_2S/Me_2Se is more stable than cis-2-CTP…Me_2S/Me_2Se at different temperatures.

Table 5.5 Zero point energy (ZPE) and basis set superposition error (BSSE) corrected binding energy (BE) of different conformers of 2-CTP…Me_2S and 2-CTP…Me_2Se complexes calculated at different levels of theory and 6-311++G(d,p) basis set. All the energy values are in kcal/mol.

Complex	BE (Kcal/mol) B3LYP-D3/6-311++G(d,p)	BE (Kcal/mol) B97-D/6-311++G(d,p)
cis-2-CTP…Me_2S	-5.82	-3.40
trans-2-CTP…Me_2S	-6.46	-4.36
cis-2-CTP…Me_2Se	-4.57	-3.75
trans-2-CTP…Me_2Se	-5.49	-4.96

Next, we have calculated the S-H stretching frequency in both cis and trans conformers of 2-CTP…Me_2S and 2-CTP…Me_2Se complexes at different levels of theory with various basis sets to reconfirm the assignment of the experimental IR spectra of the complexes. Figure 5.6 shows a comparison of the experimental IR spectra of the complexes with their theoretical IR spectra calculated at various levels of theory. The comparison reconfirms the assignment of the experimental IR spectra of the complexes provided in Figure 5.4. Thus the intense bands (34500 – 34700 cm^{-1}) in the electronic spectrum of 2-CTP…Me_2S (Figure 5.2b) are due to the less stable cis conformer of the complex while the weaker bands (34350 – 34450 cm^{-1}) are originated due to the electronic transition of the most stable (global minimum) trans conformer of the complex. A similar observation has been confirmed in the case of 2-CTP…Me_2Se complex as well. Thus the intensity of the electronic bands of the two conformers of these complexes observed in the experiment is in contradiction with their

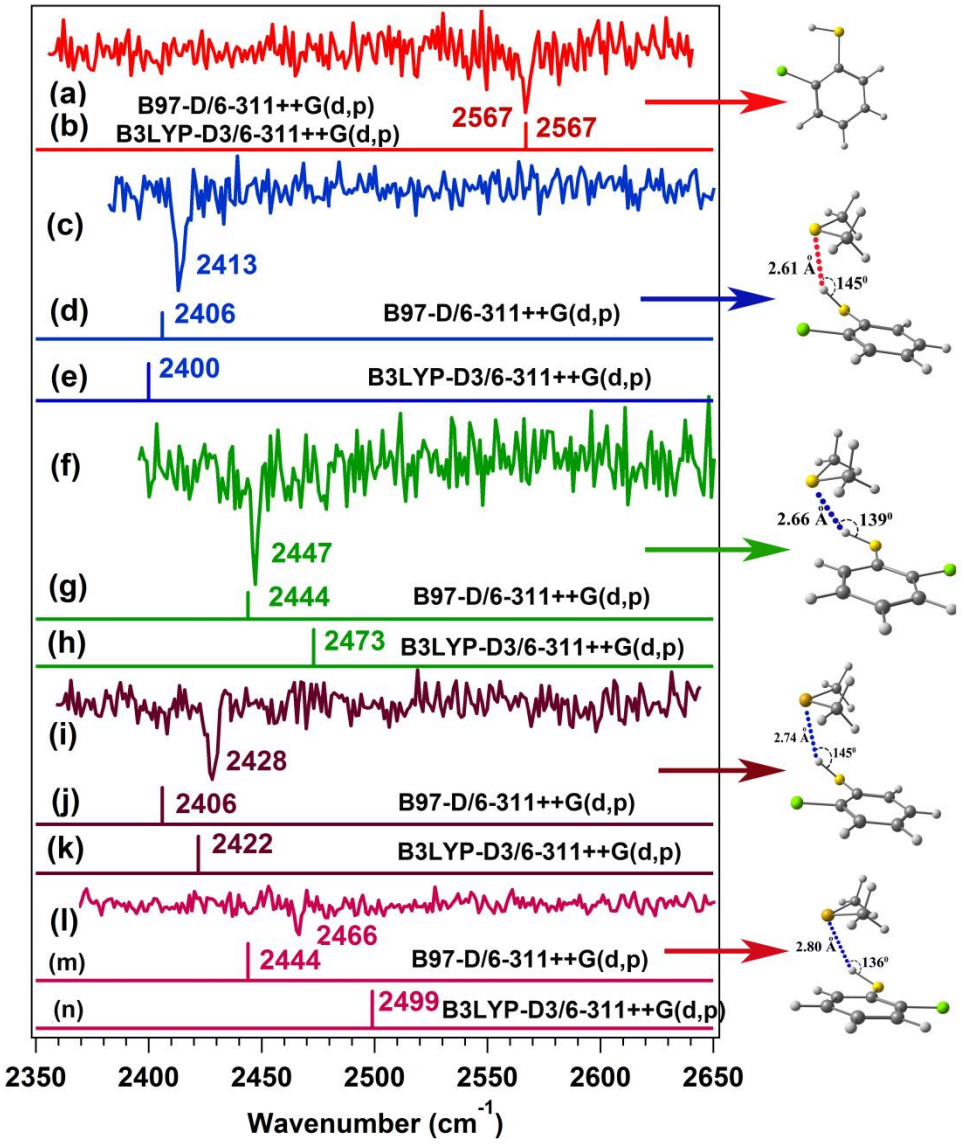

Figure 5.6: IR spectra of (a) cis-2-CTP (c) cis-2-CTP…Me_2S, (f) trans-2-CTP…Me_2S, (i)cis-2-CTP…Me_2Se and, (l) trans-2-CTP…Me_2Se by fixing the UV laser at (a) 34628 cm^{-1}, (c) 34529 cm^{-1}, (f) 34413 cm^{-1}, (i) 34545 cm^{-1}, and (l) 34401 cm^{-1} respectively. (b), (d), (g), (j) and (m) are theoretically scaled IR spectra of cis-2-CTP, cis-2-CTP…Me_2S, trans-2-CTP…Me_2S cis-2-CTP…Me_2Se and trans-2-CTP…Me_2Se respectively calculated at B97-D/6-311++G(d,p) level of theory. (b), (e), (h), (k) and (n) are theoretically scaled IR spectra of cis-2-CTP, cis-2-CTP…Me_2S, trans-2-CTP…Me_2S cis-2-CTP…Me_2Se and trans-2-CTP…Me_2Se respectively calculated at B3LYP-D3/6-311++G(d,p) level of theory. The theoretical specra shown at B97-D/6-311++G(d,p) level of theory are scaled by a scaling factor of 0.9712 and at B3LYP-D3/6-311++G(d,p) level of theory are scald by a scaling factor of 0.9557. The scaling factors used for calculation at B97-D/6-311++G(d,p) and B3LYP-D3/6-311++G(d,p) levels of theory were obtained by the ratio of experimentally observed S-H stretching frequency and theoretically calculated S-H stretching frequency of cis-2-CTP at the respective levels of theory.

Boltzmann population. However, the intensity of the electronic bands does not solely depend on the population of the molecules or complexes in the ground electronic state.

Table 5.6 Zero point energy (ZPE) and basis set superposition error (BSSE) corrected binding energy (BE) of different conformers of 2-CTP…Me_2S and 2-CTP…Me_2Se complexes calculated at the B97-D level of theory with different basis sets. All the energy values are in kcal/mol.

Complex	BE (Kcal/mol) B97-D/6-31+G(d)	BE (Kcal/mol) B97-D/6-311++G(d,p)	BE (Kcal/mol) B97-D/aug-cc-pVDZ
cis-2-CTP…Me_2S	-3.42	-3.40	-3.36
trans-2-CTP…Me_2S	-4.51	-4.36	-4.53
cis-2-CTP…Me_2Se	-3.33	-3.75	-3.87
trans-2-CTP…Me_2Se	-4.02	-4.96	-5.03

Table 5.7 Gibbs free energy of various conformers of the complexes of 2-CTP with Me_2S and Me_2Se at different temperatures calculated at the B97-D/6-311++G (d,p) level of theory. All the energy values are in kcal/mol.

T(K)	**ΔG (kcal/mol)**			
	cis-2-CTP…Me_2S	**trans-2-CTP…Me_2S**	**cis-2-CTP…Me_2Se**	**trans-2-CTP…Me_2Se**
20	-2.84	-3.82	-3.17	-4.38
40	-2.15	-3.14	-2.46	-3.67
60	-1.44	-2.46	-1.74	-2.96
80	-0.74	-1.79	-1.03	-2.24
100	-0.05	-1.12	-0.32	-1.54
120	+0.64	-0.46	+0.39	-0.85

Rather, it could be speculated that the contradictory intensity pattern of the electronic bands of the two conformers could be due to their different Franck-Condon activity, S_1state lifetime and ionization cross-sections.[205] Further theoretical calculations of the complexes in the S_1

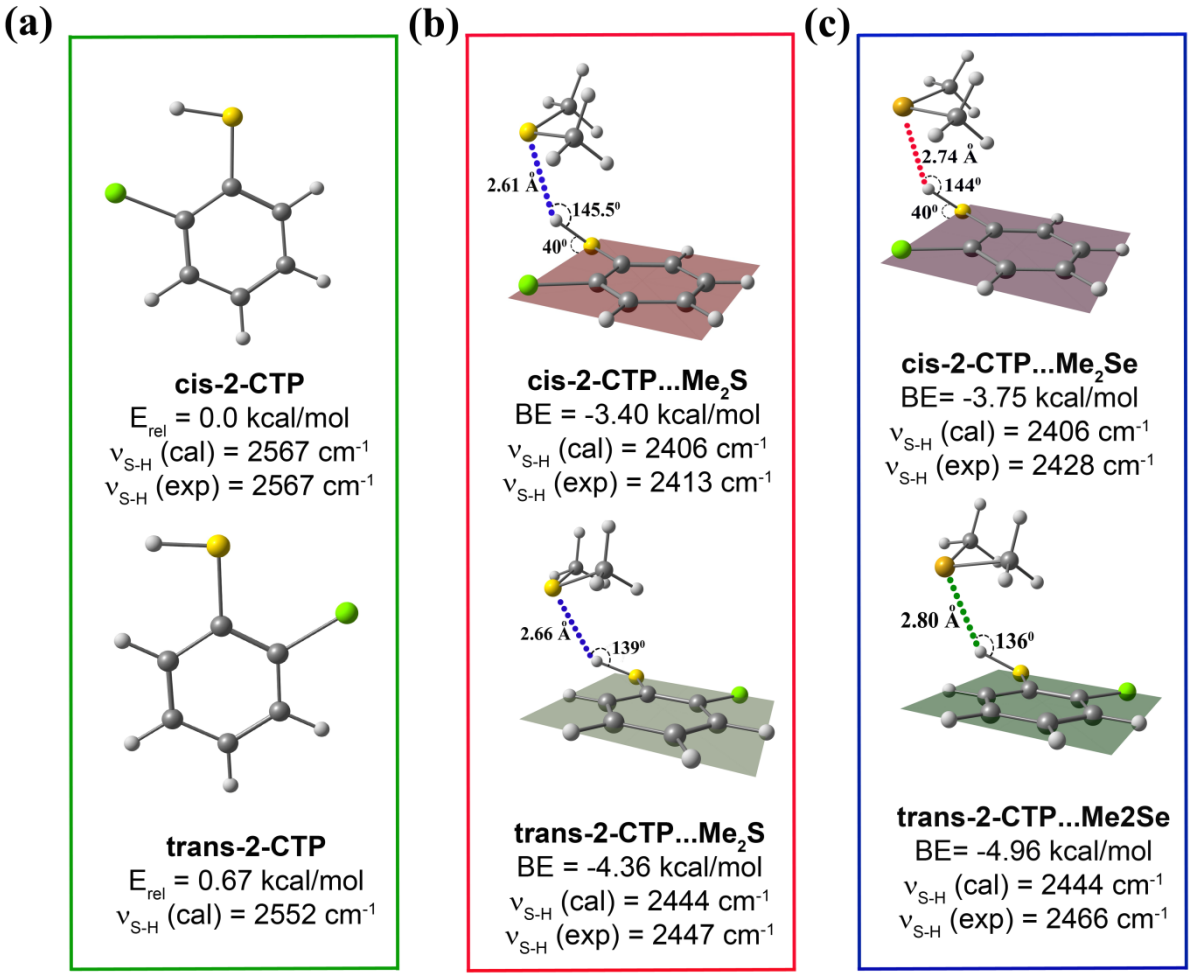

Figure 5.7: The geometries of various conformers of (a) 2-CTP with their relative energy values. (b) and (c) are the geometries of various conformers of 2-CTP with Me_2S and Me_2Serespectively with their zero point energy and BSSE corrected binding energy (BE) values. $\nu_{S\text{-}H}$(cal) represents the theoretical calculated S-H stretching frequency of 2-CTP in its complexes. All the calculations are performed at B97-D/6-311++G(d,p) level of theory.

state and their Franck-Condon Factor (FCF) calculated electronic spectra would shed light on the assignment of the experimental electronic spectra of the two conformers observed in the experiment. An alternative explanation for the observation of the intense electronic bands for the less stable cis conformer of the complexes could be a larger population of the cis conformer of the monomer (2-CTP) compared to that of the trans conformer.

5.2.5 NBO analysis

According to the Natural Bond Orbital (NBO) formalism, hydrogen bond strength in a molecule or complex can be determined in terms of second-order perturbation energy ($E^{(2)}_{i\rightarrow j^*}$), where i and j^* are hydrogen-bond donor and acceptor orbitals, respectively. The $E^{(2)}_{i\rightarrow j^*}$value due to the interaction between $\sigma_{(S)}$orbital of Me_2S and $\sigma^*_{(S-H)}$ orbital of cis-2-CTP in the cis-2-CTP…Me_2S complex is 5.16 kcal/mol (Table 5.8). On the other hand, the $E^{(2)}_{i\rightarrow j^*}$value due to the interaction between $\sigma_{(S)}$orbital of Me_2S and $\sigma^*_{(S-H)}$ of trans-2-CTP in the trans-2-CTP…Me_2S complex is 3.87 kcal/mol (Table 5.6). Thus the NBO values for the S-H…S interaction corroborate the observed red-shift in the S-H stretching frequency in the two conformers of the 2-CTP…Me_2S complex.

Table 5.8 Relation between NBO second order perturbation energy values ($E^{(2)}_{i\rightarrow j^*}$) in different conformers of 2-CTP…Me_2S complex and the red shift in S-H stretching frequency ($\Delta\nu_{S-H}$) of 2-CTP. The red shift in S-H stretching frequency is calculated with respect to S-H stretching frequency of cis-2-CTP. NBO calculation is performed at B97-D/6-311++G (d,p) level of theory.

Complex	$E^{(2)}_{i\rightarrow j^*}$ (kcal/mol) $n_{(Cl)} \rightarrow \sigma^*_{(S-H)}$	$E^{(2)}_{i\rightarrow j^*}$ (kcal/mol) $n_{(S)} \rightarrow \sigma^*_{(S-H)}$	$\Delta\nu_{S-H}$ (cm^{-1})	Δr_{S-H}(Å)[b]
cis-2-CTP…Me_2S	0.33	5.16	154	0.0133
cis-2-CTP…Me_2Se	0.70	4.83	138	0.0136
trans-2-CTP…Me_2S	0.79	3.87	120[a]	0.0085
trans-2-CTP…Me_2Se	-	3.31	100[a]	0.0107

[a]the red–shift in S-H stretching frequency in case of trans-2-CTP…Me_2S complex is calculated with respect to S-H stretching frequency in cis-2-CTP as we could not record S-H stretching frequency for trans-2-CTP.
[b]Δr_{S-H} is the increase in S-H bond length after complex formation. $\Delta r_{S-H}$for cis-2-CTP…Me2S complex is calculated with respect to S-H bond length in cis-2-CTP and for trans-2-CTP…Me_2S complex is calculated with respect to S-H bond length in trans-2-CTP.

The $E_{i\rightarrow j^*}^{(2)}$ Values for the S-H…Se hydrogen bonding interaction in thesis and trans conformers of the 2-CTP…Me_2Se complexes is 4.83 kcal/mol and 3.87 kcal/mol, respectively (Table 5.6). Similarly, the NBO values of the two conformers are in accordance with their IR red-shift values in the S-H stretch frequency.

The red-shift in the S-H stretching frequency can also be explained in terms of lengthening of the S-H bond for both the conformers of the 2-CTP...Me_2S/Me_2Se complex. In the case of the cis-2-CTP...Me_2S/Me_2Se complex, the S-H bond length of cis-2-CTP is increased by 1.33(1.36) picometer (pm) whereas for the trans-2-CTP...Me_2S/Me_2Se complex, the S-H bond length of trans-2-CTP is increased by 0.85(1.07) pm. The more bond lengthening in the S-H bond length of cis-2-CTP…Me_2S/Me_2Se shows that the S-H stretching will occur at a lower frequency.

5.2.6 Atoms-In-Molecules (AIM) analysis

AIM analysis[206,207] also provides the evidence of intramolecular hydrogen bond in 2-CTP and intermolecular hydrogen bond in the conformers of 2-CTP…Me_2S/Me_2Se complexes. The value of charge density (ρ) at the bond critical points (BCPs) in the cis-2-CTP monomer and the conformers of 2-CTP…Me_2S/Me_2Se complexes fall between 0.002-0.035 a.u. which is the proposed criteria for hydrogen bond according to AIM analysis (Figure 5.8 and Table 5.9). Similarly, the value of Laplacian of charge density ($\nabla^2\rho$) at the BCPs fall between 0.024-0.139 a.u. which also satisfy the criteria for hydrogen bond. After the complex formation between cis-2-CTP and Me_2S/Me_2Se, the BCP between the Cl and H-S bond disappears, and a new BCP arises between S-H (2-CTP) and S/Se (Me_2S/Me_2Se) in both the conformers of the complex. Thus the AIM analysis provides the evidence for the presence of the non-covalent interaction between the S-H antibonding orbital of 2-CTP and lone pair orbital of S/Se from Me_2S/Me_2Se.

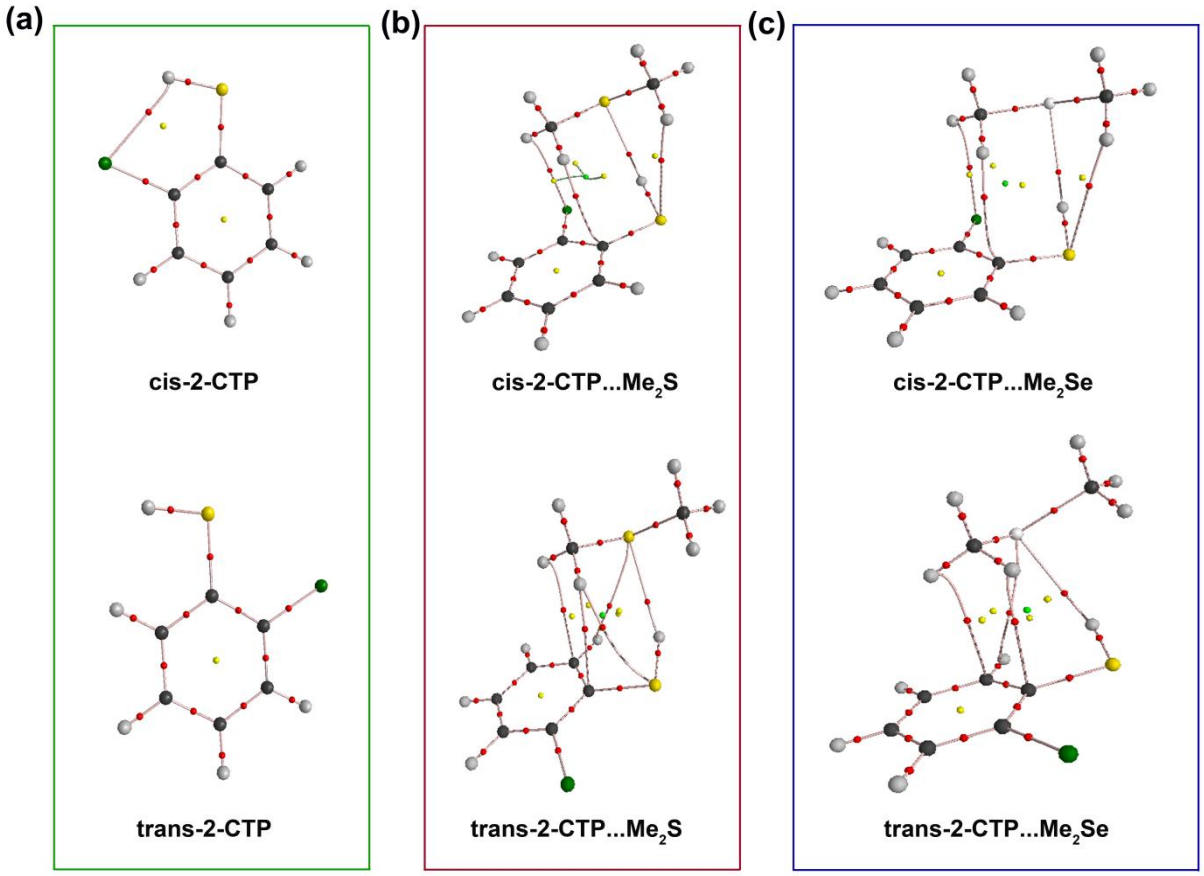

Figure 5.8: AIM analysis of the conformers of (a) 2-CTP,(b) 2-CTP…Me_2S and (c) 2-CTP…Me_2Se complex performed at the B97-D/6-311++G(d,p) level of theory. The presence of the bond critical point (BCP) between S-H of 2-CTP and Me_2S/Me_2Se in the complexes shows the hydrogen bonding interaction between 2-CTP and Me_2S(Se).

Table 5.9 AIM analysis of various geometries of the complexes of 2-CTP with Me_2S and Me_2Se performed at the B97-D/6-311++G(d,p) level of theory. The charge density (ρ) and Laplacian of charge density ($\nabla^2\rho$) are for bond critical point (BCPs) which is observed due to the formation of a hydrogen bond between 2-CTP and Me_2S/Me_2Se.

Complex	**ρ**	$\nabla^2\rho$
cis-2-CTP…Me_2S	0.0148	0.0324
cis-2-CTP…Me_2Se	0.0138	0.0308
trans-2-CTP…Me_2S	0.0136	0.0273
trans-2-CTP…Me_2Se	0.0126	0.0259

5.2.7 Energy Decomposition Analysis (EDA)

We have performed energy decomposition analysis (EDA) of various conformers of the complexes of 2-CTP with Me_2O, Me_2S, and Me_2Se to find out various components of the binding energy, which contribute to the stability of these complexes. We have decomposed the total interaction energy (ΔE_{TOTAL}) of these complexes into various components using LMO-EDA and ALMO-EDA methods. LMO-EDA method decomposes the total interaction energy (ΔE_{TOTAL}) into electrostatic (ΔE_{ES}), exchange (ΔE_{EX}), polarization (ΔE_{POL}), dispersion (ΔE_{DISP}) and repulsion (ΔE_{REP}) components. On the other hand, ALMO-EDA method decomposes the total interaction energy (ΔE_{TOTAL}) into frozen charge density (ΔE_{FRZ}), polarization (ΔE_{POL}) and charge transfer (ΔE_{CT}). Frozen charge density (ΔE_{FRZ}) is a combination of electrostatic (ΔE_{ES}), repulsion (ΔE_{REP}) and dispersion (ΔE_{DISP}) interactions. We have employed other energy decomposition methods also, like RVS-EDA and NEDA and these methods also follow the same trend as LMO-EDA and ALMO-EDA methods.

LMO-EDA calculation of both the conformers of 2-CTP…Me_2S/Me_2Se complexes at the M05-2X/cc-pVDZ level of theory (Table 5.10) reveals that the dispersion interaction plays a dominant role in the stabilization of both the conformers of 2-CTP…Me_2/Me_2Se complex but it does not provide any information about larger red shift in the S-H stretching frequency in case of cis-2-CTP…Me_2S/Me_2Se complex as compared to the S-H stretching frequency in the trans-2-CTP…Me_2S/Me_2Se complex.

ALMO-EDA calculation unearths the larger red-shift observed in the S-H stretching frequency in the case of cis-2-CTP…Me_2S/Me_2Se complex. The comparison of various energy decomposition components of both the conformers of 2-CTP…Me_2Scomplex calculated at the B97-D/6-311++G (d,p) level of theory reveals that the contribution of the charge transfer component (ΔE_{CT}) is 63% towards the total interaction energy of cis-2-

CTP…Me_2S complex whereas the same is 51.4 % towards the total interaction energy of the trans-2-CTP…Me_2S complex (Table 5.11).

Table 5.10 LMO-EDA calculation of all the conformers of complexes of 2-Chlorothiophenol (2-CTP) and 2-Chlorophenol (2-CP) with Me_2O and Me_2S calculated at M05-2X/cc-pVDZ level of theory. All the energy values are in kcal/mol.

complex	ΔE_{ES}	ΔE_{EX}	ΔE_{REP}	ΔE_{POL}	ΔE_{DISP}	ΔE_{TOTAL}
cis-2-CTP…Me_2O	-5.28	-3.97	19.3	-1.24	-13.1	-4.28
cis-2-CTP…Me_2S	-6.61	-6.41	22.65	-2.4	-11.55	-4.31
cis-2-CTP…Me_2Se	-6.21	-6.23	23.58	-2.02	-13.54	-4.43
trans-2-CTP…Me_2O	-8.55	-6.27	20.98	-2.35	-8.88	-5.06
trans-2-CTP…Me_2S	-6.99	-6.15	21.43	-2.28	-10.93	-4.94
trans-2-CTP…Me_2Se	-7.84	-7.32	25.10	-2.53	-12.83	-5.43

Patwari and co-workers have reported that electrostatic, charge transfer and polarization components contribute in the red-shift of the hydrogen bond donor whereas the dispersion interaction is contributes to the overall stabilization of the hydrogen-bonded complex. In the case of the 2-CTP…Me_2S complex, both hydrogen bond donor and hydrogen bond acceptor are less electronegative atoms; hence electrostatic contribution will not play a dominant role. Contribution of the polarization energy component is nearly the same in cis-2-CTP…Me_2S as well as trans-2-CTP…Me_2S.The charge transfer component dominates in case of cis-2-CTP…Me_2S complex which provides more red-shift in S-H stretching frequency of cis-2-CTP…Me_2S complex in spite of the fact that cis-2-CTP…Me_2S is less stable than trans-2-CTP…Me_2S.

In the case of 2-CTP…Me_2Se complex, the contribution of charge transfer component (ΔE_{CT}) is 54.7% towards the total interaction energy of cis-2-CTP…Me_2Se complex whereas the same is 48.7 % towards the total interaction energy of trans-2-CTP…Me_2Se complex. In the case of 2-CTP…Me_2Se complex, both hydrogen bond donor and hydrogen bond acceptor are

Table 5.11 ALMO-EDA calculation of different conformers of complexes of 2-Chlorothiophenol (2-CTP) and 2-Chlorophenol (2-CP) with Me_2O and Me_2S calculated at B97-D/6-311++G(d,p) level of theory. Total binding energy (E_{total}) is decomposed into frozen (ΔE_{FRZ}), polarization (ΔE_{POL}) and charge transfer (ΔE_{CT}) components. $\Delta E_{FRZ}= \Delta E_{ES} + \Delta E_{DISP} + \Delta E_{REP}$ where ΔE_{ES} is an electrostatic component, ΔE_{DISP} is dispersion component, and ΔE_{REP} is Pauli repulsion component. All the energy values are in kcal/mol. Values in parenthesis against each charge transfer term represent % contribution of charge transfer in total interaction energy.

Complex	ΔE_{FRZ}	ΔE_{POL}	ΔE_{CT}	ΔE_{TOTAL}	$\Delta\nu_{S-H}$ (cm^{-1})
cis-2-CTP…Me_2O	-3.16	-0.61	-1.06 (21.9%)	-4.83	32
cis-2-CTP…Me_2S	-1.28	-0.61	-3.21 (63%)	-5.10	154
cis-2-CTP…Me_2Se	-1.89	-0.63	-3.03 (54.7%)	-5.54	138
trans-2-CTP…Me_2O	-1.82	-1.24	-2.56(45.6%)	-5.62	97
trans-2-CTP…Me_2S	-2.00	-0.85	-3.01 (51.4%)	-5.86	120
trans-2-CTP…Me_2Se	-2.60	-0.81	-3.24 (48.7%)	-6.65	100

less electronegative atoms; hence electrostatic contribution will not play a dominant role. Contribution of the polarization energy component is nearly the same in cis-2-CTP…Me_2Se as well as trans-2-CTP…Me_2Se. The charge transfer component dominates in case of cis-2-CTP…Me_2Se complex which provides more red-shift in S-H stretching frequency of cis-2-CTP…Me_2Se complex in spite of the fact that cis-2-CTP…Me_2Se is less stable than trans-2-CTP…Me_2Se.

5.3 Conclusion

In conclusion, we have studied hydrogen bonding involving unconventional hydrogen-bond donor and acceptor atoms. We formed the complex between 2-Chlorothiophenol (2-CTP) and dimethyl sulfide (Me_2S)/dimethyl selenide (Me_2Se) in the supersonic jet to study S-H…S and S-H…Se hydrogen bonding interactions using electronic spectroscopy, UV-UV hole burn and RIDIRS coupled with quantum chemical calculations. We observed two conformers for

each of the 2-CTP…Me_2S and 2-CTP…Me_2Se complex. We observed that *cis*-2-CTP…Me_2S/Me_2Se shows more red-shift in S-H stretching frequency as compared to *trans*-2-CTP…Me_2S/Me_2Se complex although it is energetically less stable. We have compared S-H…S and S-H…Se interactions with conventional hydrogen-bonding interactions like O-H…O. We observed that these interactions are of similar strength as compared to conventional hydrogen bonding interactions. We observed large red-shift in S-H stretching frequency for both the conformers of 2-CTP…Me_2S/Me_2Se complex. This red-shift in S-H stretching frequency is comparable to O-H stretching frequency in conventional hydrogen bonding complex like phenol…H_2O. The large red-shift in S-H stretching frequency indicates a strong hydrogen-bonding complex. It is quite surprising because both hydrogen bond donor and acceptor atoms (S and Se) are less electronegative than O.

In conventional hydrogen bonding complexes, electrostatic interaction plays a dominant role in red-shift in hydrogen-bond donor atom due to the large electronegativity of donor and acceptor atoms. In conformers of 2-CTP…Me_2S/Me_2Se complex, as both S and Se are less electronegative, it is quite obvious that electrostatic will not dominate in red-shift in S-H stretching frequency of 2-CTP. To understand about the contributing factors in S-H stretching frequency, we have performed LMO-EDA, ALMO-EDA and NBO calculations. We observed that the dispersion component plays a significant role in stabilization of 2-CTP…Me_2S/Me_2Se complexes and charge transfer (CT) plays a significant role in S-H stretching frequency along with electrostatic and polarization interactions. Our results indicate that high electronegativity of hydrogen-bond donor and acceptor is no longer a necessary criterion for strong hydrogen bond. Strong hydrogen-bond can be formed even when both hydrogen-bond donor and acceptor atoms are less electronegative.

Chapter 6

Conclusion and future directions

6.1 Conclusion

In summary, we have explored direct selenium (Se) hydrogen bonding as well as water-mediated Se hydrogen bonding interactions between amino acid residues in proteins through PDB analysis coupled with gas phase electronic, IR spectroscopy and quantum chemical calculation of model complexes mimicking these interactions. The current investigation demonstrates that the most stable structure of a model complex consisting of indole, H_2O and dimethyl selenide observed in the gas phase spectroscopy mimics single water-mediated selenium hydrogen bonded structural motif present in the crystal structures of proteins. Indole and dimethyl selenide represent the amino acids tryptophan and selenomethionine, respectively. It has been found that Se hydrogen bonding is of similar strength to oxygen and nitrogen-centered hydrogen bonding. The present work establishes that water-mediated Se hydrogen bonding interactions are ubiquitous in proteins and these interactions are of similar significance to the direct Se hydrogen bonding interactions. Another interesting finding of this research is that X-H…Y hydrogen bond, i.e., S-H…S and S-H…Se can be of similar strength to any conventional strong hydrogen bond when both X and Y are weakly electronegative like a carbon atom. The unusually strong hydrogen-bond involving S and Se atoms observed in terms of IR red-shift in the X-H stretching frequency has been explained through the presence of the significant amount of charge transfer interaction as the electrostatic interaction present there is relatively weaker than that in any conventional strong hydrogen bonding interaction.

6.2 Future perspectives

In future, we would like to explore C-H…Se hydrogen bonding interaction by studying complexes between various model systems containing carbon (C) as hydrogen-bond donor and selenium (Se) as a hydrogen-bond acceptor in a supersonic jet. It is known that C (2.55) and S (2.58) have similar electronegativity. We have already explored S-H…Se interaction

observed that S-H is a strong hydrogen bond donor. It would be interesting to find out whether C-H can act as a strong hydrogen bond donor when Se is the hydrogen bond acceptor. We have theoretically studied a few model systems to investigate the strength of the C-H…Se interaction. One such example is given in Figure 6.1. We have optimized the geometry of 1,2,3,5-tetrafluorobenzene…dimethyl selenide (Me_2Se) complex and calculated the binding energy and vibrational frequencies of the complex. The binding energy of the complex is -3.49 kcal/mol, and there is a 86 cm^{-1} red shift in the C-H stretching frequency (C-H…Se) compared to that in the 1,2,3,5-tetrafluorobenzene monomer.

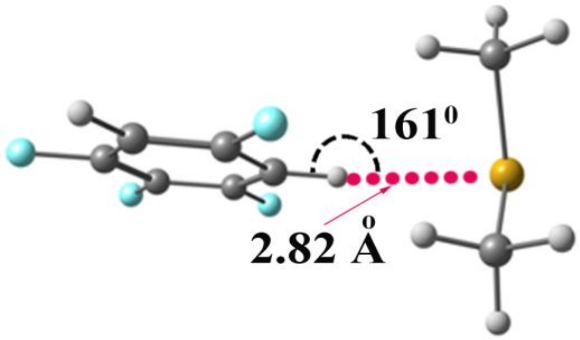

Figure 6.1: C-H…Se interaction in the optimized geometry of 1,2,3,5-tetrafluorobenzene…dimethyl selenide complex calculated at B97-D/6-311++G(d,p) level of theory.

Till now, we have studied the complexes, where Se acts as hydrogen-bond acceptor. We would like to investigate the systems where Se acts as a hydrogen bond donor. As Se (2.55), C (2.55) and S (2.58) have similar electronegativity values, it would be interesting to explore the ability of Se as a hydrogen bond donor.

We have performed *ab initio* quantum chemical calculation on the complexes of benzeneselenol (BzSeH) with dimethylsulfide (Me_2S) and dimethyl selenide (Me_2Se). We have observed that benzeneselenol forms very strong hydrogen bond with both Me_2S and Me_2Se. The red-shift values in the Se-H stretching frequency in the BzSeH…Me_2S and

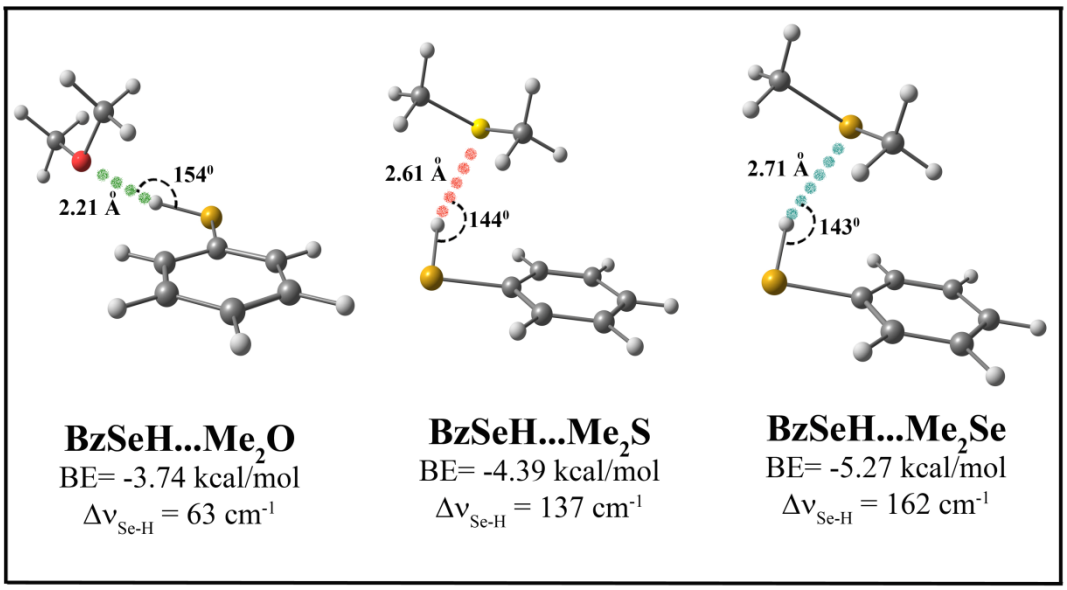

Figure 6.2: Optimized geometries of (a) benzeneselenol…dimethyl sulphide (BzSeH…Me_2S) and (b) benzeneselenol…dimethyl selenide (BzSeH…Me_2Se) complexes calculated at the B97-D/6-311++G(d,p) level of theory.

BzSeH…Me_2Se complexes with respect to that in the BzSe monomer calculated at the B97-D/6-311++G(d,p) level of theory are 137 and 162 cm^{-1}, respectively. Surprisingly, the Se-H…O hydrogen bond in BzSeH…Me_2O is relatively weaker as the calculated red-shift in the Se-H frequency in the complex compared to that in the monomer is only 63 cm^{-1}.

On the theoretical ground, we have shown that charge transfer component of the binding energies in the Se hydrogen bonded complexes plays a significant role for providing significant IR red-shift in the X-H stretching frequency despite the presence of weaker electrostatic component. However, further detailed computational studies are required to understand the nature and strength of hydrogen bonding interactions involving less electronegative and larger sized elements.

Bibiliography

(1) Desiraju, G. R.; Steiner, T. *The Weak Hydrogen Bond in Structural Chemistry and Biology*; Oxford University Press, New York, 1999.

(2) Karshikoff, A. *Non-covalent Interactions in Proteins*; Imperial College Press, 2006.

(3) Lehn, J.-M. *Supramolecular Chemistry: Concepts and Perspectives*; John Wiley & Sons, New York, 1996.

(4) Anfinsen, C. B. Principles That Govern Folding of Protein Chains. *Science* **1973**, *181*, 223-230.

(5) Mahadevi, A. S.; Sastry, G. N. Cooperativity in Noncovalent Interactions. *Chem. Rev.* **2016**, *116*, 2775-2825.

(6) Steiner, T. The Hydrogen Bond in the Solid State. *Angew. Chem. Int. Ed.* **2002**, *41*, 48-76.

(7) Jeffrey, G. A.; Saenger, W. *Hydrogen Bonding in Biological Structures*; Springer: Berlin, 1991.

(8) Jeffrey, G. A. *An Introduction to Hydrogen Bonding*; Oxford University Press: New York, 1997.

(9) Pimentel, G. C.; McClellan, A. L. *The hydrogen bond*; W.H. Freeman: San Francisco ; London, 1960.

(10) Metrangolo, P.; Meyer, F.; Pilati, T.; Resnati, G.; Terraneo, G. Halogen Bonding in Supramolecular Chemistry. *Angew. Chem. Int. Ed.* **2008**, *47*, 6114-6127.

(11) Metrangolo, P.; Resnati, G.; Pilati, T.; Biella, S. In *Halogen Bonding: Fundamentals and Applications*; Metrangolo, P., Resnati, G., Eds.; Springer Berlin Heidelberg: Berlin, Heidelberg, 2008, p 105-136.

(12) Parisini, E.; Metrangolo, P.; Pilati, T.; Resnati, G.; Terraneo, G. Halogen bonding in halocarbon–protein complexes: a structural survey. *Chem. Soc. Rev.* **2011**, *40*, 2267-2278.

(13) Metrangolo, P.; Resnati, G. Halogen Versus Hydrogen. *Science* **2008**, *321*, 918-919.

(14) Cavallo, G.; Metrangolo, P.; Milani, R.; Pilati, T.; Priimagi, A.; Resnati, G.; Terraneo, G. The Halogen Bond. *Chem. Rev.* **2016**, *116*, 2478-2601.

(15) Priimagi, A.; Cavallo, G.; Metrangolo, P.; Resnati, G. The Halogen Bond in the Design of Functional Supramolecular Materials: Recent Advances. *Acc. Chem. Res.* **2013**, *46*, 2686-2695

(16) Auffinger, P.; Hays, F. A.; Westhof, E.; Ho, P. S. Halogen bonds in biological molecules. *Proc. Natl. Acad. Sci. U.S.A.* **2004**, *101*, 16789-16794.

(17) Legon, A. C. The halogen bond: an interim perspective. *Phys. Chem. Chem. Phys.* **2010**, *12*, 7736-7747.

(18) Desiraju Gautam, R.; Ho, P. S.; Kloo, L.; Legon Anthony, C.; Marquardt, R.; Metrangolo, P.; Politzer, P.; Resnati, G.; Rissanen, K. In *Pure and Applied Chemistry* 2013; Vol. 85, p 1711.

(19) Bartlett, G. J.; Choudhary, A.; Raines, R. T.; Woolfson, D. N. n→π* interactions in proteins. *Nat. Chem. Biol.* **2010**, *6*, 615-620.

(20) Newberry, R. W.; VanVeller, B.; Guzei, I. A.; Raines, R. T. n→π* Interactions of Amides and Thioamides: Implications for Protein Stability. *J. Am. Chem. Soc.* **2013**, *135*, 7843-7846.

(21) Bartlett, G. J.; Newberry, R. W.; VanVeller, B.; Raines, R. T.; Woolfson, D. N. Interplay of Hydrogen Bonds and n→π* Interactions in Proteins. *J. Am. Chem. Soc.* **2013**, *135*, 18682-18688.

(22) Singh, S. K.; Das, A. The n [rightward arrow] [small pi]* interaction: a rapidly emerging non-covalent interaction. *Phys. Chem. Chem. Phys.* **2015**, *17*, 9596-9612.

(23) Singh, S. K.; Mishra, K. K.; Sharma, N.; Das, A. Direct spectroscopic evidence for an n-pi* interaction. *Angew. Chem. Int. Ed.* **2016**, *55*, 7801-7805.

(24) Hunter, C. A.; Sanders, J. K. M. The nature of π-π interactions. *J. Am. Chem. Soc.* **1990**, *112*, 5525-5534.

(25) Hunter, C. A.; Singh, J.; Thornton, J. M. π-π interactions: the geometry and energetics of phenylalanine-phenylalanine interactions in proteins. *J. Mol. Biol.* **1991**, *218*, 837-846.

(26) Wagner, J. P.; Schreiner, P. R. London Dispersion in Molecular Chemistry—Reconsidering Steric Effects. *Angew. Chem. Int. Ed.* **2015**, *54*, 12274-12296.

(27) Wheeler, S. E. Understanding Substituent Effects in Noncovalent Interactions Involving Aromatic Rings. *Acc. Chem. Res.* **2013**, *46*, 1029-1038.

(28) Palit, S. R.; Mukherjee, S.; De, S. K. N-H.... π hydrogen bonding. *J. Phys. Chem.* **1971**, *75*, 2404-2405.

(29) Hobza, P.; Špirko, V. r.; Havlas, Z.; Buchhold, K.; Reimann, B.; Barth, H.-D.; Brutschy, B. Anti-hydrogen bond between chloroform and fluorobenzene. *Chem. Phys. Lett.* **1999**, *299*, 180-186.

(30) Braun, J.; Neusser, H. J.; Hobza, P. N−H···π Interactions in Indole···Benzene-h_6,d_6 and Indole···Benzene-h_6,d_6 Radical Cation Complexes. Mass Analyzed Threshold Ionization Experiments and Correlated ab Initio Quantum Chemical Calculations. *J. Phys. Chem. A* **2003**, *107*, 3918-3924.

(31) Kumar, M.; Balaji, P. V. C-H…pi interactions in proteins: prevalence, pattern of occurrence, residue propensities, location, and contribution to protein stability. *J. Mol. Model.* **2014**, *20*, 2136.

(32) Ma, J. C.; Dougherty, D. A. The Cation−π Interaction. *Chem. Rev.* **1997**, *97*, 1303-1324.

(33) Gallivan, J. P.; Dougherty, D. A. Cation-π interactions in structural biology. *Proc. Natl. Acad. Sci. U.S.A.* **1999**, *96*, 9459-9464.

(34) Dougherty, D. A. The cation-π interaction. *Acc. Chem. Res.* **2013**, *46*, 885-893.

(35) Dougherty, D. A. Cation-π interactions involving aromatic amino acids. *J. Nutr.* **2007**, *137*, 1504S-1508S.

(36) Mahadevi, A. S.; Sastry, G. N. Cation−π Interaction: Its Role and Relevance in Chemistry, Biology, and Material Science. *Chem. Rev.* **2013**, *113*, 2100-2138.

(37) Mitchell, M. O.; Means, J. Cation−π Interactions in Biochemistry: A Primer. *J. Chem. Edu.* **2018**, *95*, 2284-2288.

(38) Chifotides, H. T.; Dunbar, K. R. Anion−π Interactions in Supramolecular Architectures. *Acc. Chem. Res.* **2013**, *46*, 894-906.

(39) Quiñonero, D.; Garau, C.; Rotger, C.; Frontera, A.; Ballester, P.; Costa, A.; Deyà, P. M. Anion–π Interactions: Do They Exist? *Angew. Chem. Int. Ed.* **2002**, *41*, 3389-3392.

(40) Frontera, A.; Gamez, P.; Mascal, M.; Mooibroek, T. J.; Reedijk, J. Putting Anion–π Interactions Into Perspective. *Angew. Chem. Int. Ed.* **2011**, *50*, 9564-9583.

(41) Biswas, C.; Drew, M. G. B.; Escudero, D.; Frontera, A.; Ghosh, A. Anion-π, lone-Pair-π, π-π and hydrogen-bonding interactions in a Cu11 Complex of 2-picolinate and

protonated 4,4́-bipyridine: Crystal structure and theoretical studies. *Eur. J. Inorg. Chem.* **2009**, 2238-2246.

(42) Werner, A. Ueber Haupt- und Nebenvalenzen und die Constitution der Ammoniumverbindungen. *Justus Liebigs Annalen der Chemie* **1902**, *322*, 261-296.

(43) Moore, T. S.; Winmill, T. F. CLXXVII.—The state of amines in aqueous solution. *J. Chem. Soc., Trans.* **1912**, *101*, 1635-1676.

(44) Latimer, W. M.; Rodebush, W. H. POLARITY AND IONIZATION FROM THE STANDPOINT OF THE LEWIS THEORY OF VALENCE. *J. Am. Chem. Soc.* **1920**, *42*, 1419-1433.

(45) Pauling, L. *The Nature of the Chemical Bond*; Cornell University Press: Ithaca, NY, 1960.

(46) Arunan, E.; Desiraju, G. R.; Klein, R. A.; Sadlej, J.; Scheiner, S.; Alkorta, I.; Clary, D. C.; Crabtree, R. H.; Dannenber, J. J.; Hobza, P.; Kjaergaard, H. G.; Legon, A. C.; Mennucci, B.; Nesbitt, D. J. Definition of the hydrogen bond (IUPAC Recommendations 2011). *Pure and Applied Chemistry* **2011**, *83*, 1637-1641.

(47) Emsley, J. Very strong hydrogen bonding. *Chem. Soc. Rev.* **1980**, *9*, 91-124.

(48) Pimentel, G. C.; McClellan, A. L. HYDROGEN BONDING. *Ann. Rev. Phys. Chem.* **1971**, *22*, 347-385.

(49) Etter, M. C. Encoding and decoding hydrogen-bond patterns of organic compounds. *Acc. Chem. Res.* **1990**, *23*, 120-126.

(50) Alkorta, I.; Rozas, I.; Elguero, J. Non-conventional hydrogen bonds. *Chem. Soc. Rev.* **1998**, *27*, 163-170.

(51) Grabowski, S. J. Ab Initio Calculations on Conventional and Unconventional Hydrogen BondsStudy of the Hydrogen Bond Strength. *J. Phys. Chem. A* **2001**, *105*, 10739-10746.

(52) Hibbert, F.; Emsley, J. In *Advances in Physical Organic Chemistry*; Bethell, D., Ed.; Academic Press: 1990; Vol. 26, p 255-379.

(53) Kitaura, K.; Morokuma, K. A new energy decomposition scheme for molecular interactions within the Hartree-Fock approximation. *Int. J. Quantum Chem.* **1976**, *10*, 325-340.

(54) Saggu, M.; Levinson, N. M.; Boxer, S. G. Direct Measurements of Electric Fields in Weak OH···π Hydrogen Bonds. *J. Am. Chem. Soc.* **2011**, *133*, 17414-17419.

(55) Saggu, M.; Levinson, N. M.; Boxer, S. G. Experimental Quantification of Electrostatics in X–H···π Hydrogen Bonds. *J. Am. Chem. Soc.* **2012**, *134*, 18986-18997.

(56) Nishio, M. CH/[small pi] hydrogen bonds in crystals. *CrystEngComm* **2004**, *6*, 130-158.

(57) Nishio, M. The CH/[small pi] hydrogen bond in chemistry. Conformation, supramolecules, optical resolution and interactions involving carbohydrates. *Phys. Chem. Chem. Phys.* **2011**, *13*, 13873-13900.

(58) Nishio, M.; Umezawa, Y.; Fantini, J.; Weiss, M. S.; Chakrabarti, P. CH-[small pi] hydrogen bonds in biological macromolecules. *Phys. Chem. Chem. Phys.* **2014**, *16*, 12648-12683.

(59) Mohan, N.; Vijayalakshmi, K. P.; Koga, N.; Suresh, C. H. Comparison of aromatic NH···π, OH···π, and CH···π interactions of alanine using MP2, CCSD, and DFT methods. *J. Comput. Chem.* **2010**, *31*, 2874-2882.

(60) Kitaura, K.; Morokuma, K. *Int. J. Quantum Chem.* **1976**, *10*, 325.

(61) Umeyama, H.; Morokuma, K. *J. Am. Chem. Soc.* **1977**, *99*, 1316.

(62) Sato, N.; Seki, K.; Inokuchi, H. Polarization Energies of Organic Solids Determined by Ultraviolet Photoelectron Spectroscopy. *J. Chem. SOC., Faraday Trans. 2* **1981**, *77*, 1621-1633.

(63) Atkins, P.; Paula, J. D. ATKIN'S PHYSICAL CHEMISTRY 8th EDITION. 633.

(64) Watson, J. D.; Crick, F. H. C. Molecular Structure of Nucleic Acids. *Nature* **1953**, *171*, 737-738.

(65) Stadtman, T. C. Selenium Biochemistry. *Proteins containing selenium are essential components of certain bacterial and mammalian enzyme systems* **1974**, *183*, 915-922.

(66) Stadtman, T. C. SELENOCYSTEINE. *Annu. Rev. Biochem.* **1996**, *65*, 83-100.

(67) Salon, J.; Sheng, J.; Jiang, J.; Chen, G.; Caton-Williams, J.; Huang, Z. Oxygen Replacement with Selenium at the Thymidine 4-Position for the Se Base Pairing and Crystal Structure Studies. *J. Am. Chem. Soc.* **2007**, *129*, 4862-4863.

(68) Salon, J.; Jiang, J.; Sheng, J.; Gerlits, O. O.; Huang, Z. Derivatization of DNAs with selenium at 6-position of guanine for function and crystal structure studies. *Nucleic Acids Res.* **2008**, *36*, 7009-7018.

(69) Mundlapati, V. R.; Sahoo, D. K.; Ghosh, S.; Purame, U. K.; Pandey, S.; Acharya, R.; Pal, N.; Tiwari, P.; Biswal, H. S. Spectroscopic Evidences for Strong Hydrogen Bonds with Selenomethionine in Proteins. *J. Phys. Chem. Lett.* **2017**, *8*, 794-800.

(70) June Sutor, D. The C–H… O Hydrogen Bond in Crystals. *Nature* **1962**, *195*, 68-69.

(71) Ferguson, G.; Tyrrell, J. C-H...O Hydrogen Bonding. *Chem. Comm.* **1965**, 195-196.

(72) Keegstra, E. M. D.; Spek, A. L.; Zwikker, J. W.; Jenneskens, L. W. The crystal structure of 2-methoxy-1,4-benzoquinone: molecular recognition involving intermolecular dipole–dipole- and C–H ⋯ O hydrogen bond interactions. *J. Chem. Soc., Chem. Comm.* **1994**, 1633-1634.

(73) Sharma, C. V. K.; Desiraju, G. R. C–H ⋯ O hydrogen bond patterns in crystalline nitro compounds: studies in solid-state molecular recognition. *J. Chem. Soc., Perkin Trans. 2* **1994**, 2345-2352.

(74) Allen, F. H.; Bird, C. M.; Rowland, R. S.; Raithby, P. R. Resonance-Induced Hydrogen Bonding at Sulfur Acceptors in R1R2C=S and R1CS2- Systems. *Acta Crystallographica Section B* **1997**, *53*, 680-695.

(75) Allen, F. H.; Bird, C. M.; Rowland, R. S.; Raithby, P. R. Hydrogen-Bond Acceptor and Donor Properties of Divalent Sulfur (Y-S-Z and R-S-H). *Acta Crystallographica Section B* **1997**, *53*, 696-701.

(76) Peng, J.; Barr, M. E.; Ashburn, D. A.; Odom, J. D.; Dunlap, R. B.; Silks, L. A. Synthesis and Characterization of Chiral Oxazolidine-2-selones: A General One-Step Procedure from Readily Available Oxazolines. *J. Org. Chem.* **1994**, *59*, 4977-4987.

(77) Bhattacharyya, P.; Novosad, J.; Phillips, J.; Slawin, A. M. Z.; Williams, D. J.; Woollins, J. D. Bis(bidentate) complexes of iminobis(diphenylphosphine chalcogenides)[M{N(XPPh2)2-X,X′}2](X = S or Se; M = Ni, Pd or Pt). *J. Chem. Soc., Dalton Trans.* **1995**, 1607-1613.

(78) Iwaoka, M.; Tomoda, S. First Observation of a C-H...Se "Hydrogen Bond". *J. Am. Chem. Soc.* **1994**, *116*, 4463-4464.

(79) Badger, R. M.; Bauer, S. H. Spectroscopic Studies of the Hydrogen Bond. II. The Shift of the O–H Vibrational Frequency in the Formation of the Hydrogen Bond. *J. Chem. Phys.* **1937**, *5*, 839-851.

(80) Badger, R. M.; Bauer, S. H. Spectroscopic Studies of the Hydrogen Bond I. A Photometric Investigation of the Association Equilibrium in the Vapor of Acetic Acid. *J. Chem. Phys.* **1937**, *5*, 605-608.

(81) Buděšínský, M.; Fiedler, P.; Arnold, Z. Triformylmethane: An Efficient Preparation, Some Derivatives, and Spectra. *Synthesis* **1989**, *1989*, 858-860.

(82) Hobza, P.; Havlas, Z. Blue-Shifting Hydrogen Bonds. *Chem. Rev.* **2000**, *100*, 4253-4264.

(83) Legon, A. C. Tilden Lecture. The properties of hydrogen-bonded dimers from rotational spectroscopy. *Chem. Soc. Rev.* **1990**, *19*, 197-237.

(84) Xue, Z.; Suhm, M. A. Probing the stiffness of the simplest double hydrogen bond: The symmetric hydrogen bond modes of jet-cooled formic acid dimer. *J. Chem. Phys.* **2009**, *131*, 054301.

(85) Kumler, W. D. The Effect of the Hydrogen Bond on the Dielectric Constants and Boiling Points of Organic Liquids. *J. Am. Chem. Soc.* **1935**, *57*, 600-605.

(86) Shallcross, F. V.; Carpenter, G. B. The crystal structure of cyanoacetylene. *Acta Crystallogr* **1958**, *11*, 490-496.

(87) Dougill, M. W.; Jeffrey, G. A. The structure of dimethyl oxalate. *Acta Crystallogr* **1953**, *6*, 831-837.

(88) Desiraju, G. R. The C-H...O Hydrogen-Bond in Crystals - What Is It. *Acc. Chem. Res.* **1991**, *24*, 290-296.

(89) Kirchner, M. T.; Bläser, D.; Boese, R.; Thakur, T. S.; Desiraju, G. R. Weak C-H···O hydrogen bonds in anisaldehyde, salicyl-aldehyde and cinnamaldehyde. *Acta Crystallographica Section C: Crystal Structure Communications* **2011**, *67*, o387-o390.

(90) Desiraju, G. R. C-H···O and other weak hydrogen bonds. From crystal engineering to virtual screening. *Chem. Comm.* **2005**, 2995-3001.

(91) Thakur, T. S.; Kirchner, M. T.; Bläser, D.; Boese, R.; Desiraju, G. R. C-H···F-C hydrogen bonding in 1,2,3,5-tetrafluorobenzene and other fluoroaromatic compounds and the crystal structure of alloxan revisited. *CrystEngComm* **2010**, *12*, 2079-2085.

(92) Thalladi, V. R.; Weiss, H.-C.; Bläser, D.; Boese, R.; Nangia, A.; Desiraju, G. R. C−H···F Interactions in the Crystal Structures of Some Fluorobenzenes. *J. Am. Chem. Soc.* **1998**, *120*, 8702-8710.

(93) Wulf, O. R.; Liddel, U.; Hendricks, S. B. The Effect of Ortho Substitution on the Absorption of the OH Group of Phenol in the Infrared1. *J. Am. Chem. Soc.* **1936**, *58*, 2287-2293.

(94) Yoshida, Z.-i.; Osawa, E. Hydrogen Bonding of Phenol to π Electrons of Aromatics, Polyolefins, Heteroaromatics, Fulvenes, and Azulenes1. *J. Am. Chem. Soc.* **1966**, *88*, 4019-4026.

(95) McPhail, A. T.; Sim, G. A. Hydroxyl–benzene hydrogen bonding: an X-ray study. *Chem. Comm.* **1965**, 124-126.

(96) Davies, T.; Staveley, L. A. K. The behaviour of the ammonium ion in the ammonium salt of tetraphenylboron by comparison of the heat capacities of the ammonium, rubidium, and potassium salts. *Trans. Faraday Soc.* **1957**, *53*, 19-30.

(97) Leist, R.; Frey, J. A.; Ottiger, P.; Frey, H.-M.; Leutwyler, S.; Bachorz, R. A.; Klopper, W. Nucleobase–Fluorobenzene Interactions: Hydrogen Bonding Wins over π Stacking. *Angew. Chem. Int. Ed.* **2007**, *46*, 7449-7452.

(98) Karthikeyan, S.; Venkatnarayan, R.; Mishra, B. K. Influence of the Substituents on the CH…π Interaction: Benzene-Methane Complex. *J. Phys. Chem. A* **2013,** *117*, 6687-6694.

(99) Ottiger, P.; Pfaffen, C.; Leist, R.; Leutwyler, S.; Bachorz, R. A.; Klopper, W. Strong N−H···π Hydrogen Bonding in Amide−Benzene Interactions. *J. Phys. Chem. B* **2009**, *113*, 2937-2943.

(100) Rodham, D. A.; Suzuki, S.; Suenram, R. D.; Lovas, F. J.; Dasgupta, S.; Goddard, W. A.; Blake, G. A. Hydrogen bonding in the benzene-ammonia dimer. *Nature* **1993**, *362*, 735-737.

(101) Suzuki, S.; Green, P. G.; Bumgarner, R. E.; Dasgupta, S.; Goddard, W. A.; Blake, G. A. Benzene Forms Hydrogen Bonds with Water. *Science* **1992**, *257*, 942-945.

(102) Kollman, P. A.; Allen, L. C. Theory of the hydrogen bond. *Chem. Rev.* **1972**, *72*, 283-303.

(103) Biswal, H. S. In *Noncovalent Forces*; Scheiner, S., Ed.; Springer International Publishing: Cham, 2015, p 15-45.

(104) Mundlapati, V. R.; Sahoo, D. K.; Ghosh, S.; Purame, U. K.; Pandey, S.; Acharya, R.; Pal, N.; Tiwari, P.; Biswal, H. S. Spectroscopic Evidences for Strong Hydrogen Bonds with Selenomethionine in Proteins. *J. Phys. Chem. Lett.* **2017**, *8*, 794-800.

(105) Hansen, A. S.; Du, L.; Kjaergaard, H. G. Positively Charged Phosphorus as a Hydrogen Bond Acceptor. *J. Phys. Chem. Lett.* **2014**, *5*, 4225-4231.

(106) Brammer, L. Metals and hydrogen bonds. *Dalton Trans.* **2003**, 3145-3157.

(107) Brammer, L.; Charnock, J. M.; Goggin, P. L.; Goodfellow, R. J.; Orpen, A. G.; Koetzle, T. F. The role of transition metal atoms as hydrogen bond acceptors: a neutron diffraction study of [NPrn4]2[PtCl4]·cis-[PtCl2(NH2Me)2] at 20 K. *J. Chem. Soc., Dalton Trans.* **1991**, 1789-1798.

(108) Braga, D.; Grepioni, F.; Desiraju, G. R. Crystal Engineering and Organometallic Architecture. *Chem. Rev.* **1998**, *98*, 1375-1406.

(109) Braga, D.; Grepioni, F.; Tedesco, E.; Biradha, K.; Desiraju, G. R. Hydrogen Bonding in Organometallic Crystals. 4. M−H- - -O Hydrogen-Bonding Interactions. *Organometallics* **1996**, *15*, 2692-2699.

(110) Sahoo, D. K.; Jena, S.; Dutta, J.; Rana, A.; Biswal, H. S. Nature and Strength of M–H···S and M–H···Se (M = Mn, Fe, & Co) Hydrogen Bond. *J. Phys. Chem. A* **2019**, *123*, 2227-2236.

(111) Arunan, E.; Desiraju, G. R.; Klein, R. A.; Sadlej, J.; Scheiner, S.; Alkorta, I.; Clary, D. C.; Crabtree, R. H.; Dannenberg, J. J.; Hobza, P.; Kjaergaard, H. G.; Legon, A. C.; Mennucci, B.; Nesbitt, D. J. Defining the hydrogen bond: An account (IUPAC Technical Report). *Pure and Applied Chemistry* **2011**, *83*, 1619-1636.

(112) Biswal, H. S.; Chakraborty, S.; Wategaonkar, S. Experimental evidence of O-H-S hydrogen bonding in supersonic jet. *J. Chem. Phys.* **2008**, *129*.

(113) Biswal, H. S.; Wategaonkar, S. Nature of the N−H···S Hydrogen Bond. *J. Phys. Chem. A* **2009**, *113*, 12763-12773.

(114) Bhattacharyya, S.; Bhattacherjee, A.; Wategaonkar, S. Nature and strength of sulfur-centred hydrogen bonds: laser spectroscopic investigations in the gas phase and quantum-chemical calculations AU - Biswal, Himansu S. *Int. Rev. Phys. Chem.* **2015**, *34*, 99-160.

(115) Biswal, H. S.; Chakraborty, S.; Wategaonkar, S. Experimental evidence of O–H—S hydrogen bonding in supersonic jet. *J. Chem. Phys.* **2008**, *129*, 184311.

(116) Andersen, C. L.; Jensen, C. S.; Mackeprang, K.; Du, L.; Jørgensen, S.; Kjaergaard, H. G. Similar Strength of the NH···O and NH···S Hydrogen Bonds in Binary Complexes. *J. Phys. Chem. A* **2014**, *118*, 11074-11082.

(117) Dey, A.; Mondal, S. I.; Sen, S.; Ghosh, D.; Patwari, G. N. Electrostatics determine vibrational frequency shifts in hydrogen bonded complexes. *Phys. Chem. Chem. Phys.* **2014**, *16*, 25247-25250.

(118) Madzhidov, T. I.; Chmutova, G. A. The nature of hydrogen bonds with divalent selenium compounds. *Journal of Molecular Structure: THEOCHEM* **2010**, *959*, 1-7.

(119) Takano, K.; Funahashi, J.; Yamagata, Y.; Fujii, S.; Yutani, K. Contribution of water molecules in the interior of a protein to the conformational stability. *J. Mol. Biol.* **1997**, *274*, 132-142.

(120) Smalley, R. E.; Wharton, L.; Levy, D. H. Molecular optical spectroscopy with supersonic beams and jets. *Acc. Chem. Res.* **1977**, *10*, 139-145.

(121) Levy, D. H. Laser Spectroscopy of Cold Gas-Phase Molecules. *Ann. Rev. Phys. Chem.* **1980**, *31*, 197-225.

(122) Levy, D. H. The spectroscopy of very cold gases. *Science* **1981**, *214*, 263-269.

(123) Wiley, W. C.; McLaren, I. H. Time-of-Flight Mass Spectrometer with Improved Resolution. *Review of Scientific Instruments* **1955**, *26*, 1150-1157.

(124) Duarte, F. J. K., P.; Hillman, L. W.; Liao, P. F. *Dye laser principles*; Elsevier Science, 2012.

(125) Liao, P. F. K., P.; Duarte, F. J.; Hillman, L. W. *Dye Laser Principles: With Applications*; Elsevier, 2012.

(126) Sorokin, P. L., J. IBM *J. Res. Dev.* **1966**, *10*.

(127) Lubman, D. M. Optically selective molecular mass spectrometry. *Anal. Chem.* **1987**, *59*, 31A-40A.

(128) Page, R. H.; Shen, Y. R.; Lee, Y. T. Infrared–ultraviolet double resonance studies of benzene molecules in a supersonic beam. *J. Chem. Phys.* **1988**, *88*, 5362-5376.

(129) Ehrlich, S.; Moellmann, J.; Grimme, S. Dispersion-Corrected Density Functional Theory for Aromatic Interactions in Complex Systems. *Acc. Chem. Res.* **2012**, *46*, 916-926.

(130) Zhao, Y.; Truhlar, D. G. Density Functionals for Noncovalent Interaction Energies of Biological Importance. *J. Chem. Theory Comput.* **2006**, *3*, 289-300.

(131) Hohenstein, E. G.; Chill, S. T.; Sherrill, C. D. Assessment of the Performance of the M05−2X and M06−2X Exchange-Correlation Functionals for Noncovalent Interactions in Biomolecules. *J. Chem. Theory Comput.* **2008**, *4*, 1996-2000.

(132) Grimme, S. Semiempirical GGA-type density functional constructed with a long-range dispersion correction. *J. Comput. Chem.* **2006**, *27*, 1787-1799.

(133) Grimme, S.; Ehrlich, S.; Goerigk, L. Effect of the Damping Function in Dispersion Corrected Density Functional Theory. *J. Comput. Chem.* **2011**, *32*, 1456-1465.

(134) Boys, S. F.; Bernardi, F. The calculation of small molecular interactions by the differences of separate total energies. Some procedures with reduced errors. *Mol. Phys.* **1970**, *19*, 553-566.

(135) Frisch, M. J.; Trucks, G. W.; Schlegel, H. B.; Scuseria, G. E.; Robb, M. A.; Cheeseman, J. R.; Scalmani, G.; Barone, V.; Mennucci, B.; Petersson, G. A.; Nakatsuji, H.; Caricato, M.; Li, X. H., H. P.; Izmaylov, A. F. B., J.; Zheng, G.; Sonnenberg, J. L.; Hada, M.; Ehara, M.; Toyota, K.; Fukuda, R.; Hasegawa, J.; Ishida, M.; Nakajima, T.; Honda, Y.; Kitao, O.; Nakai, H.; Vreven, T.; Montgomery, J., J. A.; Peralta, J. E.; Ogliaro, F.; Bearpark, M.; Heyd, J. J.; Brothers, E.; Kudin, K. N.; Staroverov, V. N.; Kobayashi, R.; Normand, J.; Raghavachari, K.; Rendell, A.; Burant, J. C.; Iyengar, S. S.; Tomasi, J.; Cossi, M.; Rega, N.; Millam, N. J.; Klene, M.; Knox, J. E.; Cross, J. B.; Bakken, V.; Adamo, C.; Jaramillo, J.; Gomperts, R.; Stratmann, R. E.; Yazyev, O.; Austin, A. J.; Cammi, R.; Pomelli, C.; Ochterski, J. W.; Martin, R. L.; Morokuma, K.; Zakrzewski, V. G.; Voth, G. A.; Salvador, P.; Dannenberg, J. J.; Dapprich, S.; Daniels, A. D.; Farkas, Ö.; Foresman, J. B.; Ortiz, J. V.; Cioslowski, J.; Fox, D. J. *Gaussian 09, Revision D.01*, Gaussian, Inc., Wallingford CT, 2009.

(136) Frisch, M. J.; Trucks, G. W.; Schlegel, H. B.; Scuseria, G. E.; Robb, M. A.; Cheeseman, J. R.; Scalmani, G.; Barone, V.; Petersson, G. A.; Nakatsuji, H.; Li, X.; Caricato, M.; Marenich, A. V.; Bloino, J.; Janesko, B. G.; Gomperts, R.; Mennucci, B.; Hratchian, H. P.; Ortiz, J. V.; Izmaylov, A. F.; Sonnenberg, J. L.; Williams; Ding, F.; Lipparini, F.; Egidi,

F.; Goings, J.; Peng, B.; Petrone, A.; Henderson, T.; Ranasinghe, D.; Zakrzewski, V. G.; Gao, J.; Rega, N.; Zheng, G.; Liang, W.; Hada, M.; Ehara, M.; Toyota, K.; Fukuda, R.; Hasegawa, J.; Ishida, M.; Nakajima, T.; Honda, Y.; Kitao, O.; Nakai, H.; Vreven, T.; Throssell, K.; Montgomery Jr., J. A.; Peralta, J. E.; Ogliaro, F.; Bearpark, M. J.; Heyd, J. J.; Brothers, E. N.; Kudin, K. N.; Staroverov, V. N.; Keith, T. A.; Kobayashi, R.; Normand, J.; Raghavachari, K.; Rendell, A. P.; Burant, J. C.; Iyengar, S. S.; Tomasi, J.; Cossi, M.; Millam, J. M.; Klene, M.; Adamo, C.; Cammi, R.; Ochterski, J. W.; Martin, R. L.; Morokuma, K.; Farkas, O.; Foresman, J. B.; Fox, D. J. *Gaussian 16, Revision B.01*, Gaussian, Inc.,Wallingford, CT, 2016.

(137) Su, P.; Li, H. Energy decomposition analysis of covalent bonds and intermolecular interactions. *J. Chem. Phys.* **2009**, *131*, 014102.

(138) Schmidt, M. W.; Baldridge, K. K.; Boatz, J. A.; Elbert, S. T.; Gordon, M. S.; Jensen, J. H.; Koseki, S.; Matsunaga, N.; Nguyen, K. A.; Su, S.; Windus, T. L.; Dupuis, M.; Montgomery Jr, J. A. General atomic and molecular electronic structure system. *J. Comput. Chem.* **1993**, *14*, 1347-1363.

(139) Khaliullin, R. Z.; Cobar, E. A.; Lochan, R. C.; Bell, A. T.; Head-Gordon, M. Unravelling the Origin of Intermolecular Interactions Using Absolutely Localized Molecular Orbitals. *J. Phys. Chem. A* **2007**, *111*, 8753-8765.

(140) Shao, Y.; Gan, Z.; Epifanovsky, E.; Gilbert, A. T. B.; Wormit, M.; Kussmann, J.; Lange, A. W.; Behn, A.; Deng, J.; Feng, X.; Ghosh, D.; Goldey, M.; Horn, P. R.; Jacobson, L. D.; Kaliman, I.; Khaliullin, R. Z.; Kuś, T.; Landau, A.; Liu, J.; Proynov, E. I.; Rhee, Y. M.; Richard, R. M.; Rohrdanz, M. A.; Steele, R. P.; Sundstrom, E. J.; Woodcock, H. L.; Zimmerman, P. M.; Zuev, D.; Albrecht, B.; Alguire, E.; Austin, B.; Beran, G. J. O.; Bernard, Y. A.; Berquist, E.; Brandhorst, K.; Bravaya, K. B.; Brown, S. T.; Casanova, D.; Chang, C.-M.; Chen, Y.; Chien, S. H.; Closser, K. D.; Crittenden, D. L.; Diedenhofen, M.; DiStasio, R. A.; Do, H.; Dutoi, A. D.; Edgar, R. G.; Fatehi, S.; Fusti-Molnar, L.; Ghysels, A.; Golubeva-Zadorozhnaya, A.; Gomes, J.; Hanson-Heine, M. W. D.; Harbach, P. H. P.; Hauser, A. W.; Hohenstein, E. G.; Holden, Z. C.; Jagau, T.-C.; Ji, H.; Kaduk, B.; Khistyaev, K.; Kim, J.; Kim, J.; King, R. A.; Klunzinger, P.; Kosenkov, D.; Kowalczyk, T.; Krauter, C. M.; Lao, K. U.; Laurent, A. D.; Lawler, K. V.; Levchenko, S. V.; Lin, C. Y.; Liu, F.; Livshits, E.; Lochan, R. C.; Luenser, A.; Manohar, P.; Manzer, S. F.; Mao, S.-P.; Mardirossian, N.; Marenich, A. V.; Maurer, S. A.; Mayhall, N. J.; Neuscamman, E.; Oana, C. M.; Olivares-Amaya, R.; O'Neill, D. P.; Parkhill, J. A.; Perrine, T. M.; Peverati, R.; Prociuk, A.; Rehn, D. R.; Rosta, E.; Russ, N. J.; Sharada, S. M.; Sharma, S.; Small, D. W.; Sodt, A. Advances in molecular quantum chemistry contained in the Q-Chem 4 program package. *Mol. Phys.* **2015**, *113*, 184-215.

(141) Stevens, W. J.; Fink, W. H. Frozen fragment reduced variational space analysis of hydrogen bonding interactions. Application to the water dimer. *Chem. Phys. Lett.* **1987**, *139*, 15-22.

(142) Chen, W.; Gordon, M. S. Energy Decomposition Analyses for Many-Body Interaction and Applications to Water Complexes. *J. Phys. Chem.* **1996**, *100*, 14316-14328.

(143) Weinhold, F.; Landis, C. R. *Valency and Bonding: A Natural Bond Orbital Donor-Acceptor Perspective*, Cambridge University Press: Cambridge, 2005.

(144) Reed, A. E.; Curtiss, L. A.; Weinhold, F. Intermolecular interactions from a natural bond orbital, donor-acceptor viewpoint. *Chem. Rev.* **1988**, *88*, 899-926.

(145) Huggins, M. L. HYDROGEN BRIDGES IN ORGANIC COMPOUNDS*. *J. Org. Chem.* **1936**, *01*, 407-456.

(146) Huggins, M. L. 50 Years of Hydrogen Bond Theory. *Angew. Chem. Int. Ed.* **1971**, *10*, 147-152.

(147) G C Pimentel, a.; McClellan, A. L. Hydrogen Bonding. *Annu. Rev. Phys. Chem.* **1971**, *22*, 347-385.

(148) Hager, J. W.; Demmer, D. R.; Wallace, S. C. Electronic spectra of jet-cooled indoles: evidence for the 1La state. *J. Phys. Chem.* **1987**, *91*, 1375-1382.

(149) Watanabe, T.; Ebata, T.; Tanabe, S.; Mikami, N. Size-selected vibrational spectra of phenol-$(H_2O)_n$ (n=1--4) clusters observed by IR--UV double resonance and stimulated Raman-UV double resonance spectroscopies. *J. Chem. Phys.* **1996**, *105*, 408-419.

(150) Carney, J. R.; Hagemeister, F. C.; Zwier, T. S. The hydrogen-bonding topologies of indole--$(water)_n$ clusters from resonant ion-dip infrared spectroscopy. *J. Chem. Phys.* **1998**, *108*, 3379-3382.

(151) Andersen, C. L.; Jensen, C. S.; Mackeprang, K.; Du, L.; Jørgensen, S.; Kjaergaard, H. G. Similar Strength of the NH···O and NH···S Hydrogen Bonds in Binary Complexes. *J. Phys. Chem. A* **2014**, *118*, 11074.

(152) Bhattacherjee, A.; Wategaonkar, S. Nature and Hierarchy of Noncovalent Interactions in Gas-Phase Binary Complexes of Indole and Benzimidazole with Ethers. *J. Phys. Chem. A* **2017**, *121*, 8815-8824.

(153) Du, L.; Tang, S. S.; Hansen, A. S.; Frandsen, B. N.; Maroun, Z.; Kjaergaard, H. G. Subtle differences in the hydrogen bonding of alcohol to divalent oxygen and sulfur. *Chem. Phys. Lett.* **2017**, *667*, 146-153.

(154) Khaliullin, R. Z.; Cobar, E. A.; Lochan, R. C.; Bell, A. T.; Head-Gordon, M. Unravelling the origin of intermolecular interactions using absolutely localized molecular orbitals. *J. Phys. Chem. A* **2007**, *111*, 8753-8765.

(155) Sanchez-de-Armas, R.; Ahlquist, M. S. G. On the nature of hydrogen bonds to platinum(II) - which interaction can predict their strength? *Phys. Chem. Chem. Phys.* **2015**, *17*, 812-816.

(156) Lao, K. U.; Herbert, J. M. Energy Decomposition Analysis with a Stable Charge-Transfer Term for Interpreting Intermolecular Interactions. *J. Chem. Theory Comput.* **2016**, *12*, 2569-2582.

(157) Stone, A. J. Natural Bond Orbitals and the Nature of the Hydrogen Bond. *J. Phys. Chem. A* **2017**, *121*, 1531-1534.

(158) National Center for Biotechnology Information. PubChem Database. Selenomethionine, CID=15103, https://pubchem.ncbi.nlm.nih.gov/compound/15103

(159) Burley, S. K.; Petsko, G. A. Aromatic-aromatic interaction: a mechanism of protein structure stabilization. *Science* **1985**, *229*, 23-28.

(160) Dill, K. A. Dominant Forces in Protein Folding. *Biochemistry* **1990**, *29*, 7133-7155.

(161) Saenger, W. STRUCTURE AND DYNAMICS OF WATER SURROUNDING BIOMOLECULES. *Annu. Rev. Biophys. Biophys. Chemistry* **1987**, *16*, 93-114.

(162) Finney, J. L.; Eley Daniel, D.; Richards Rex, E.; Franks, F. The organization and function of water in protein crystals. *Philos. Trans. R. Soc. B* **1977**, *278*, 3-32.

(163) Wolfenden, R.; Andersson, L.; Cullis, P. M.; Southgate, C. C. B. Affinities of Amino-Acid Side-Chains for Solvent Water. *Biochemistry* **1981**, *20*, 849-855.

(164) Edsall, J. T.; Mckenzie, H. A. Water and Proteins .2. The Location and Dynamics of Water in Protein Systems and Its Relation to Their Stability and Properties. *Adv. Biophys.* **1983**, *16*, 53-183.

(165) Buckle, A. M.; Cramer, P.; Fersht, A. R. Structural and energetic responses to cavity-creating mutations in hydrophobic cores: Observation of a buried water molecule and the hydrophilic nature of such hydrophobic cavities. *Biochemistry* **1996**, *35*, 4298-4305.

(166) Sleigh, S. H.; Tame, J. R. H.; Dodson, E. J.; Wilkinson, A. J. Peptide binding in OppA, the crystal structures of the periplasmic oligopeptide binding protein in the unliganded form and in complex with lysyllysine. *Biochemistry* **1997**, *36*, 9747-9758.

(167) Chen, J. M.; Xu, S. L.; Wawrzak, Z.; Basarab, G. S.; Jordan, D. B. Structure-based design of potent inhibitors of scytalone dehydratase: Displacement of a water molecule from the active site. *Biochemistry* **1998**, *37*, 17735-17744.

(168) Baldwin, E. T.; Bhat, T. N.; Gulnik, S.; Liu, B. S.; Topol, I. A.; Kiso, Y.; Mimoto, T.; Mitsuya, H.; Erickson, J. W. Structure of Hiv-1 Protease with Kni-272, a Tight-Binding Transition-State Analog Containing Allophenylnorstatine. *Structure* **1995**, *3*, 581-590.

(169) Loris, R.; Maes, D.; Poortmans, F.; Wyns, L.; Bouckaert, J. A structure of the complex between concanavalin A and methyl-3,6-di-O-(alpha-D-mannopyranosyl)-alpha-D-mannopyranoside reveals two binding modes. *J. Biol. Chem.* **1996**, *271*, 30614-30618.

(170) Wang, Y. X.; Freedberg, D. I.; Wingfield, P. T.; Stahl, S. J.; Kaufman, J. D.; Kiso, Y.; Bhat, T. N.; Erickson, J. W.; Torchia, D. A. Bound water molecules at the interface between the HIV-1 protease and a potent inhibitor, KNI-272, determined by NMR. *J. Am. Chem. Soc.* **1996**, *118*, 12287-12290.

(171) Helms, V.; Wade, R. C. Thermodynamics of Water Mediating Protein-Ligand Interactions in Cytochrome P450cam - a Molecular-Dynamics Study. *Biophys. J.* **1995**, *69*, 810-824.

(172) Li, Z.; Lazaridis, T. Water at biomolecular binding interfaces. *Phys. Chem. Chem. Phys.* **2007**, *9*, 573-581.

(173) Williams, M. A.; Goodfellow, J. M.; Thornton, J. M. Buried Waters and Internal Cavities in Monomeric Proteins. *Protein Science* **1994**, *3*, 1224-1235.

(174) Jiang, L.; Kuhlman, B.; Kortemme, T. A.; Baker, D. A "solvated rotainer" approach to modeling water-mediated hydrogen bonds at protein-protein interfaces. *Proteins* **2005**, *58*, 893-904.

(175) Fenwick, R. B.; Oyen, D.; Dyson, H. J.; Wright, P. E. Slow Dynamics of Tryptophan-Water Networks in Proteins. *J. Am. Chem. Soc.* **2018**, *140*, 675-682.

(176) Otting, G.; Liepinsh, E.; Wuthrich, K. Protein Hydration in Aqueous-Solution. *Science* **1991**, *254*, 974-980.

(177) Otting, G.; Liepinsh, E. Protein Hydration Viewed by High-Resolution Nmr-Spectroscopy - Implications for Magnetic-Resonance Image-Contrast. *Acc. Chem. Res.* **1995**, *28*, 171-177.

(178) Ernst, J. A.; Clubb, R. T.; Zhou, H. X.; Gronenborn, A. M.; Clore, G. M. Use of Nmr to Detect Water within Nonpolar Protein Cavities - Response. *Science* **1995**, *270*, 1848-1849.

(179) Clore, G. M.; Bax, A.; Wingfield, P. T.; Gronenborn, A. M. Identification and Localization of Bound Internal Water in the Solution Structure of Interleukin-1-Beta by Heteronuclear 3-Dimensional H-1 Rotating-Frame Overhauser N-15-H-1 Multiple Quantum Coherence Nmr-Spectroscopy. *Biochemistry* **1990**, *29*, 5671-5676.

(180) Ernst, J. A.; Clubb, R. T.; Zhou, H. X.; Gronenborn, A. M.; Clore, G. M. Demonstration of Positionally Disordered Water within a Protein Hydrophobic Cavity by Nmr. *Science* **1995**, *267*, 1813-1817.

(181) Berman, H. M.; Westbrook, J.; Feng, Z.; Gilliland, G.; Bhat, T. N.; Weissig, H.; Shindyalov, I. N.; Bourne, P. E. The Protein Data Bank. *Nucleic Acids Res.* **2000**, *28*, 235-242.

(182) Wang, G.; Dunbrack, R. L., Jr PISCES: a protein sequence culling server. *Bioinformatics* **2003**, *19*, 1589-1591.

(183) Word, J. M.; Lovell, S. C.; LaBean, T. H.; Taylor, H. C.; Zalis, M. E.; Presley, B. K.; Richardson, J. S.; Richardson, D. C. Visualizing and quantifying molecular goodness-of-fit: Small-probe contact dots with explicit hydrogen atoms. *J. Mol. Biol.* **1999**, *285*, 1711-1733.

(184) Bondi, A. van der Waals Volumes and Radii. *J. Phys. Chem.* **1964**, *68*, 441-451.

(185) Biswal, H. S.; Shirhatti, P. R.; Wategaonkar, S. O−H···O versus O−H···S Hydrogen Bonding. 2. Alcohols and Thiols as Hydrogen Bond Acceptors. *J. Phys. Chem. A* **2010**, *114*, 6944-6955.

(186) Kumar, S.; Biswas, P.; Kaul, I.; Das, A. Competition between Hydrogen Bonding and Dispersion Interactions in the Indole···Pyridine Dimer and $(Indole)_2$···Pyridine Trimer Studied in a Supersonic Jet. *J. Phys. Chem. A* **2011**, *115*, 7461.

(187) Zwier, T. S. Laser Spectroscopy of Jet-Cooled Biomolecules and Their Water-Containing Clusters: Water Bridges and Molecular Conformation. *J. Phys. Chem. A* **2001**, *105*, 8827-8839.

(188) Carney, J. R.; Zwier, T. S. Infrared and Ultraviolet Spectroscopy of Water-Containing Clusters of Indole, 1-Methylindole, and 3-Methylindole. *J. Phys. Chem. A* **1999**, *103*, 9943-9957.

(189) Su, P.; Li, H. Energy decomposition analysis of covalent bonds and intermolecular interactions. *J. Chem. Phys.* **2009**, *131*, 14102-14115.

(190) Stevens, W. J.; Fink, W. H. *Chem. Phys. Lett.* **1987**, *139*, 15.

(191) Phipps, M. J. S.; Fox, T.; Tautermann, C. S.; Skylaris, C. K. Energy decomposition analysis approaches and their evaluation on prototypical protein-drug interaction patterns. *Chem. Soc. Rev.* **2015**, *44*, 3177-3211.

(192) Mishra, K. K.; Singh, S. K.; Ghosh, P.; Ghosh, D.; Das, A. The nature of selenium hydrogen bonding: gas phase spectroscopy and quantum chemistry calculations. *Phys. Chem. Chem. Phys.* **2017**, *19*, 24179-24187.

(193) Biswal, H. S.; Wategaonkar, S. Sulfur, Not Too Far Behind O, N, and C: SH···π Hydrogen Bond. *J. Phys. Chem. A* **2009**, *113*, 12774-12782.

(194) Bhattacherjee, A.; Matsuda, Y.; Fujii, A.; Wategaonkar, S. The Intermolecular S□H···Y (Y=S,O) Hydrogen Bond in the H2S Dimer and the H2S–MeOH Complex. *ChemPhysChem* **2013**, *14*, 905-914.

(195) Lobo, I. A.; Robertson, P. A.; Villani, L.; Wilson, D. J. D.; Robertson, E. G. Thiols as Hydrogen Bond Acceptors and Donors: Spectroscopy of 2-Phenylethanethiol Complexes. *J. Phys. Chem. A* **2018**, *122*, 7171-7180.

(196) Das, A.; Mandal, P. K.; Lovas, F. J.; Medcraft, C.; Walker, N. R.; Arunan, E. The H2S Dimer is Hydrogen-Bonded: Direct Confirmation from Microwave Spectroscopy. *Angew. Chem. Int. Ed.* **2018**, *57*, 15199-15203.

(197) Gregoret, L. M.; Rader, S. D.; Fletterick, R. J.; Cohen, F. E. Hydrogen bonds involving sulfur atoms in proteins. *Proteins* **1991**, *9*, 99-107.

(198) Zhou, P.; Tian, F.; Lv, F.; Shang, Z. Geometric characteristics of hydrogen bonds involving sulfur atoms in proteins. *Proteins* **2009**, *76*, 151-163.

(199) Ovejas, V.; Fernández-Fernández, M.; Montero, R.; Longarte, A. On the ultrashort lifetime of electronically excited thiophenol. *Chem. Phys. Lett.* **2016**, *661*, 206-209.

(200) Devine, A. L.; Nix, M. G. D.; Dixon, R. N.; Ashfold, M. N. R. Near-Ultraviolet Photodissociation of Thiophenol. *J. Phys. Chem. A* **2008**, *112*, 9563-9574.

(201) Lim, J. S.; Choi, H.; Lim, I. S.; Park, S. B.; Lee, Y. S.; Kim, S. K. Photodissociation Dynamics of Thiophenol-d1: The Nature of Excited Electronic States along the S−D Bond Dissociation Coordinate. *J. Phys. Chem. A* **2009**, *113*, 10410-10416.

(202) Han, S.; You, H. S.; Kim, S.-Y.; Kim, S. K. Dynamic Role of the Intramolecular Hydrogen Bonding in Nonadiabatic Chemistry Revealed in the UV Photodissociation Reactions of 2-Fluorothiophenol and 2-Chlorothiophenol. *J. Phys. Chem. A* **2014**, *118*, 6940-6949.

(203) Martin, D. E.; Robertson, E. G.; Thompson, C. D.; Morrison, R. J. S. Resonant 2-photon ionization study of the conformation and the binding of water molecules to 2-phenylethanethiol (PhCH2CH2SH). *J. Chem. Phys.* **2008**, *128*, 164301.

(204) Iwasaki, A.; Fujii, A.; Watanabe, T.; Ebata, T.; Mikami, N. Infrared Spectroscopy of Hydrogen-Bonded Phenol−Amine Clusters in Supersonic Jets. *J. Phys. Chem.* **1996**, *100*, 16053-16057.

(205) Gord, J. R.; Hewett, D. M.; Hernandez-Castillo, A. O.; Blodgett, K. N.; Rotondaro, M. C.; Varuolo, A.; Kubasik, M. A.; Zwier, T. S. Conformation-specific spectroscopy of capped, gas-phase Aib oligomers: tests of the Aib residue as a 310-helix former. *Phys. Chem. Chem. Phys.* **2016**, *18*, 25512-25527.

(206) Bader, R. F. W. Atoms in molecules. *Acc. Chem. Res.* **1985**, *18*, 9-15.

(207) Bader, R. F. W. *Atoms in Molecules: A Quantum Theory*; Clarendon Press: Oxford, U.K., 1990.